

# NAVAL POSTGRADUATE SCHOOL

## Monterey, California



## THESIS

**U.S. AND AUSTRALIAN MINE WARFARE SONAR  
PERFORMANCE ASSESSMENT USING SWAT AND  
HODGSON MODELS**

by

Barbra K. Dubsky

September 2000

Thesis Advisors:

Robert H. Bourke  
James H. Wilson

Approved for public release; distribution is unlimited

DTIC QUALITY INSPECTED 4

20001205 023

<b>REPORT DOCUMENTATION PAGE</b>			Form Approved OMB No. 0704-0188	
Public reporting burden for this collection of information is estimated to average 1 hour per response, including the time for reviewing instruction, searching existing data sources, gathering and maintaining the data needed, and completing and reviewing the collection of information. Send comments regarding this burden estimate or any other aspect of this collection of information, including suggestions for reducing this burden, to Washington headquarters Services, Directorate for Information Operations and Reports, 1215 Jefferson Davis Highway, Suite 1204, Arlington, VA 22202-4302, and to the Office of Management and Budget, Paperwork Reduction Project (0704-0188) Washington DC 20503.				
1. AGENCY USE ONLY (Leave blank)		2. REPORT DATE September 2000		3. REPORT TYPE AND DATES COVERED Master's Thesis
TITLE AND SUBTITLE : U.S. And Australian Mine Warfare Sonar Performance Assessment Using Swat And Hodgson Models			5. FUNDING NUMBERS	
6. AUTHOR(S) Dubsky, Barbra K.				
7. PERFORMING ORGANIZATION NAME(S) AND ADDRESS(ES) Naval Postgraduate School Monterey, CA 93943-5000			8. PERFORMING ORGANIZATION REPORT NUMBER	
9. SPONSORING / MONITORING AGENCY NAME(S) AND ADDRESS(ES) N/A			10. SPONSORING / MONITORING AGENCY REPORT NUMBER	
11. SUPPLEMENTARY NOTES The views expressed in this thesis are those of the author and do not reflect the official policy or position of the Department of Defense or the U.S. Government.				
12a. DISTRIBUTION / AVAILABILITY STATEMENT Approved for public release; distribution is unlimited			12b. DISTRIBUTION CODE	
13. ABSTRACT (maximum 200 words) <p>The purpose of this thesis was to investigate a shallow coastal region to compile a detailed environmental picture of its sediment composition and water characteristics and from this model MCM sonar performance at the FBE-H exercise location as a means to determine what parameters exerted the greatest effect on performance. Seven parameters were intercompared to assess their sensitivity in detecting mines: bottom type, SSP, water depth/sonar depth, mine depth, frequency, sonars and models. Performance was assessed using several measures of effectiveness including the signal to noise ratio and initial detection range. Variations in these measures were analysed by investigating how TL and RL responded to changing parameters.</p> <p>No one single parameter was identified that affected sonar performance significantly above all others. Of the environmental parameters considered, variations in bottom type exerted the most influence on TL and RL and ultimately on sonar performance. TL was clearly a significant factor when the bottom type is comprised of absorptive, fine-grained material. Of the sonar parameters, frequency exerted a significant impact on performance with TL the most sensitive term in this comparison. A higher TL associated with higher frequency reduced the signal level and consequently the bottom RL. The higher frequency displayed a stronger SNR than the lower frequency over short ranges, however the higher frequency was limited by TL at greater ranges with the lower frequency achieving greater initial detection ranges.</p>				
14. SUBJECT TERMS Reverberation, Bottom Backscatter, Mine Warfare, PC SWAT Model			15. NUMBER OF PAGES 214	
			16. PRICE CODE	
17. SECURITY CLASSIFICATION OF REPORT  Unclassified	18. SECURITY CLASSIFICATION OF THIS PAGE  Unclassified	19. SECURITY CLASSIFICATION OF ABSTRACT  Unclassified	20. LIMITATION OF ABSTRACT  UL	

THIS PAGE INTENTIONALLY LEFT BLANK

**Approved for public release: distribution unlimited**

**U.S. AND AUSTRALIAN MINE WARFARE SONAR PERFORMANCE  
ASSESSMENT USING SWAT AND HODGSON MODELS**

Barbra K. Dubsky  
Lieutenant, Royal Australian Navy  
B.Sc., University College of the University of New South Wales, 1992

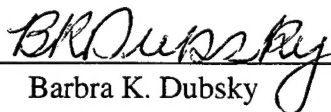
Submitted in partial fulfillment of the  
requirements for the degree of

**MASTER OF SCIENCE IN PHYSICAL OCEANOGRAPHY**


from the

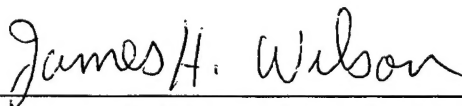
**NAVAL POSTGRADUATE SCHOOL  
September 2000**

Author:

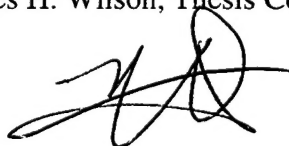
  
Barbra K. Dubsky

Approved by:

  
Robert H. Bourke, Thesis Advisor



James H. Wilson, Thesis Co-Advisor



Roland W. Garwood, Chairman  
Department of Oceanography



THIS PAGE INTENTIONALLY LEFT BLANK

## ABSTRACT

The purpose of this thesis was to investigate a shallow coastal region to compile a detailed environmental picture of its sediment composition and water characteristics and from this model MCM sonar performance at the FBE-H exercise location as a means to determine what parameters exerted the greatest effect on performance. Seven parameters were intercompared to assess their sensitivity in detecting mines: bottom type, SSP, water depth/sonar depth, mine depth, frequency, sonars and models. Performance was assessed using several measures of effectiveness including the signal to noise ratio and initial detection range. Variations in these measures were analysed by investigating how TL and RL responded to changing parameters.

No one single parameter was identified that affected sonar performance significantly above all others. Of the environmental parameters considered, variations in bottom type exerted the most influence on TL and RL and ultimately on sonar performance. TL was clearly a significant factor when the bottom type is comprised of absorptive, fine-grained material. Of the sonar parameters, frequency exerted a significant impact on performance with TL the most sensitive term in this comparison. A higher TL associated with higher frequency reduced the signal level and consequently the bottom RL. The higher frequency displayed a stronger SNR than the lower frequency over short ranges, however the higher frequency was limited by TL at greater ranges with the lower frequency achieving greater initial detection ranges.

THIS PAGE INTENTIONALLY LEFT BLANK

# TABLE OF CONTENTS

<b>I.</b>	<b>INTRODUCTION .....</b>	<b>1</b>
<b>A.</b>	<b>BACKGROUND .....</b>	<b>1</b>
<b>B.</b>	<b>MINE WARFARE .....</b>	<b>1</b>
	1. Mine Threat .....	1
	2. Mine Countermeasures (MCM).....	3
	3. Current Procedures for Route Surveys and Q-routes .....	4
	4. About FBE-H.....	9
<b>C.</b>	<b>STUDY AREAS .....</b>	<b>10</b>
<b>D.</b>	<b>ACOUSTICS .....</b>	<b>11</b>
	1. Bottom Loss .....	12
	2. Bottom Reverberation .....	13
	a. Bottom Composition.....	14
	b. Grazing Angle.....	15
	c. Frequency.....	18
	d. High Frequency Bottom Backscattering off Panama City, Florida.....	20
<b>E.</b>	<b>OBJECTIVES .....</b>	<b>20</b>
<b>II.</b>	<b>ENVIRONMENT .....</b>	<b>37</b>
<b>A.</b>	<b>OCEANOGRAPHY .....</b>	<b>37</b>
	1. General Circulation .....	37
	2. Water Mass Characteristics .....	38
	3. Mesoscale Features .....	39
	4. Northeast Gulf of Mexico .....	41
	a. Observed Seasonal Coastal Currents .....	42
	b. River Runoff .....	42
	c. Tides.....	45
	d. Meteorological Effects on the Gulf of Mexico.....	45
	5. Environmental Characterization of the Two Study Areas.....	47
	a. Circulation .....	47
	b. Water Properties.....	48
	c. Aperiodic Variability.....	50
<b>B.</b>	<b>BOTTOM BATHYMETRY AND COMPOSITION.....</b>	<b>51</b>
	1. Bathymetry .....	51
	a. Panama City Shelf.....	51
	b. Mississippi-Alabama Continental Shelf.....	52
	2. Sediments .....	53
	a. Overview of the Northeast Gulf of Mexico.....	54
	b. Mississippi Delta .....	54
	c. Panama City Shelf.....	56
	d. Mississippi-Alabama Shelf.....	58

III.	MODEL AND SONAR PARAMETERS .....	79
A.	SONARS AND MINES .....	79
1.	RAN Type 2093.....	79
2.	USN Generic MIW Sonar .....	80
3.	Mines .....	80
B.	MODELS.....	81
1.	PC SWAT.....	81
2.	HODGSON .....	85
3.	Model Parameters .....	88
IV.	RESULTS.....	99
A.	OVERVIEW .....	99
B.	COMPARISONS .....	100
1.	Bottom Type.....	100
2.	Season and SSP.....	104
3.	Water Depth and Sonar Depth .....	107
4.	Target .....	109
5.	Frequency.....	111
6.	Sonars .....	113
7.	Models .....	115
V.	CONCLUSIONS AND RECOMMENDATIONS .....	137
A.	CONCLUSIONS.....	137
B.	RECOMMENDATIONS .....	142
	LIST OF REFERENCES .....	145
	APPENDIX A. MODEL RUNS .....	153
	INITIAL DISTRIBUTION LIST .....	193

## LIST OF FIGURES

Figure 1.	The mine warfare environment is divided into five depth zones as shown here, with specific types of mines employed in each zone.....	23
Figure 2.	Bottom composition, per cent estimation of mine burial and bottom roughness combine with NOMBO density to achieve a particular bottom category .....	24
Figure 3.	Two areas will be studied. The first is the portion of the West Florida Shelf adjacent to Panama City, from Cape San Blas to the DeSoto Canyon. The second area is the Mississippi Alabama Shelf adjacent to Gulfport, from the Mississippi River Delta to the DeSoto Canyon.....	25
Figure 4.	A compilation of high frequency measurements in the range of 24 to 100 kHz for a variety of bottom types show that the backscattering strength changes for changing type .....	26
Figure 5.	Smoothed curves of bottom backscattering strength as a function of grazing angle illustrate the dependence on both grazing angle and bottom type ..	27
Figure 6.	The slope of the bottom backscattering strength increases with decreasing angle at grazing angles less than $10^\circ$ , as observed by Boehme et al., (1985) and Jackson et al. (1986). The bottom material consisted of silty sand with buried shell fragments .....	28
Figure 7.	Bottom scattering strength does appear to be dependent on frequency for the smoother bottoms such as mud and sand. The data for the $10^\circ$ grazing information is from McKinney and Anderson (1964).....	29
Figure 8.	Backscattering strength is dependent on frequency for higher incident angles (smaller grazing angles). In (a) there is a clear frequency dependence of the backscattering strength. Here the line was established to be to the fourth power of frequency. Frequency dependence increases with increasing incidence angle as shown in (b).....	30
Figure 9.	The bottom backscattering strength increases with increasing grazing angle for the fine sand bottom off Panama City. Both panels (20-90 kHz and 110-180 kHz) indicate this dependence .....	31
Figure 10.	The backscattering strength as $10 \log \mu$ shows a dependence on frequency, increasing by about 1.5 dB/octave.....	32
Figure 11.	The Intra America Seas (IAS) are the semi-enclosed waters of the western tropical North Atlantic. ....	63
Figure 12.	Temperature-salinity diagram that describes the water masses of the IAS.....	64
Figure 13.	The mean path of the Loop Current is illustrated here. Its northern extent is variable and can in fact intrude onto the continental shelf as occurred in February 1977.....	65
Figure 14.	The Loop Current intruded onto the shelf to the east of Louisiana in March 1998 as depicted here by temperature contours ( $^\circ\text{C}$ ) .....	66
Figure 15.	The sixty-four year average river discharge from the Mississippi River	

	is a maximum in spring and a minimum in Fall ( $\times 1000 \text{ m}^3 \text{ s}^{-1}$ ).....	67
Figure 16.	The Mississippi River's outflow is onto the Mississippi-Alabama shelf to the east and the Louisiana-Texas shelf to the west. The shaded region indicates the flood plains of the Mississippi and its tributaries.....	68
Figure 17.	The K1 tide displayed here dominates the diurnal tide along with the O1 constituent. The amplitude is in cm and the Greenwich phase angle in degrees in parentheses. ....	69
Figure 18.	The main semi-diurnal tide is the M2, with amplitude in cm and Greenwich phase angle in degrees in parentheses.....	70
Figure 19.	Observed mean current vectors over the Mississippi-Alabama shelf indicate that the mean flow is to the west, most notably on the outer shelf. Thick arrows are near surface currents, thin arrows are mid depth vectors and dashed arrows are near bottom currents, all in cm/s .....	71
Figure 20.	The shallow and deep water profiles for the two regions over the two seasons are displayed here. For the shallow region, temperature, salinity and sound speed profiles for the Panama City Shelf and the Mississippi-Alabama Shelf in fall are displayed, with an additional SSP for Mississippi-Alabama in spring for a flood event. For the deep water region, all three profiles have the Panama City Shelf and the Mississippi-Alabama Shelf in both fall and spring....	72
Figure 21.	A number of locations with hard bottom features have been studied as shown here, starting in 1957. The shaded or boxed areas have been identified as containing hard bottom features and were examined by various studies, as outlined in the legend .....	73
Figure 22.	The surficial sediments on the Florida-Mississippi-Alabama shelf are illustrated here. The sediments, from the Mississippi Delta east to Cape San Blas, are described as a number of clastic sand, mud and transitional facies .....	74
Figure 23.	Triangular diagrams for the 8 deposits from Figure 22 are shown here. The three poles are terrigenous sand, carbonate sand, and silt and clay. The frequency of occurrence in percent per 5 percent compositional triangle is illustrated within the shaded region.....	75
Figure 24.	The location of the delta lobes of the Mississippi River delta plain has migrated over time.....	76
Figure 25.	The coarsest material settles out first and nearest to the channel, followed at greater distances by finer and finer material .....	77
Figure 26.	Profiles of geoacoustic properties for a site off Panama City show very little variability with depth. Displayed here are (a) porosity, (b) mean grain size, (c) sound velocity, and (d) attenuation .....	78
Figure 27.	Curves for the bottom loss model in PC SWAT for a variety of bottom types and valid over the frequency range 20 to 30 kHz, as a function of grazing angle. $M_z$ is grain size in logarithmic units. ....	91
Figure 28.	Model curves for backscattering strength at 30 kHz for a variety of bottom types. Data is available for frequencies in the range of 10 to 100 kHz....	92
Figure 29.	Navy standard high frequency bottom loss (HFBL) curves as a function of grazing angle for the frequency band 1-4 kHz .....	93

Figure 30.	Comparison of sand (—) and clay (---) bottoms for the 2093 sonar operating in shallow water at 40 kHz.	119
Figure 31.	Comparison of sand (—) and clay (---) bottoms for the US sonar operating in shallow water at 35 kHz.	120
Figure 32.	Ray trace diagram for the shallow water environment on the Mississippi-Alabama shelf. The top figure is for August-September (A40_06) and the middle figure is for a flood event in spring (A40_12) when there is a strong positive sound speed gradient with the sonar at 3 m for both cases. The bottom figure is for a flood event in spring with the sonar at 10 m (A40_13).	121
Figure 33.	Comparison of sand (—) and muddy sand (--) bottoms for the 2093 sonar operating in deep water at 40 kHz.	122
Figure 34.	Comparison of the fall (—) and spring flood (---) SSPs in shallow water for the 2093 sonar at 40 kHz.	123
Figure 35.	Comparison of the spring SSP with the source above the layer (—) and below (---) the layer when searching for a bottom target.	124
Figure 36.	Comparison of the fall (—) and spring (---) SSPs in deep water for the US sonar	125
Figure 37.	Comparison of shallow (—) and deep (---) water conditions on the Panama City shelf for the 2093 sonar at 40 kHz.	126
Figure 38.	Comparison of shallow (—) and deep (---) water conditions on the Panama City shelf for the US sonar.	127
Figure 39.	Comparison of moored mines over a sand (—) bottom and a muddy sand (---) bottom for the 2093 sonar at 40 kHz.	128
Figure 40.	Comparison of moored (—) and bottom (---) mines over a muddy sand bottom for the 2093 sonar at 40 kHz.	129
Figure 41.	Comparison of bottom (—) and buried (---) mines on the Mississippi-Alabama shelf (clay bottom) for the 2093 sonar at 40 kHz.	130
Figure 42.	Comparison of the 2093 sonar at 40 kHz (—) and at 90 kHz (---) over a sandy bottom in shallow water.	131
Figure 43.	Comparison of the 2093 sonar at 40 kHz (—) and at 90 kHz (---) over a clay bottom in shallow water.	132
Figure 44.	Comparison of the Australian Type 2093 sonar (—) and the US sonar (---) over a sandy bottom.	133
Figure 45.	Comparison of the Australian Type 2093 sonar (—) and the US sonar (---) over a clay bottom.	134
Figure 46.	Analysis of the US sonar over a sandy bottom, comparing the three sonar parameters of source level, beamwidth and pulse length against the baseline parameters listed in Table 6.	135
Figure A 1.	S_A40_01	153
Figure A 2.	S_A40_02	154
Figure A 3.	S_A40_03	155
Figure A 4.	S_A40_04	156
Figure A 5.	S_A40_05	157
Figure A 6.	S_A40_06	158



Figure A 7.	S_A40_07.....	159
Figure A 8.	S_A40_08.....	160
Figure A 9.	S_A40_09.....	161
Figure A 10.	S_A40_10.....	162
Figure A 11.	S_A40_11.....	163
Figure A 12.	S_A40_12.....	164
Figure A 13.	S_A40_13.....	165
Figure A 14.	S_A90_01.....	166
Figure A 15.	S_A90_02.....	167
Figure A 16.	S_A90_03.....	168
Figure A 17.	S_A90_04.....	169
Figure A 18.	S_A90_05.....	170
Figure A 19.	S_A90_06.....	171
Figure A 20.	S_A90_07.....	172
Figure A 21.	S_A90_08.....	173
Figure A 22.	S_A90_09.....	174
Figure A 23.	S_A90_10.....	175
Figure A 24.	S_A90_11.....	176
Figure A 25.	S_U35_01.....	177
Figure A 26.	S_U35_02.....	178
Figure A 27.	S_U35_03.....	179
Figure A 28.	S_U35_04.....	180
Figure A 29.	S_U35_05.....	181
Figure A 30.	S_U35_06.....	182
Figure A 31.	S_U35_07.....	183
Figure A 32.	S_U35_08.....	184
Figure A 33.	S_U35_09.....	185
Figure A 34.	S_U35_10.....	186
Figure A 35.	S_U35_11.....	187
Figure A 36.	H_A40_01.....	188
Figure A 37.	H_A40_06.....	189
Figure A 38.	H_A90_01.....	190
Figure A 39.	H_A90_06.....	191

## LIST OF TABLES

Table 1.	Bottom Profile Groups .....	33
Table 2.	Clutter Category .....	33
Table 3.	Sediment Classification .....	34
Table 4.	US MIW Bottom Composition .....	35
Table 5.	Bottom Types .....	36
Table 6.	Sonar Parameters .....	94
Table 7.	PC SWAT Input Parameters.....	95
Table 8.	HODGSON Additional Parameters.....	96
Table 9.	Matrix of Model Runs .....	97
Table 10.	The Results from the SWAT Runs.....	136

THIS PAGE INTENTIONALLY LEFT BLANK

## **ACKNOWLEDGMENTS**

I would like to thank Professors Bourke and Wilson for their guidance, encouragement and instruction whilst researching and preparing this study.

I also thank CMDR Brenton Smyth, RAN for assisting in establishing contacts within DSTO. Thanks also to Dr. Stuart Anstee of DSTO, Australia for providing the parameters for the Type 2093 sonar and his constant and always timely advice on related issues.

Thanks also go to Mr. Steve Haeger and Ms Gabrielle Malley of NAVO for their assistance with the environmental data for the regions in this study. I would also like to thank Dr. Gary Sammelmann of CSS for his support and advice for using the model PC SWAT.

THIS PAGE INTENTIONALLY LEFT BLANK

# **I. INTRODUCTION**

## **A. BACKGROUND**

Mine Warfare is a component of naval warfare that is heavily affected by the environment. From the performance of mine hunting sonars being influenced by the water column or the bottom type, to ability of divers to conduct tasks in conditions of high current or low visibility, to the ability of the bottom to mask mines with other bottom features or allow burial in softer sediments, many aspects are influenced by the conditions in which they are operating. Knowledge of this environment is an enormous asset, which would allow decisions from the strategic level down to the tactical level to be made to enhance operational capability.

This study will focus on the impact of the environment on mine hunting sonar performance, examining the sensitivity of performance to each component of the environment, and also sensitivity to, essentially, fixed parameters such as the frequency of the sonar. In determining which factor or factors have the greatest impact on sonar performance, that is, when a parameter is altered and the sonar performance is either seriously degraded or enhanced, efforts could be concentrated to investigate this parameter to improve predictions in the future.

## **B. MINE WARFARE**

### **1. Mine Threat**

The history of the use of mines in naval warfare is a long one, sometimes said to date back as early as 1585 (Levie, 1992), and has been a continuous part of it ever since.

Many types of naval mines have been developed over the centuries leading to various categorisations or classification of mines, e.g., according to their intended target, (as anti-submarine, anti-ship or anti-landing) or by their method of delivery (submarine, ship/surface or air delivered). More commonly, naval mines are categorised as either moored, bottom, drifting or rising mines; or according to their actuation, as either contact, influence or controlled. Influence mines are further classified as acoustic, magnetic or pressure sensitive or a combination (Brown, 1991; Levie, 1992). Although drifting mines were limited by the Hague Convention of 1907 and are not in the U.S. Navy inventory, nations such as Iran have recently used them in the Persian Gulf region (Gerken, 1989). As such, they are addressed here.

As noted in the U.S. Naval Mine Warfare Plan (2000), the mine environment has been divided into five depth zones or regimes (Figure 1). The Deep Water Zone is considered to occupy water deeper than 300 feet, with mines in this regime generally of the rising or moored types, although some deep water bottom mines exist that can be deployed in this zone. The Shallow Water Zone is between 40 and 300 feet, typically associated with bottom, moored and rising mines. From 10 to 40 feet is the Very Shallow Water Zone, where typically bottom, moored, controlled and buried types are employed. The Surf Zone extends from waters less than 10 feet deep to the beach, including the intertidal region. This zone generally uses anti-invasion mines, controlled mines, buried mines and other obstacles. Finally is the Craft Landing Zone (CLZ), which is the beach itself. The mine threat in this zone is generally similar to that in the Surf Zone, but with the possible addition of conventional land mines.

Due to the cost effectiveness and ease of deployment of a sea mine, it is a highly sought after weapon by many nations. These factors combined with the historical success of simple contact and influence mines, suggests that these weapons will continue to be a part of modern warfare. This has been displayed as recently as the 1992 Gulf War, when Iraq demonstrated a significant mining capability laying approximately 1,300 mines, although many were nonfunctioning or ineffectively laid. Despite this, three mines were successful in seriously damaging two U.S. warships. With a combined cost of an estimated \$11,500 for the mines, approximately \$28 million in damages was inflicted. (U.S. Naval Mine Warfare Plan, 2000)

## **2. Mine Countermeasures (MCM)**

Naval mine countermeasures (MCM) include all possible means of preventing sea mines from destroying ships and submarines, both offensive and defensive. This involves a broad range of tasks, ranging from preventing the enemy from laying mines, preventing own ships from actuating mines (using methods such as degaussing), to finding mines once laid (termed mine hunting), and sweeping, destroying or neutralising the mines (Gerken, 1989). If mines are deployed, a number of MCM options are available as outlined by the U.S. Naval Mine Warfare Plan, 2000. The options include localising and avoiding mines or minefields, localising and selectively clearing mines (for tactical breakthrough and short-term operations), minesweeping, and/or minehunting and neutralisation. This study will focus on minehunting.

MCM will refer to active minehunting for the remainder of this study. The MCM sonars operate at much higher frequencies and thus much shorter ranges than Anti-



Submarine Warfare (ASW) sonars. The usual frequency range for MCM sonars is of the order of 35 to 700 kHz with bandwidths that spread by 10 to 20 per cent either side of the centre frequency. Most MCM sonars employ a dual-frequency capability. They operate at lower frequency to survey a specific area, allowing detection at greater ranges (several hundred meters) and use higher frequency (thus higher definition and shorter ranges) to classify and identify a mine like object (MILO). (Friedman, 1997; Lathrop, 1995)

Environmental conditions greatly influence the success of MCM operations. Variations in environmental parameters such as bathymetry, salinity, temperature, tidal range, currents, water clarity and seafloor structure can alter and, in some cases, significantly degrade sensor performance, thus reducing operational capabilities (Oceanography and Mine Warfare, 1999).

Dedicated U.S. MCM vessels in use today are the MCM-1 (Avenger) class and the Minehunter Coastal, MHC-51 (Osprey) class. Both are equipped with the variable depth sonar (VDS) AN/SQQ-32. The Royal Australian Navy's (RAN) MCM vessels are the Huon class MHC with the VDS Type 2093 and the Bay class Inshore Minehunters (MHI) fitted with the hull-mounted DSQS-11M. (Jane's Fighting Ships, 1999-2000)

### **3. Current Procedures for Route Surveys and Q-routes**

To clear an area of a mine threat, the use of sonar to detect and locate the mines requires a long duration operation where the sea bed is surveyed for the presence of bottom contacts. In times of conflict, the duration to conduct this type of operation is far too great. The concept of a "route survey" has been introduced to overcome this limitation. It involves a suitably equipped vessel collecting accurate hydrographic and

side scan sonar (SSS) data, initially along strategic routes (Q-routes) and then later collecting similar data in areas of less operational importance. The survey data would include all sonar contacts in the area with an appropriate classification for each contact. (Gerken, 1989)

The Q-route concept was adopted by the U.S. Navy during World War II and was modified to meet U.S. requirements. It is also a part of the Australian MCM Plan. A Q-route, or port breakout route, normally begins at a harbour entrance and extends out to sea, ending at a designated depth where the mine threat is no longer considered significant. Ideally, these routes would be well surveyed and regular and comprehensive surveys would be conducted in peacetime. Certain types of bottom sediment are favorable to the minehunting task. Sediments that do not impede minehunting are those where mines cannot be buried in mud or hidden among rocky outcrops. If these bottom areas were selected and surveyed during peacetime, they would only require a few sweeps during periods of mine threat to ensure that a high probability of safe transit existed. (Gerken, 1989; Hinge, 1992)

Laying Q-routes and conducting route surveys, even before mines have been deployed, allows for the identification of all mine-like objects, and facilitates finding mines once laid. If the decision was made not to clear an area of mines during a time of conflict when ports may possibly be mined, the Q-route would be selected as the egress path and its integrity could be rapidly checked. The data that had been previously collected during route surveys can be recalled and the minehunting vessel can be redeployed along the Q-route, investigating only those contacts that have not previously

been encountered. Thus rapid detection and clearance, as required, is achieved; this procedure is called change detection. (Gerken, 1989)

The Mine Warfare Campaign Plan initiated by the Chief of Naval Operations (CNO N85) has specifically tasked the Naval Oceanographic Office (NAVOCEANO) to collect oceanographic data to describe environmental conditions along predetermined Q-routes, Carrier Operation Areas (CVOAs) and along critical sea lanes of communication (SLOCs) (Null, 2000). The Mine Warfare (MIW) community, in conjunction with NAVOCEANO, is currently formulating route survey environmental databases. One of the objectives of the establishment of these databases is to consolidate all of the environmental data collected by MIW forces with the data routinely collected and stored by NAVOCEANO. These merged data sets can then be made available to MIW units to support operations. This collection, analysis, assessment and proper data basing and eventual fleet dissemination of mine-like contacts (MILCOs), non-mine-like bottom objects (NOMBOs) and other environmental data in critical areas allows realistic time lines to be established for entry during times of conflict (Null, 2000). Without this specific information, significant time delays or risks to shipping could occur. More specifically, the seafloor can be categorised depending on environmental qualities that are optimum for MCM, chiefly;

- topographically featureless regions delineated from more geological complex areas;
- low clutter regions delineated from high clutter regions; and

- low bottom reverberation areas delineated from higher reverberation areas (Null, 2000).

Environmental data that describes the reflective nature of the seafloor and the level of backscattered acoustic energy are essential to the determination of sonar performance. NAVOCEANO's bottom characteristic database is intended to provide, in a simplistic fashion, the information required to assist in minehunting. It consists of four parameters or layers: surface sediment type, bottom roughness, clutter density and bottom features. Bottom features are physiographic parameters of the bottom that are not directly related to grain size, such as pockmarks and oil or gas seepage, and provides statistical information such as number of pockmarks per area. MIW units collect the other three parameters. COMINELWARCOM TACMEMO MZ6000-01-99 (COMINELWARCOM, 1999) outlines procedures for collecting and processing this environmental data by MIW units and this process will be outlined here.

Acoustic imagery from AN/SQQ-32 surveys can provide estimates of bottom roughness, clutter density and ridging. Table 1 and Table 2 provide classification boundaries for categorising the degree of bottom roughness and clutter density, respectively. The roughness is defined as the percentage of the search area that can be considered to be smooth, moderate or rough. This categorisation is subjective and is based on the size and extent of sand ridges, outcroppings or other bottom structures. Ridging is the estimated height of sand ridges or other bottom roughness features from crest to trough, to the nearest tenth of a meter.

The clutter density is defined as the number of NOMBOs per unit area (kilometer<sup>2</sup> or nautical mile<sup>2</sup>). NOMBO density influences the amount of incorrectly identified mines and thus the time needed to complete a mine hunting mission (Oceanography and Mine Warfare, 1999). It is translated into a clutter category number as shown in Table 2.

As outlined in COMINEWARCOM TACMEMO MZ6000-01-99, this data should be logged every 5 minutes during route survey operations. Track lines should be run at 250 m spacing to maximize coverage of the route, time permitting.

Surface sediment type is based on grain size. Various texts and papers outline such classifications, all having similar categorisations. Komar (1998) outlines sediment grain size in both millimetres and  $\phi$  units. The  $\phi$  scale is related to the diameter (D) in millimetres by  $D = (1/2)^\phi$ .

Table 3 outlines these categories, from boulders to clay. For reporting bottom types during route survey databases, the sediment size is categorised into bottom composition categories as defined in Table 4.

Of the parameters discussed above, bottom composition and bottom roughness are combined with an estimation of mine burial (in percentage) to form a mine warfare bottom type as defined in COMINEWARCOM TACMEMO MZ6000-01-99. Bottom categories range from best case "A" defined as a seafloor with characteristics optimum for minehunting (e.g., hard sand bottom) to the worst case "D", typified by a potential for high-mine burial (Oceanography and Mine Warfare, 1999). Table 5 outlines these bottom types.

The process outlined above, i.e., combining bottom roughness, bottom composition and per cent predicted mine burial to achieve a bottom category, is then combined with NOMBO's per unit area. This procedure is summarised in Figure 2 to categorize the sea floor.

Oceanography and Mine Warfare (1999) outlines a significant shortfall with this technique of route surveying. Current doctrine does not adequately account for the highly variable conditions that are often encountered in MCM operational areas. For example, the sonar search width is highly dependent on prevalent environmental conditions, however, this sonar width is a fixed quantity for all environments. Thus, in a changing environment two consequences arise. Firstly, environmental variations can result in data voids, referred to as "holidays", when the assumed sonar detection width is greater than the actual detection width. Secondly, redundant coverage and thus wasted time will result when the assumed sonar width is less than the actual sonar detection width for the specific environment.

#### **4. About FBE-H**

Fleet Battle Experiment Hotel (FBE-H) was the eighth exercise in the series conducted by the Navy Warfare Development Command and is outlined on their web page. The MIW component of FBE-H provided guidelines for this study in terms of location, platform and timing. It was conducted in the Gulf of Mexico and Southern United States from 25 August to 15 September and focused on joint operations in the littoral zone. The MIW component was conducted on the Panama City Shelf, where the

survey of the approaches to Panama City is expected to take twelve days. The exercise was then be relocated and the landing took place at Gulfport, Mississippi.

### **C. STUDY AREAS**

Two particular areas will be examined in this study to model sonar performance. Both are located in the northeast Gulf of Mexico and are the regions of interest for FBE-H. The continental margin of the Gulf of Mexico, adjacent to Mississippi, Alabama and Florida, is referred to by the acronym MAFLA, and is shown in Figure 3. The MAFLA encompasses both areas that will be examined.

The first area is located on the northwestern portion of the West Florida Shelf, adjacent to Panama City. The West Florida Shelf is a broad shallow region off the west coast of Florida extending from the southernmost tip of Florida, adjacent to the Strait of Florida, to the DeSoto Canyon, seaward of Pensacola near the Florida/Alabama border. The area of interest is the continental shelf extending from Cape San Blas, northwest to the eastern extent of the DeSoto Canyon. For the purpose of this study, this region will be referred to as the Panama City Shelf.

The second area to be examined is the Mississippi-Alabama Shelf (sometimes referred to as the Louisiana-Mississippi-Alabama Shelf), in the west of the MAFLA. It extends from the Mississippi River Delta east to the western extent of the DeSoto Canyon. This region will be referred to as the Mississippi-Alabama Shelf.

Minehunting during FBE-H will take place on the Panama City Shelf. It is a relatively uniform region with regard to sediments on the shelf. The Mississippi-

Alabama Shelf was chosen as a second study region as the landing is taking place at Gulfport. It has more variation in the sediments on the shelf and should provide a good contrast in operational performance.

#### **D. ACOUSTICS**

The sea bottom effects sound propagation by reflection, scattering and transmission into the sediment. Other factors that effect underwater sound are the water column and the state of the sea. The water column effects sound speed (being a function of temperature, pressure and salinity), absorption and scattering, while surface reflection and scattering vary with sea state. Scattering, as described here, is the reradiation of a portion of the acoustic energy by the volume, the bottom and/or the surface, and is termed reverberation in monostatic active sonars (Urlick, 1983).

In the shallow water environment, the effects of the bottom become significant due to the nearness of the seabed, and detailed knowledge of the bottom environment is essential for knowledge of sound propagation and detection ranges. How bottom reverberation and transmission loss (TL) change with changing frequency and bottom types is of critical importance to sonar performance. Studies on bottom interaction in acoustic performance began during World War II where a series of transmission measurements at high frequencies (12 and 24 kHz) were made, examining both bottom reflection (incorporated in TL) and backscattering (incorporated in reverberation level – RL) (Urlick, 1983). These two components (bottom TL and RL) will be examined relative to mine hunting sonar frequencies.



## **1. Bottom Loss**

The seafloor is able to reflect and scatter sound from its interface as well as allow penetration into the substrate. With penetration into the sediment, refraction, absorption and transmission occur, as well as further reflection and scattering at medium changes. Thus transmission loss at the seabed is made up of many components.

Additionally, the bottom is highly variable in composition, it may vary from hard rock to soft mud, and this creates high variability in acoustic properties. Also, it is often layered, with density and sound speed changing gradually or abruptly with depth. (Urick, 1983).

In *Physics of Sound of the Sea* (1946), an experiment is described, which used predominantly high frequency sonars in World War II that, examined the reflection from varying bottom types. It was found, using a 24 kHz source, that sand, rock and stony (defined as pre-dominantly cobble, gravel and shell) categories were termed "well-reflecting" bottom types, with stony being more reflective than all other types of bottoms and sand more reflective than rock. More variability was seen with mud, with generally poor reflectivity, and where bottoms consisted of both sand and mud, the reflection was intermediate between well and poorly reflecting bottoms and generally followed that of the dominant grain size, either the sand or the very fine particles (mud).

Winn et al. (1983), analysed reflections from the uppermost 10-12 cm of the surface sediment from an 18 kHz echosounder and indicated a relationship between the mean grain size of the surface sediment samples and the reflection strength. They demonstrated a log-linear relationship, with a minimum in reflection strength at the

smallest grain sizes (clay and mud in this experiment) and increasing with increasing grain size. Investigations of acoustic penetration into the seabed as a function of grain size were conducted. Where sands and gravels constituted the surface sediment cover, penetration was very limited, with most of the acoustic energy being reflected from the topmost layer. Penetration was fair to good in muds and clays, but the depth of penetration was usually limited by the presence of interstitial sands or an underlying strong reflector. (Winn and Becker, 1983; McKinney and Anderson, 1964)

Hamilton (1974(a); 1980) discussed the frequency dependence of attenuation in sedimentary material. Experimental evidence over a wide range of frequencies (from 10 Hz to 1 MHz) indicated that the dependence of attenuation on frequency for both mud and sand is approximately a first-power dependence ( $f^1$ ). For silt-clay or mud bottoms, the dependence was more closely approximated by  $f^1$  than  $f^{1/2}$  or  $f^2$ , which others had concluded, but an exact dependence was not verified.

## **2. Bottom Reverberation**

Bottom reverberation is the scattering of sound by various kinds of nonuniformities and irregularities of the ocean bottom. Dependence on bottom characteristics, grazing angle and frequency have all been examined and will be discussed here.

Reported measurements of backscattering strengths of the ocean bottom made during World War II were primarily at 24 kHz and at small grazing angles. In general, reverberation was highest over rock, less over sand-and-mud or mud and least over sand.

In some cases reverberation over sand was high, especially after a storm when rippling of the bottom may have been the cause. (Physics of Sound of the Sea, 1946)

Since World War II, numerous experiments have been carried out extending the range of frequencies, grazing angles and bottom characteristics examined. Chapman et al. (1997) examined a series of shallow water experiments, conducted from 1964 to 1992 at frequencies ranging from 8-290 kHz. The experiments were conducted over a wide range of bottom conditions and grazing angles and indicated that scattering strength was either independent of frequency or only weakly dependent on it

*a. Bottom Composition*

Bottom composition appears to exert an influence on scattering strength, more so than frequency. As discussed above, reverberation does vary over varying bottom types, as displayed in Figure 4.

Bunchuk and Zhitkovskii (1980) determined that regions with different types of bottoms form a sequence in order of decreasing backscattering strength, that order being rock; clay-silt and silt; and sand. They observed only slight differences with the greatest gradation differing by only 10 dB. Jackson et al. (1986) reported on bottom backscatter measurements that were made at six shallow water sites over the frequency range 20-85 kHz. They determined that the highest scattering strengths were observed over a gravel bottom, were lower for sand combined with shell or rock and lowest for sand and silt.

Beyond considering merely bottom type, early researchers determined that the magnitude and nature of the scattering was a function of both the particle size and the

surface (bottom) relief (McKinney and Anderson, 1964). The two are not independent and both are important; however they concluded that bottom relief was the major factor in the backscattering of sound. A relationship between sediment type and back scattering strength was evident in the observations, implying that the particle size has some effect. However, that effect exists because the composition of the sediment influences the type of bottom relief and structure of the bottom. Data in Wong and Chesterman (1968), Bunchuk and Zhitkovskii (1980) and Jackson et al. (1986) revealed that scattering strength can differ by 10-15 dB for sediments having similar grain size.

#### *b. Grazing Angle*

Figure 5 illustrates smoothed curves of scattering strength as a function of grazing angle from a large variety of sources. It indicates that scattering strength tends to be independent of grazing angle at small angles and that a Lambert's law relationship, which relates backscattering strength ( $S_B$ ) to grazing angle ( $\theta$ ), appeared to provide a good approximation to the data at angles below  $45^\circ$  (Urick 1983). Lambert's law is:

$$S_B = 10 \log \mu + 10 \log \sin^2 \theta$$

where  $\mu$  is Mackenzie's constant, a measure of the degree of bottom roughness.  $10 \log \mu$  equals the backscattering strength in dB at normal incidence if Lambert's law is valid at normal incidence (Boehme et al., 1985)

McKinney and Anderson (1964) discussed results for different sediments and the dependence on grazing angle for frequencies of 12.5 to 290 kHz. Backscattering strength for sand was thought to be essentially independent of angle for grazing angles

near  $2^\circ$ . With increasing grazing angle there was a steady increase in backscattering strength until the range of  $10^\circ$  to  $30^\circ$  where the rate became close to the dependence predicted by Lambert's law. Beyond this, a smaller rate of increase of backscattering strength at larger values of grazing angle was thought to be due to an increase in penetration (and consequent absorption) of sound into the bottom, occurring when the grazing angle was larger than the critical angle. A critical angle of  $30^\circ$  is a reasonable value for sands, and for angles greater than this, energy penetrates into the substrate and is partially absorbed thus reducing the backscattered energy. However, as the grazing angle approaches  $90^\circ$  (near incidence), the backscattered energy would again increase due to specular reflection (for a flat bottom). For gravel a similar pattern was observed; however, the backscattering strength increased more rapidly with increasing grazing angle. For mud a critical angle of  $10^\circ$  was considered reasonable, and at lower values of grazing angle the dependence was approximately  $\sin \theta$ , not  $\sin^2 \theta$  in accordance with Lambert's law.

This pattern of three scattering regimes has been seen in various experiments whose results are discussed in Chapman et al. (1997). One experiment compared slopes of scattering strength versus grazing angle over a complete range of grazing angles for sand, clay and gravel bottoms. The three scattering regimes were consistent with those of other observers. Below  $10^\circ$  the scattering strength slopes often exceeded that of Lambert's law; in the region between  $20^\circ$  and  $60^\circ$  they were generally flatter; and above  $60^\circ$  the slopes rose very rapidly.

Scanlon (1995) modelled reverberation levels over varying bottom types. He noted that bottom backscattering strength over mostly coarse sand bottoms closely approximated that given by Lambert's law, a  $\sin^2 \theta$  relationship. However, for an absorptive bottom, such as mud, energy enters the sediment and is attenuated within the sediment. In this case bottom backscatter does not obey Lambert's law, instead it is assumed to be a function of  $\sin \theta$ , consistent with volume scattering (as observed by McKinney and Anderson, 1964 and Briggs, 1994). These relationships were tested during Exercise LWAD 99-1, and found to agree as stated above, i.e., with bottom back scattering strength over a silty clay bottom having a  $\sin \theta$  relationship and that over a sandy bottom exhibiting a  $\sin^2 \theta$  relationship (Schalm, 1999).

Results from the early experiments which concluded that scattering strength was independent of grazing angle at small angles, has been called into question. Wong and Chesterman (1968) examined back scattering strengths at small grazing angles (between  $0.4^\circ$  and  $8^\circ$ ) and noted that on a few occasions there was a weak angular dependence at very low grazing angles. The estimated bottom backscattering strength slope was observed to increase with decreasing grazing angle (below about  $3^\circ$ ) for sand bottoms by Boehme et al. (1985). They concluded that this behaviour was a result of energy backscattered from the water surface. Jackson et al. (1986) also noted this behaviour of the scattering strength curves having steep slopes for the smallest grazing angles for bottoms consisting of silty sand with shell, fine sand and shell, medium sand and sandy silt as illustrated in Figure 6. They observed a rapid decrease in backscattering

strength for decreasing grazing angle at 5-10°, usually set by interfering surface reverberation as Boehme et al. (1985) concluded.

*c. Frequency*

As previously mentioned, it appeared that scattering strength was independent of or only weakly dependent on frequency. However, there does appear to be some dependence for certain bottom types. Figure 7 shows a definite frequency variation for two data sets, one at a grazing angle of 30° and the other at a grazing angle of 10°, both extending over a wide range of frequencies.

There appears to be a rise in scattering strength for sand and silt bottoms with frequency, however there is little or no frequency dependence for the rock, sand and rock, and silt and shell bottoms. Urick (1983) attributed this behaviour to a difference in the scale of bottom roughness. Back scattering coefficients are independent of frequency when the roughness of the bottom is large compared to the wavelength. When the bottom has an appreciable portion of its roughness spectrum at roughness's small compared to the wavelength, the scattering strength increases with frequency. Thus the variation of bottom backscattering with frequency appears to be very complex because it is influenced by both bottom composition and bottom roughness (AOMC Training Publication).

Zhitkovskii and Lysanov (1967) also discussed frequency dependence variation with different bottom types. They noted that essentially the relief of the bottom determines the nature of frequency dependence of the scattered signal. For a region that has a highly structured bottom relief pattern, where the scattering is diffusive at all angles of incidence, the scattering does not exhibit frequency dependence. The frequency

dependence was determined in the vicinity of abyssal plains, which are characteristically flat and composed of clays (very fine grained sediment). For small incidence angles ( $<10-15^\circ$ ), scattering is due largely to reflection from the bottom. For large angles of incidence (small grazing angles) a strong frequency dependence is observed as displayed in Figure 8 (a), where the scattering intensity varies in proportion to  $f^4$ . Frequency dependence of scattering increases with increasing angle of incidence, as is illustrated in Figure 8(b), with incidence angles of  $14^\circ$ ,  $20^\circ$  and  $40^\circ$ .

A weak frequency dependence was observed for sand bottoms over a variety of frequencies and grazing angles (Boehme et al., 1985; McKinney and Anderson, 1964; Jackson et al., 1986; Stanic et al., 1989). Over the frequency range of 30 to 95 kHz they noted that bottom backscattering strength increased with frequency at a rate of  $10 \log f^n$  where  $1 \leq n \leq 1.5$  (variation due to scatter in data points) (Boehme et al., 1985). This is in close agreement with McKinney and Anderson (1964) who observed that backscattering strength increased with frequency at a rate of  $10 \log f^{1.6}$  for sand.

Measured scattering strengths over a coarse shell bottom were nearly identical to two other areas with bottoms consisting of coarse shell as discussed in Stanic et al. (1989). At all three sites the sediments below the coarse shell surface were different. This would indicate that the primary scattering mechanism, especially above 20 kHz, the minimum frequency examined here, was the surface roughness. In the three shell areas, backscattering strengths were on average 8-10 dB higher than those measured at smooth sand locations.



*d. High Frequency Bottom Backscattering off Panama City, Florida*

In an experiment conducted 30 km south of Panama City, Florida, Stanic et al. (1988) made bottom backscattering measurements. This is the region where FBE-H will be held. The bottom is comprised of fine sand (the sediments will be discussed in more detail in Chapter II) and a clear dependence of bottom backscattering strength on grazing angle was noted as illustrated in Figure 9. For both 20-90 kHz and 110-180 kHz the backscattering strength increased with increasing grazing angle. Scattering strengths tended to exhibit a  $\sin^2 \theta$  dependence as expected in areas with sand bottoms.

As shown in Figure 10, only a weak frequency dependency is noted in the bottom backscatter. The scattering strengths for this sandy smooth bottom region increased by about 1.5 dB/octave, similar to those observed in other regions of similar sedimentary composition.

**E. OBJECTIVES**

The objectives of this thesis are to:

- i. Assess the environmental picture of the two regions, highlighting the differences. With this information the resulting sonar performance will be explained in terms of the environment.
- ii. Determine the effects of different environmental parameters and different sonar parameters on sonar performance for mine hunting sonars.

These objectives will be met by first specifying environmental parameters in Chapter II. The performance of two sonars will be compared. The two sonars to be used are the Royal Australian Navy (RAN) TSM 2093 and a U.S. Generic Mine Warfare Sonar (Chapter III). Using the Shallow Water Acoustic Toolchest (SWAT) and Hodgson® models (both discussed in Chapter III), the environmental information and sonar parameters will be used to determine sonar performance. These results will allow the comparison of the two models and comparison of the two sonars (Chapter IV). Typical reasonable values of sonar parameters are used to keep the model runs unclassified.

THIS PAGE INTENTIONALLY LEFT BLANK

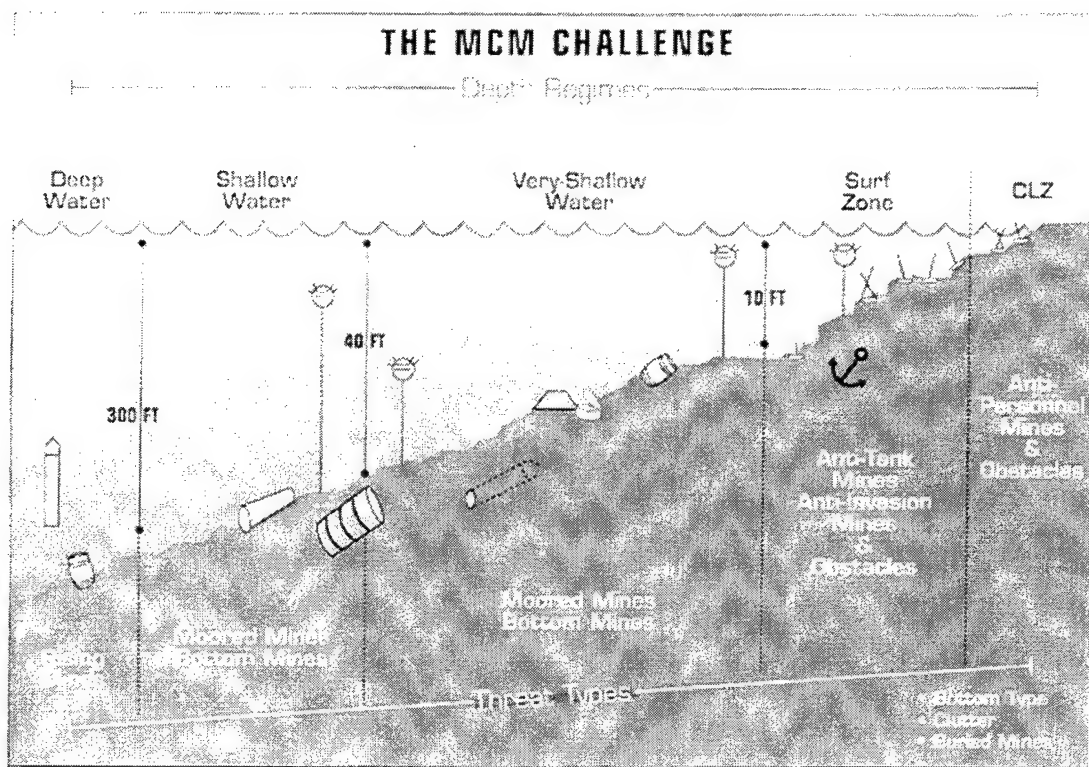


Figure 1. The mine warfare environment is divided into five depth zones as shown here, with specific types of mines employed in each zone (from U.S. Naval Mine Warfare Plan, 2000).

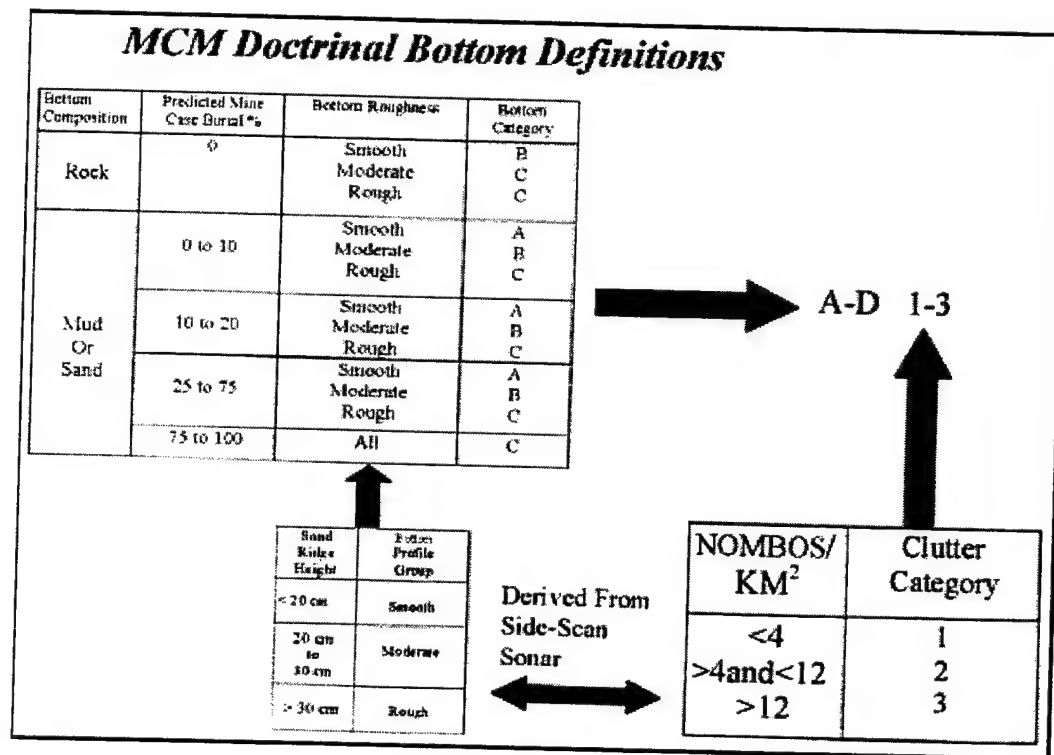


Figure 2. Bottom composition, per cent estimation of mine burial and bottom roughness combine with NOMBOS density to achieve a particular bottom category (from Oceanography and Mine Warfare, 1999).

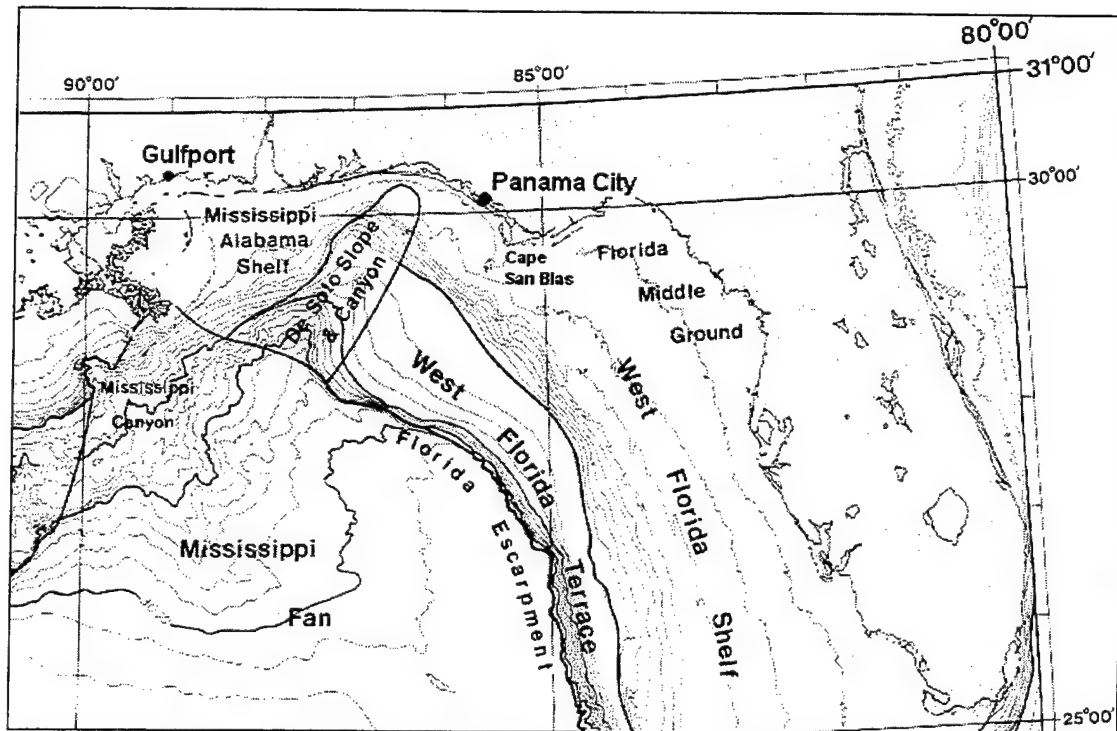


Figure 3. Two areas will be studied. The first is the portion of the West Florida Shelf adjacent to Panama City, from Cape San Blas to the DeSoto Canyon. The second area is the Mississippi Alabama Shelf adjacent to Gulfport, from the Mississippi River Delta to the DeSoto Canyon. (After Bryant et al., 1991)

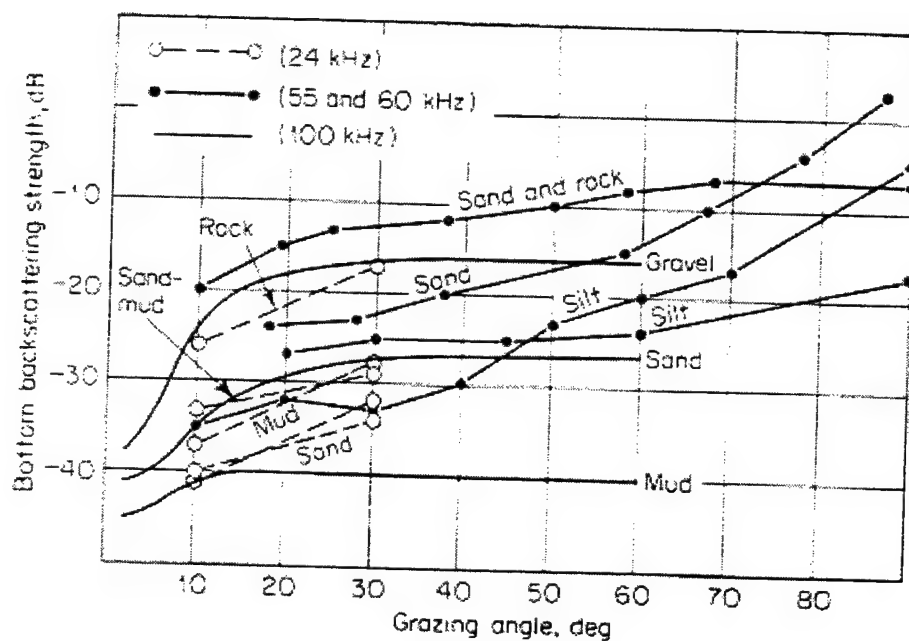


Figure 4. A compilation of high frequency measurements in the range of 24 to 100 kHz for a variety of bottom types show that the backscattering strength changes for changing type (after Urick, 1983).

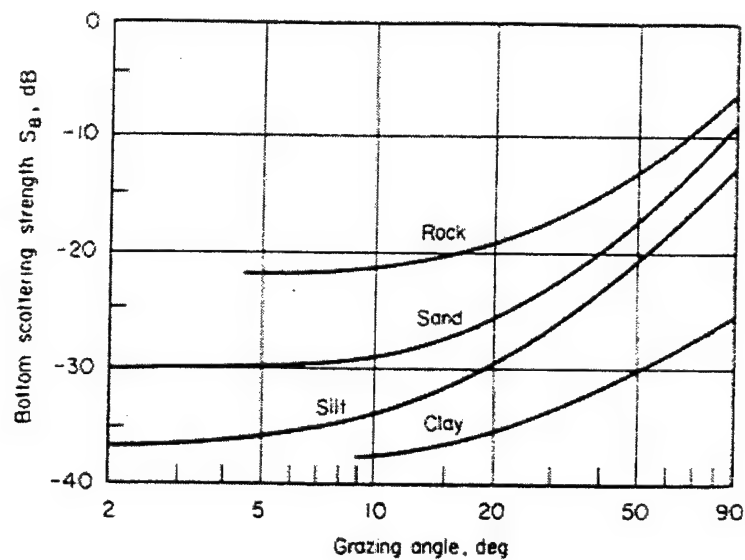


Figure 5. Smoothed curves of bottom backscattering strength as a function of grazing angle illustrate the dependence on both grazing angle and bottom type (from Urick, 1983).



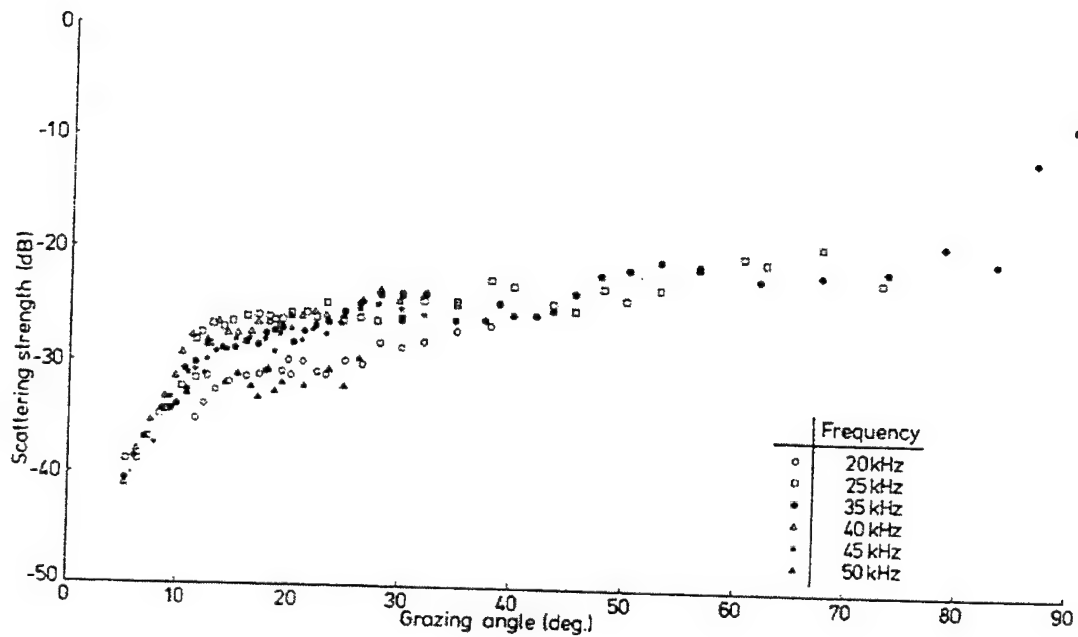


Figure 6. The slope of the bottom backscattering strength increases with decreasing angle at grazing angles less than  $10^\circ$ , as observed by Boehme et al., (1985) and Jackson et al. (1986). The bottom material consisted of silty sand with buried shell fragments. (From Jackson et al., 1986)

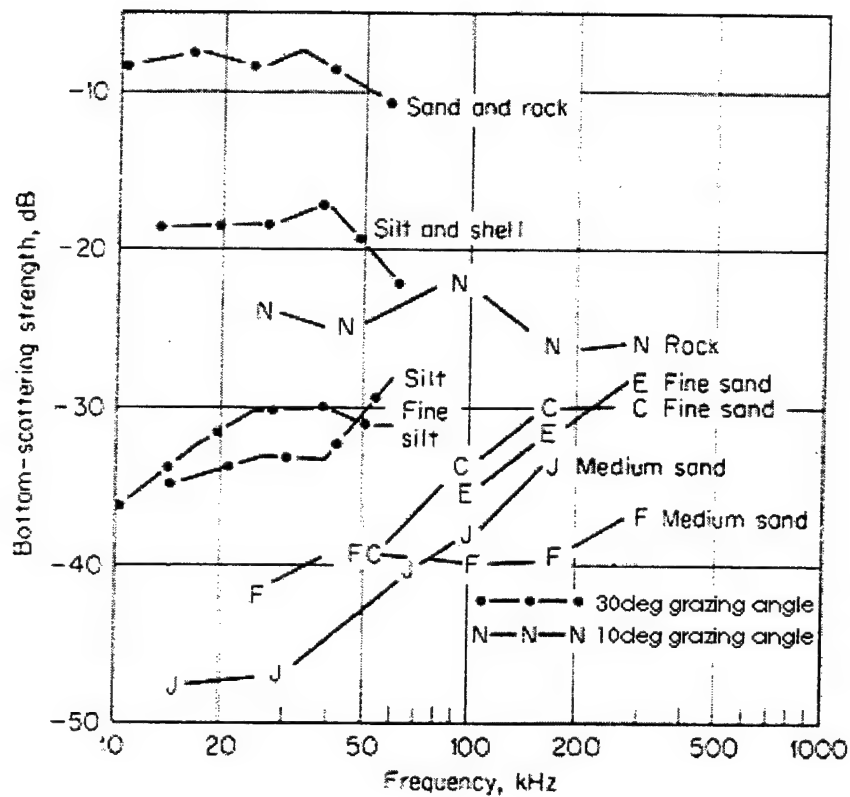


Figure 7. Bottom scattering strength does appear to be dependent on frequency for the smoother bottoms such as mud and sand. The data for the 10° grazing information is from McKinney and Anderson (1964). (After Urick, 1983)

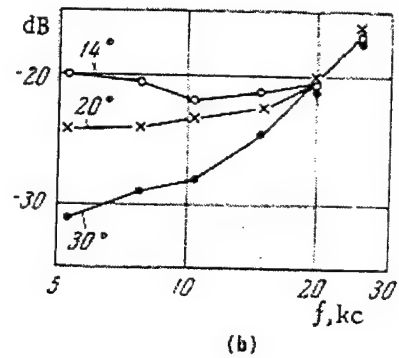
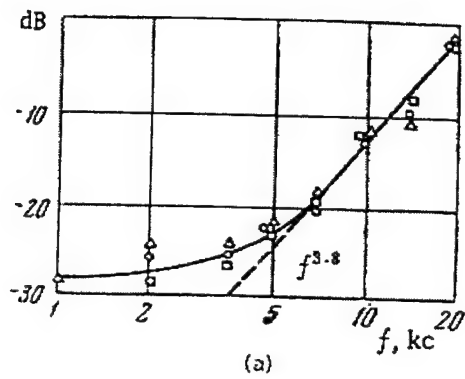


Figure 8. Backscattering strength is dependent on frequency for higher incident angles (smaller grazing angles). In (a) there is a clear frequency dependence of the backscattering strength. Here the line was established to be to the fourth power of frequency. Frequency dependence increases with increasing incidence angle as shown in (b). (After Zhitkovskii and Lysanov, 1967)

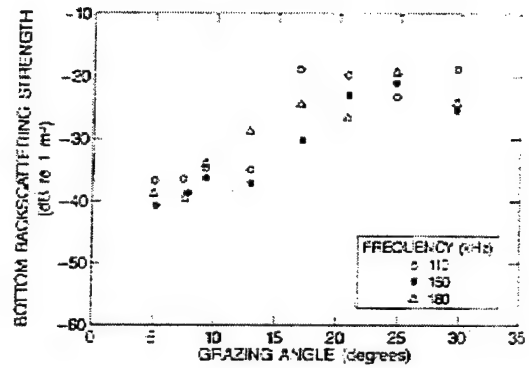
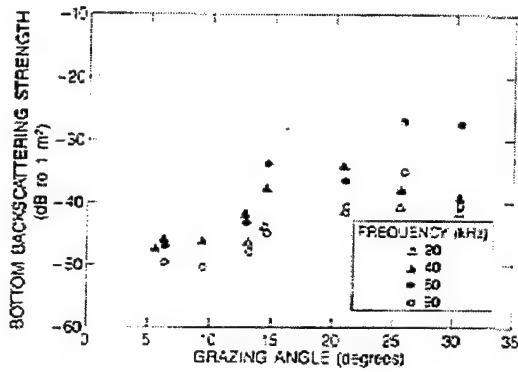


Figure 9. The bottom backscattering strength increases with increasing grazing angle for the fine sand bottom off Panama City. Both panels (20-90 kHz and 110-180 kHz) indicate this dependence. (From Stanic et al., 1988)

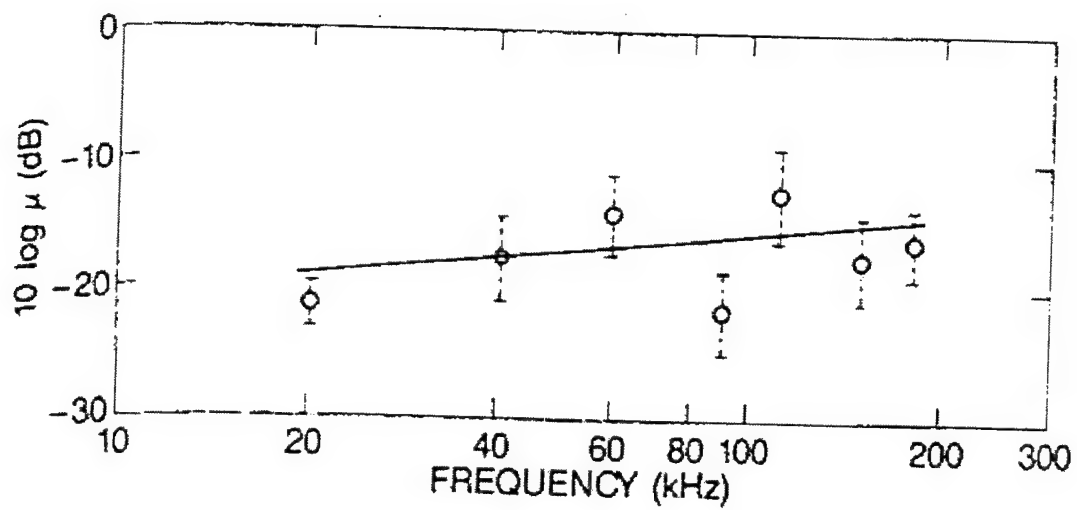


Figure 10. The backscattering strength as  $10 \log \mu$  shows a dependence on frequency, increasing by about 1.5 dB/octave (from Stanic et al., 1988).

Bottom Roughness (%)	Bottom Roughness Ridge Height (m/ft)	Bottom Profile Group
<5	<0.2/<0.5	Smooth
5-15	0.2-0.3/0.5-1.0	Moderate
>15	>0.3/>1.0	Rough

Table 1. Bottom Profile Groups (after COMINELARCOM TACMEMO MZ6000-01-99)

NOMBOs/km <sup>2</sup>	NOMBOs/nm <sup>2</sup>	Clutter Category
<4	<15	1
4-12	15-40	2
>12	>40	3

Table 2. Clutter Category (from COMINELARCOM TACMEMO MZ6000-01-99)

Size Nomenclature	Diameter	
	Millimetres	$\phi$ units
Boulders	>256	>-8
Cobbles	64 to 256	-6 to -8
Pebbles	4 to 64	-2 to -6
Granule	2 to 4	-1 to -2
Very Coarse Sand	1 to 2	0 to -1
Coarse Sand	0.5 to 1	1 to 0
Medium Sand	0.25 to 0.5	2 to 1
Fine Sand	0.125 to 0.25	3 to 2
Very Fine Sand	0.0625 to 0.125	4 to 3
Silt	0.0039 to 0.0626	8 to 4
Clay	< 0.0039	> 8

Table 3. Sediment Classification (taken, in part, from Komar, 1998)

Code	Meaning
10	Sand
11	Sand, very coarse (>2mm)
12	Sand, coarse (0.5 to 2.0mm)
13	Sand, medium (0.25 to 0.5,,)
14	Sand, fine (0.125 to 0.25mm)
15	Sand very fine (0.083 to 0.125mm)
20	Gravel
30	Limestone
40	Mud
50	Clay
60	Coral
70	Rock

Table 4. US MIW Bottom Composition (from COMINEWARCOM  
TACMEMO MZ6000-01-99)



A	Stable and smooth flat bottom. Ripples less than 15 cm deep and/or moderate mine burial possible, but never exceeding 15 cm.
B	Rather stable and smooth but uneven bottom. Holes, bumps, ridges, and folds up to 30 cm and/or mine burial possible, but never exceeding 30 cm.
C	Rough bottom. Holes, bumps, ridges, and folds exceeding 30 cm and/or a lot of seaweed. Mine burial likely (exceeding 30 cm), but never complete.
DR	Mines are likely to be hidden completely by irregularities of the bottom.
DV	Mines are likely to be hidden completely by seaweed.
DB	Mines are likely to be hidden completely owing to complete burial (mines may be buried permanently or break surface from time to time).
DH	Mines are likely to be hidden completely in deep hollows or crevices or by cliffs.
DZ	Mines are likely to be hidden completely for other reasons.

Table 5. Bottom Types (From COMINEWARCOM TACMEMO MZ6000-01-99)

## **II. ENVIRONMENT**

### **A. OCEANOGRAPHY**

#### **1. General Circulation**

The semi-enclosed waters of the western tropical North Atlantic are referred to as the Intra-Americas Seas (IAS) (Mooers & Maul, 1998). Figure 11 illustrates this region, in which the Gulf of Mexico is encompassed. The circulation of this region is a part of the North Atlantic anticyclonic gyre, with flow on the western boundary from the equator to the poles.

The circulation of the IAS is dominated by throughflow through deep and narrow passages, as described by Mooers and Maul (1998). The inflow is derived from the tropical and subtropical North Atlantic Ocean. It enters the Caribbean Sea through several passages, flowing west and north through this sea (known here as the Yucatan Current), then exiting through the Yucatan Channel into the Gulf of Mexico. Here it penetrates north as the Loop Current into the eastern Gulf of Mexico where it sheds anticyclonic rings, before turning anticyclonically to exit through the Straits of Florida. The sill depth of the Yucatan Channel is 1900 m with an observed transport of 19.2 Sv, whereas the sill depth of the Straits of Florida is 750 m with an observed transport of 32 Sv. (Mooers and Maul, 1998)

## 2. Water Mass Characteristics

Prior to describing the coastal waters off the Florida, Mississippi and Alabama shelves, we first examine the characteristics and origins of the waters within the IAS.

Mooers and Maul (1998) describe these water masses with a temperature and salinity diagram (Figure 12). The surface waters are of tropical Atlantic Ocean origin, with temperatures of  $28^{\circ}\text{C}$  and salinities of 36 psu. These waters flow into the Caribbean Sea through the Antilles Passages and flow out the Straits of Florida with almost the same general temperature and salinity properties. Below the surface is the subtropical underwater (SUW), typically at 200 m, of central tropical Atlantic origin ( $T \approx 22^{\circ}\text{C}$ ,  $S \approx 36.7\text{psu}$ ). The Loop Current and its anticyclonic rings are identified by the SUW and will be discussed later. Below this is the Western North Atlantic Central Water (WNACW) with typical temperatures ranging from  $8^{\circ}\text{C}$  to  $20^{\circ}\text{C}$  and salinity range from 35.2 to 36.3 psu. The characteristic salinity minimum of the Antarctic Intermediate Water (AAIW) near 34.8 psu with  $T \approx 7^{\circ}\text{C}$  is located at about 700 m, and can be traced through the Gulf of Mexico and the northern Straits of Florida. The deepest waters, below 1000 m, are of slightly increased salinity from the mid-depth waters of the Atlantic. It is common to use the depth of certain isotherms to locate water masses and typically the  $15^{\circ}\text{C}$  isotherm at 200 m or the  $22^{\circ}\text{C}$  isotherm at 100 m can be used reliably to locate the edge of the Loop Current.

Outside of the water of this throughflow, the waters of the IAS are typically reduced in salinity ( $S \approx 36.2\text{ psu}$ ) due to mixing with the ambient waters. The ambient

waters are usually highly influenced by freshwater of river origin or due to precipitation exceeding evaporation (Mooers and Maul, 1998).

### **3. Mesoscale Features**

The Loop Current is the major oceanographic feature in the Gulf of Mexico. It is a western boundary current, which separates from the continental shelf north of Yucatan Strait. The extent of penetration and location of the loop is variable, and it periodically sheds eddies which propagate westward. Figure 13 illustrates the general path of the Loop Current. The main path of the current generally penetrates north to about 27°N, however, it can be located farther north and intrude onto the shelf. Conversely, when an anticyclonic eddy (or ring) separates from the northern part of the Loop Current, the main current does not extend north of 25°N. This occurs on average every 11 months (Tomczak and Godfrey, 1994).

Evidence suggests that the minimum northward penetration of the Loop Current generally occurs in winter months, with a migration of the Loop Current northward increasing during winter and spring, reaching a maximum in early summer. It is then, in the summer, that larger anticyclonic eddies probably separate from the current. There is, however, substantial deviation from this "average" sequence of events with the period between eddy separations being as short as 8 months and as long as 17 months. Also, there is evidence that the Loop Current has intruded onto the shelf in winter. (Vukovich, 1979)

These rings are anticyclonic and are clearly identified by their water properties with SUW found at their core. This high salinity water is entrapped upon separation from

the Loop Current and is clearly distinguishable from the surrounding water – commonly referred to as the Gulf of Mexico common water (Elliot, 1982).

The Loop Current influences the outer shelf, and when large intrusions of Loop Current water penetrate to the inner shelf, it dominates the local circulation over time intervals of two to three weeks (Boicourt et al., 1998). The variation in location of the Loop Current and the intrusions onto the shelf also facilitates the local exchange of water masses (Huh et al., 1981). In particular, Loop Current water influences the region of the DeSoto Canyon, the preferred site for the Loop Current to extrude water onto the shelf, and has been observed to penetrate nearly to the coast. This takes place primarily in the upper part of the water column (Brink, 1994).

An intrusion of a plume following the trend of the DeSoto Canyon occurred in February 1977 and is discussed by Huh et al. (1981). The northward edge of the warm current was observed to move rapidly onto the continental shelf, affecting shelf waters to within 8 km of the shore. The intrusion brings warm, salty water onto the shelf, and is a major mechanism for sudden modification of coastal and shelf waters with the development of oceanic fronts. Filaments of adjacent cold shelf waters with cyclonic curvature were entrained into the plume, creating modified Loop Current water.

The movement of the Loop Current onto the shelf facilitates an easterly current, thus the mean flow on the shelf is dependent on the degree of intrusion of the Current (Boicourt et al., 1998). Schroeder et al. (1994) discussed observations of an eastward flow on the shelf. When the Loop Current or a Loop Current eddy is present on the shelf, it dominates the flow and a mean eastward flow above 200 m is observed.

Also, oscillatory flow south of the Mississippi River delta was observed for many months prior to the Loop Current penetrating to the vicinity of the delta when a strong eastward mean flow developed and persisted for over four months.

Aside from the main body of the Loop Current, filaments can also impinge on the shelf, stretching over considerable distances, in some cases meandering hundreds of kilometres northward. These events are characterised by water of higher temperatures and salinity throughout the water column, being pushed onto the western portion of the shelf and flowing clockwise to the northeast (Figure 14) (Kelly and Vastano, 1994). Located to the east of the plume is a southwestward return flow with opposite water mass characteristics. Measurements of salinity and temperature taken at site A (Figure 14) indicate that bottom temperatures rose abruptly by more than 2°C and salinity by about 1 psu. Generally these intrusions vary in vertical extent but have a characteristic horizontal width over the shelf of 30-45 km. Further studies have shown a temperature increase above the mean in one or more subsurface measurements which persisted for at least ten days and reached a peak deviation of at least one degree (Kelly, 1994).

In some months, particularly June-September, no evidence of the Loop Current at the surface may be present due to surface heating during this season. This does not mean that the feature does not exist, rather that there is no surface thermal contrast to identify it. (Vukovich, 1979)

#### **4. Northeast Gulf of Mexico**

The continental shelf of the northeastern Gulf of Mexico has a complicated circulation, variable in both space and time. Forcing of these patterns is due to tides,

winds, river flow and the Loop Current, some of which have a seasonal cycle. The spatial variations may be complex and are dependent on the relative strengths of the forcing functions. The time scales may be seasonal (such as river output), they may have a response time of months, e.g., Loop Current intrusions, or may have responses as short as several hours with the passage of a storm system (Niiler, 1994).

*a. Observed Seasonal Coastal Currents*

Winter, spring and fall seasons all have mean alongshore flows to the west, with summer flow patterns somewhat different. Observations indicate in summer that easterly and westerly currents may equally dominate the flow, though it is not considered a flow reversal. Throughout the year, the cross-shore flows appear consistent in magnitude with an apparent lack of direction, with onshore velocities increasing in spring and becoming weaker in winter but no other trend evident in other seasons. (Dinnell et al., 1997)

Over the west Louisiana-Texas shelf (the region immediately to the west of the Mississippi delta) the mean nearshore flow is downcoast (to the west away from the Mississippi output) during all but the summer months. During late summer and spring, the combination of winds and decreasing discharge from the Mississippi River system forces the flow back upcoast (eastward), penetrating into Louisiana waters. (Boicourt et al., 1998)

*b. River Runoff*

The northern regions of the Gulf of Mexico are influenced by the seasonal runoff from the Mississippi River and Mobile Bay. River discharge peaks in spring, with

May being at the end of the period of maximum average discharge; conversely, the minimum discharge occurs in the fall, with November generally being the period of minimum average discharge by this river system. (Li et al., 1997)

The average discharge of the Mississippi River is  $14,000 \text{ m}^3\text{s}^{-1}$  (Schroeder et al., 1994). Figure 15 illustrates a sixty-four year average of river discharge for the Mississippi River. The flood plains of the Mississippi River and its region of outflow are displayed in Figure 16. Roughly half of the discharge exits westward onto the west Louisiana shelf and the other half exits eastward onto the east Louisiana-Mississippi-Alabama shelf (Boicourt et al., 1998). The result of freshwater being discharged onto the shelf is discussed in Blanton (1994). The freshwater discharge forms plumes of low-salinity (low-density) water. The lower density of this water causes it to override ambient shelf water of higher density and a coastal front is formed. An offshore pressure gradient is formed and Coriolis turns this flow to the right, thus a baroclinic coastal current (buoyant flow) is directed to the west on the Mississippi-Alabama shelf from Mobile Bay, and south of the Mississippi delta to the Louisiana-Texas shelf from the Mississippi River.

Thus dynamically, it is expected that buoyancy flow will be to the west in our region of interest, but some of the Mississippi River water does influence the shelf (approximately 30%) in the northeastern Gulf of Mexico (Garvine, 1994).

Despite the fact that much of the runoff from the Mississippi flows westward, it is still the largest source of freshwater to the Louisiana-Mississippi-Alabama shelf, followed in importance by the Alabama and Tombigbee Rivers. These two rivers



converge to form the Mobile River system flowing into Mobile Bay, Alabama as illustrated in Figure 16. It provides a significant amount of water ( $2,200 \text{ m}^3\text{s}^{-1}$ ) to the northeastern portions of the shelf. West of Mobile Bay is the Chandeleur Sound where numerous rivers contribute an average discharge of just over  $1,200 \text{ m}^3\text{s}^{-1}$ . (Schroeder et al., 1994) When the Loop Current penetrates far enough north, some of the river water is entrained into the Loop Current and transported to the Strait of Florida (especially under periods of eastward winds) (Mooers and Maul, 1998).

The westward and southward flowing low salinity plumes from the Mississippi Delta discharge into deep water. The Froude number, the ratio of the fluid speed to a measure of internal wave speed (Gill, 1982), is high for the Mississippi discharge. This indicates that as the plumes move out toward deeper water, they remain mostly intact and do not mix with the surrounding waters until in deeper water. The plumes quickly separate from the bottom and spread buoyantly. When mixing does occur, the plumes are highly responsive to both wind forcing and entrainment of momentum from ambient currents. The low salinity plume from Mobile Bay behaves in a similar way, but significant mixing occurs within the Bay. This causes the Froude number of the discharge to be much less than in the Mississippi discharge. Thus, it doesn't remain as an intact feature and it further mixes with the ambient waters much more easily. (Boicourt et al., 1998)

Fresh water is delivered from Mobile Bay onto the shelf mainly through a single pass. Alternatively, multiple passes associated with the Mississippi Sound results in a more distributed source of freshwater onto the shelf. Variation in the fate of this

freshwater is controlled by seasonal buoyancy driven coastal current, (relatively slow) cross shelf exchange via mixing, and (more rapid) cross shelf exchanges driven by either wind events or Loop Current intrusions onto the shelf. (Schroeder, 1994) The latter process results in the greatest variability in fresh water flow.

*c. Tides*

Tides and tidal currents in the Gulf of Mexico are relatively weak, less than 1 m and  $0.1 \text{ ms}^{-1}$ , respectively (Mooers and Maul, 1998). The K1 (the Soli-lunar diurnal) and O1 (main lunar diurnal) constituents, both nearly uniform in amplitude and phase, dominate the diurnal tide in the Gulf of Mexico across the Gulf. These diurnal constituents are dominant over the majority of the Gulf. The amplitude and phase of the K1 constituent is displayed in Figure 17 (Clarke, 1994).

The main semi-diurnal tide in the Gulf is the M2 (main lunar semi-diurnal) constituent Figure 18). This tide varies spatially across the Gulf and is strongly amplified across the wide West Florida Shelf (typical of semi-diurnal amplification across wide non-polar continental shelves). However, in our area of interest, the component contributes only a small fraction to the tidal range and is invariant in amplitude between the two locations (Clarke, 1994).

*d. Meteorological Effects on the Gulf of Mexico*

The wind regime over the northeastern Gulf of Mexico shelf is modulated by the position and strength of the Bermuda High, a semi-permanent subtropical anticyclone over the Atlantic (Boicourt et al., 1998). It dominates the weather patterns of

late spring and summer, when it is strongest, and is located to the southeast of the Gulf of Mexico. It directs a southeasterly flow over the northeast shelf. (Schroeder et al., 1994)

In addition to this semi-permanent feature, the summer and early fall are strongly influenced by the more dramatic events of intense tropical cyclones. Typically four tropical storms will reach hurricane intensity in the IAS each year (Mooers and Maul, 1998). Although tropical storms and hurricanes propagate rapidly through the area, the associated high winds can produce rapid changes in water properties and circulation patterns. The responses to these systems include rapid vertical mixing (and thus cooling of the surface waters) and strong currents. Additionally, in the summer local conditions are influenced by the daytime sea breeze and its nocturnal counterpart the land breeze, both resulting from differential heating of the land (Schroeder et al., 1994).

The Bermuda High weakens during the fall and retreats southward (Schroeder et al., 1994). The northeastern Gulf of Mexico shelf then comes under the influence of the westerlies. During winter the primary synoptic scale features are the weekly cold front passages (sometimes bringing cold air outbreaks), prevalent until the end of spring. (Mooers and Maul, 1998)

Wind driven currents are strongest in winter when the shelf is influenced by these cold fronts from the north, progressing eastward. Cyclones also form in the Texas/western Gulf of Mexico region and typically track across the northern Gulf of Mexico in a matter of days moving ashore from Louisiana to Florida. Both of these types of storms affect processes in the gulf directly by the addition of fresh water through precipitation and also by increasing fresh water discharges as storms move ashore

(Ruscher, 1994). These cold air outbreaks occur on 3 to 10 day intervals. They can rapidly change the water column by cooling and vertical mixing, and additionally increase the exchange between the shelf waters and the Loop Current (Boicourt et al., 1998).

## **5. Environmental Characterization of the Two Study Areas**

### ***a. Circulation***

The first study area is the Panama City shelf, the northern portion of the West Florida shelf. Most of the literature describes the circulation on the West Florida shelf in its entirety, and will be discussed as such here.

The West Florida shelf generally receives little fresh water from rivers, being outside the normal influence of the Mississippi River system's discharge. With lack of strong buoyancy forcing concurrent with the variability inherent in both the predominant wind forcing and occasional Loop Current interaction, there is no definitive characterization of a mean or a seasonally varying flow; it is primarily driven by the wind (Boicourt et al., 1998). Clarke (1994) discusses the flow on this shelf, due to the tides, wind, fresh water input from coastal streams and springs (although small) and the Loop Current. The main wind forcing takes place in winter as the atmospheric fronts move over the shelf from the north. Current meter observations consistently showed that the low frequency flow (several day periodicity) was wind driven on the inner and mid shelf, and to a smaller extent on the outer shelf where the Loop Current processes may become important. The Loop Current is expected to influence the outer shelf flow over the length of the West Florida shelf. Occasionally near the narrower regions of the shelf, large intrusions of the Loop Current can penetrate to the inner shelf and will then dominate the

circulation for a period of two to three weeks, resulting in eastward or southward flow in these circumstances (Boicourt et al., 1998).

On the Louisiana-Mississippi-Alabama Shelf, the second study region, river runoff is highly variable, with the inputs from the Mississippi River and the rivers that form the Mobile River system. The buoyancy forcing is strong in this region. The mean flow, although variable, is westward throughout much of spring, summer and fall and is illustrated in Figure 19 where current meter measurements taken on the shelf show this mean westward flow. The mean flow turns south off the western barrier islands in front of the Chandeleur Islands (Kennicutt et al., 1995). The most variation has been seen during winter, at the time when the mean flow is strongly responsive to wind forcing (Schroeder et al., 1994). The mean flow of the outer shelf is expected to be highly dependent on the degree of intrusion of the Loop Current in the eastern Gulf of Mexico, as seen on the West Florida shelf (Boicourt et al., 1998).

***b. Water Properties***

The sea surface temperatures range from 14°C in January to 30°C in August. Variations from the mean are most pronounced in winter and spring and accompany weather systems. As previously stated, surface water temperatures decrease during and after the passage of a cold front. The southerly winds that precede the passage of a cold front bring warm water from farther offshore. It is only during winter and spring that offshore surface waters are substantially warmer than local coastal waters. (Salsman and Ciesluk, 1978)

For the Panama City Shelf, the vertical temperature structure is nearly isothermal from summer through fall to 30 m, with temperature decreasing at all depths below this. During spring, the warming of the surface waters causes the thermocline to shoal to near 10 m and as the season progresses the thermocline gradually retreats to deeper water again (Salsman and Ciesluk, 1978). The temperature structure of the water column on the Mississippi-Alabama shelf shows less seasonal variation, with a shallow (15-20 m) mixed layer in all seasons and temperature decreasing below this. When a weather event passes to mix the water column and drain heat from it, the decrease can be evident at shallow depths.

The salt content of the Gulf waters is high throughout the year with surface values exceeding 34 psu inshore and 35 psu offshore, increasing farther seaward (Salsman and Ciesluk, 1978). A salinity gradient is also present in the east-west direction, with salinity increasing to the east away from the river discharges on the western portion of the shelf. On the Panama City Shelf the variation of salinity with depth and with season is minor whereas a marked decrease in salinity is noted in waters on the Mississippi-Alabama Shelf in the spring and an increased likelihood of a significant fresh water event.

Over the shallow shelf environment, temperature and salinity exert the greatest effect on sound speed. A large change is caused by the annual temperature variation, with surface values near 1500 m/s expected in winter months increasing to 1540 m/s in summer (Salsman and Ciesluk, 1978). Spatial variations occur with the salinity variations due to the freshwater input on the Mississippi-Alabama shelf, with

correspondingly lower sound speed in that region compared with the Panama City Shelf and periods of positive gradients created when a fresh water event has occurred. Figure 20 illustrates the temperature, salinity and sound speed profiles for the two regions in the seasons fall and spring that were used in this study (Malley, 2000).

*c. Aperiodic Variability*

The largest variations in the circulation and water properties occur with northward penetration of the Loop Current coinciding with increased discharge from the Mississippi River.

A well-documented flood event in 1993 discharged sizable amounts of fresh water into the Gulf of Mexico during the normally dry summer months and is discussed by Ortner et al. (1995). As previously stated, the Mississippi River plume normally flows westward, against the coast. However, an eastward and southeastward movement of the plume into the region of the Loop Current was forced by a persistent eastward wind component in that region at that time. Additionally, the Loop Current was located well north, intruding on the shelf, which allowed entrainment and transport of the Mississippi River water.

The flooding event was reflected in unusually high river discharge from many other rivers in the region, (though these only amounted to 10% of the Mississippi discharge). Low salinity values of 26 psu were detected in an area just south of the Florida panhandle and extended easterly and to the south towards the Florida Peninsula. This atypical eastward flow of the river was confirmed by satellite imagery showing an eastward turbidity plume (Tomas, 1994).

## **B. BOTTOM BATHYMETRY AND COMPOSITION**

This study focuses on the two regions outlined in Chapter I and displayed in Figure 3, the Panama City Shelf and the Mississippi-Alabama Shelf. The DeSoto Canyon divides these two regions, creating an abrupt change in the subbottom properties. The canyon delineates the edge of the large carbonate province of the West Florida Shelf comprised of relatively uniform sands from the more spatially varying sedimentary composition west (Antoine, 1972).

### **1. Bathymetry**

#### ***a. Panama City Shelf***

As outlined in Chapter I, this study is concerned primarily with the northwestern portion of the West Florida Shelf, the Panama City Shelf.

Much of this region is described as characteristically flat and featureless (Salsman and Ciesluk, 1978). Subdued, north-south trending ridges dominate the shelf. These ridges are slightly asymmetrical with the steep sides facing east. They have wavelengths of about 200 to 1000 m and amplitudes of 1 to 3 m. Thus, there are relatively large expanses between ridges, which are essentially flat. (Briggs, 1994)

Wave induced sand ripples with heights up to 3 cm and wavelengths of 7 to 13 cm are often present in shallow waters off the beaches. These small ripples are observed to only exist for a day or so before being flattened. These ripples also occur farther offshore and have been observed with heights of up to 15 cm and with wavelengths of about 1 m, however large storms are needed for their generation.



Salsman and Ciesluk (1978) discussed many of the features of the Panama City Shelf. Typically, the shelf break occurs about 65 km offshore in approximately 50 m of water. The bottom deepens rapidly seaward of the break and the shelf break is rather abrupt in places. Limestone outcrops are scattered throughout the area. These formations are reef-like and are found at depths of 18 to 70 m, though most do not protrude more than a few meters above the surrounding sediment. Remnants of an ancient forest have been discovered in water 18 m deep south of Panama City Beach, and at shallower depths (6 to 15 m) in the land-cut portion of the bay entrance. Most of the wood has been identified as pine, with only small amounts of hardwood found.

***b. Mississippi-Alabama Continental Shelf***

The Mississippi-Alabama Shelf has recently been studied by Schroeder et al. (1994). It is triangular in shape, bounded on the west by the Chandeleur Islands and the Mississippi River Delta where the shelf has a maximum width of approximately 125 km. It progressively narrows eastward to the western rim of the DeSoto Canyon where the width is only about 25 km. A prominent characteristic of this shelf is the abrupt 90° change, from the east-west orientation of the Mississippi-Alabama barrier island coastline to the north-south trend of the Chandeleur Islands and the Mississippi River delta/Louisiana coastline. This change is also reflected in the sediment variation.

The shelf is a gently sloping, flat plain interspersed by scattered clusters of elevated mounds along the outer shelf (Schroeder et al., 1994). Thousands of carbonate mounds have been found along the outer continental shelf (OCS), ranging from less than a few meters in diameter to nearly a kilometer across. Figure 21 illustrates regions where

features have been studied. They are found mostly in two isobath-parallel bands, near the shelf edge in water depths of about 100-110 m and at about 75-80 m depth, which is at the deeper end of the region for this study. Mound heights were found to range from less than 1 m to 15-18 m and diameters varying from a few meters to nearly a kilometer. Some of the pinnacles are atop what is described as a hard bottom, are slightly elevated and have sizes of several tens of meters across to hundreds of meters across. Also found in the shallower of the two depth zones were isobath-parallel ridges which are virtually continuous structures of varying length (the longest 15 km, others much smaller and discontinuous) and height (1 to 8 m) trending east-west. (USGS Report (1), 1998; Laswell et al., 1992)

As well as these clusters of pinnacles, salt domes are prevalent on the shelf, usually subsurface. These features are most prevalent in the west, and as the DeSoto Canyon is approached, they generally decrease in number with very few found east of the canyon (Antoine, 1972).

## **2. Sediments**

Marine sediments in the littoral regions are predominantly derived from land. In general, sediments on the continental shelf are deposited in a systematic way with the nearshore region covered by deposits of sand grading outward to a mud bottom in deep water. This is an ideal concept and many regional exceptions abound. From the continental shelf to the continental slope, sediments generally consist of a layer of fine silt and mud, unless the slope is too steep to retain sediment. (Gulluly, 1968)

*a. Overview of the Northeast Gulf of Mexico*

The northeast Gulf of Mexico encompasses both the Panama City Shelf and the Mississippi-Alabama Shelf. Barrier islands and lagoons are nearly continuous along its shoreline from the Mississippi Delta continuing all the way to the Florida Peninsula, extending for 400 km. The sands of the barrier island-lagoon complex and adjacent beaches are quartz-rich. They are composed of clean, fine to medium-grained sand (Coleman et al., 1991).

These sands are a part of the MAFLA sand sheet, a clastic sand body which extends west of Cape San Blas to the Mississippi River, grading westward to the muds derived from the Mississippi River (Doyle and Sparks, 1980). The shelf is characterized by a relict topography covered by a thin sand and mud sheet.

Figure 22 illustrates the broad suite of surface sediments found along the northeast Gulf of Mexico (Coleman et al., 1991). The compositional makeup of these regions is displayed in Figure 23.

Apart from this sand sheet, the two regions differ considerably, from the relatively invariant West Florida Shelf to the complicated Mississippi-Alabama Shelf that is influenced by the Mississippi River. Both areas will be discussed below after first addressing the Mississippi delta and its impact on the shelf composition of the Gulf of Mexico.

*b. Mississippi Delta*

The Mississippi River delta is the major mode of sediment transport and deposition responsible for the huge volume of sediment found in the Gulf of Mexico

basin (Coleman et al., 1991). The sediment input to the delta is approximately  $2.7 \times 10^7$  tons/year ( $2.4 \times 10^{11}$  kg) (Johns, 1992). It is one of the world's largest deltas, with a coverage of 28,600 km<sup>2</sup>, with 4,700 km<sup>2</sup> (16%) being submerged. The subaqueous portion of the Mississippi River delta plain consists of the area of the Gulf of Mexico offshore of the Mississippi River delta, below low tide level, that actively receives riverborne sediments. During times of high river discharge, rapid movement of the delta is common, causing the delta lobes to move considerably over time as shown in Figure 24.

The Mississippi River carries little coarse sediment; the flood plain is chiefly composed of silt and fine sand (Gilluly et al., 1968). The sediment laden fresh riverwater discharges into the Gulf of Mexico and spreads as a buoyant plume. With increasing distance from the mouth, water velocity decelerates and the coarser sediments are rapidly dropped out of suspension. Farther offshore deposition of fine sands, silts and minor amounts of clay forms takes place. Farther seaward, deposition is characterized by the presence of fine-grained clays; this region is referred to as the prodelta. As these marine sediments are rapidly deposited and are unconsolidated at all distances from the source, excess pore water pressures exist. (Coleman et al., 1991) Figure 25 illustrates the sedimentation pattern of the Mississippi Delta.

Areas in the immediate vicinity of the deltas receive large volumes of sediment, whereas regions removed from the site of active sedimentation accumulate only thin layers of riverine sediment (Coleman et al., 1991). As the regions of the delta lobes have changed with time, location of active sedimentation has also changed with time.

c. *Panama City Shelf*

The Panama City Shelf is the eastern half of the MAFLA sand sheet. The clean quartz-rich sands here are referred to as the Cape San Blas sand facies (as illustrated in Figure 22) and are typically 2 to 10 m thick (Briggs, 1994). Within this sand sheet, linear shoals are present, probably representing relict nearshore topography (the beach and barrier system). Small bedforms actively migrate on the shelf, which indicates modern-day reworking of these relict topographic features. (Coleman et al., 1991)

Along the Panama City Shelf, variations in sediments tend to parallel the adjacent coastline and shelf edge (Coleman et al., 1991). As Figure 22 illustrates, the shelf adjacent to Panama City shows limited variation. The quartz rich sand of the Cape San Blas sand facies dominates the shelf, then transitions to the outer rim of the northwest Florida shelf which consists of a lime-mud facies, a mixture of calcium carbonate, quartz and terrigenous clays. The transition zone, consisting of calcareous muddy sands and silts, separates the sand facies from the lime-mud facies (Coleman et al., 1991). Doyle and Sparks (1980) state that the transition zone also contains shell.

The relatively large, flat expanse of the sand sheet is essentially of uniform sediment characteristics. These sediments are moderately to poorly sorted fine to coarse sands (Briggs, 1994; Fleischer and Sawyer, 1999). Only slight variations in sediment properties have been noted due to the bottom stirring associated with the passage of a hurricane. For example, after Hurricane Earl a discontinuous layer of soft mud covering most bedforms was noted, predominantly located in bedform troughs.

The mixture for the facies is 90% terrigenous sand and 10% carbonate sand on the Cape San Blas sand facies. The average mean grain diameter is 0.165 mm with almost no sediment coarser than 2 mm, and classified as mostly fine to medium grained with some coarse sand (Ludwick, 1964).

Briggs (1994) examined five experimental sites in the Gulf of Mexico for sediment properties. One site was located on the shelf adjacent to Panama City in 34 m of water. He found that the compressional wave velocity ratio, attenuation, porosity and mean grain size exhibited relatively low variability when compared with the other experimental sites. Figure 26 displays the vertical distribution of sediment geoacoustic properties for the core samples collected from the Panama City site.

Values of sediment porosity averaged 39.0% and ranged from 34.6 to 42.5%, decreasing with depth. Little depth dependence in mean grain size was observed with most phi values ranging from 2.3 to 2.8. The mean compressional wave speed ratio ( $C_{\text{sediment}}/C_{\text{water}}$ ) was 1.113, with a coefficient of variation of 0.87%. This variation is small compared with other compressional speed ratios, even other sandy sites. The only discernible trend in the sediment sound speed ratio was a slight increase from the surface to a depth of 4 cm, then remaining constant thereafter. The final panel of Figure 26 shows values of sediment compressional wave attenuation, which averaged  $0.58 \text{ dB m}^{-1} \text{ kHz}^{-1}$  and ranged from  $0.42$  to  $0.98 \text{ dB m}^{-1} \text{ kHz}^{-1}$ . The variability of attenuation values at various depths in the sediment was relatively low and caused by the presence of buried mollusk-shell fragments. (Briggs, 1994)

The West Florida lime-mud facies is located on the continental shelf off the extreme western Florida coast seaward of the 80-90 m depth contour, as illustrated in Figure 22. The sediment comprises of a mixture of calcium carbonate, quartz and clay minerals in two distinct combinations (Figure 23). One is 4% terrigenous sand, 21% carbonate sand and 75% silt and clay, where the other is 10% terrigenous sand, 50% carbonate sand and 40% silt and clay. The average median grain diameter of the sediment is 0.050 mm. (Ludwick, 1964)

*d. Mississippi-Alabama Shelf*

Sediments on the Mississippi-Alabama shelf vary significantly spatially. Grain sizes vary from the clay-rich, fine-grained sediments associated with the Mississippi River delta complex to the coarse-grained shell sediments found on the eastern shelf (Kennicutt et al., 1995). This is illustrated in Figure 22 with the sediment composition in Figure 23.

The sound and bay deposits are an almost unified body of silt and clay sized particles. The riverborne sediments are deposited behind the barrier islands in natural settling basins. Tidal currents move the unsettled sediments through the passes between the islands where they are then deposited. The bulk of the fine sediment is deposited in water less than 18 m deep and in a zone about 11 km wide to the south of the islands. The median grain diameter of the sound and bay deposits was found to be 0.002 mm, with 5% terrigenous sand and 95% silt and clay. (Ludwick, 1965)

The barrier islands, lagoons and beaches, are quartz-rich as previously discussed. They are well-sorted, medium-grained particles. The diameter of the coarsest

grain is on the average 2.0 mm, with the maximum found to measure 7.0 mm. The northern boundary of this deposit is in contact with the sound and bay silty clays. For the most part, this contact (boundary) is well defined and the transition zone is less than half a kilometer. The contact between the barrier island sands and the offshore silty clays that are flushed between the islands is less clear and expected to inter-leave. (Ludwick, 1965)

The Mississippi-Alabama sand sheet, with the same quartz rich sand as found off the Panama City shelf, is the most extensive component of the mineral suite. As with the Florida shelf, the sediment variations run parallel to the Mississippi-Alabama coastline and shelf edge in the eastern portion of this region beginning at the DeSoto Canyon. As the Mississippi Delta is approached, this trend changes dramatically, with the sediment variation on the shelf running parallel to the Louisiana coast, now perpendicular to the Mississippi-Alabama coast and shelf edge, and the sediments become more variable. The sand fraction decreases rapidly west of Mobile Bay (Doyle and Sparks, 1980).

The modal mixture for the sand facies is 93% terrigenous sand and 7% carbonate sand. The average median diameter is 0.180 mm, or fine sand, and there was very little sediment coarser than 2 mm in this facies. Near the southern edge of this sand sheet, pebbles ranging in size from 2 to 15 mm were observed in silty and clayey sands. (Ludwick, 1965)

Offshore of Mississippi and Alabama a lime-mud facies exists, and is comprised of two parts; the reef facies and the inter-reef facies. Great variability is present from place to place with two dominant compositions. One is carbonate sand



referred to as the reef phase (20% terrigenous sand, 70% carbonate sand and 10% silt and clay) and the second a sand-silt-clay mixture referred to as the inter-reef phase (30% terrigenous sand, 20% carbonate sand and 30% silt and clay). The median grain size in the reef facies is 0.710 mm with 19% of the sediment coarser than 2 mm. The median grain size of the inter-reef zone is 0.120 mm with only 4% coarser than 2 mm. Molluscan debris is present in the inter-reef areas, with sediments coarser than 4 mm. (Ludwick, 1964) It is in the region of the reef facies that the carbonate mounds occur as discussed in USGS Report (1) (1998).

These calcareous pinnacles are not similar in character to other pinnacles observed in the northwestern Gulf of Mexico, which are often salt or shale diapirs. Instead, they are calcareous reefs, no longer actively growing. The sediments in this region are generally mud and sand in varying amounts (as described in the preceding paragraphs), with a general trend of increasing percentage of mud sediments proceeding westward across the region. There are also varying amounts of carbonate debris made up of shell, other fragments from infauna and occasionally carbonate fragments from the mounds. (USGS Report -1, 1998)

The Mississippi-Alabama Shelf is not directly influenced by the Mississippi Delta, which deposits most of its load directly south to the shelf edge or carried westward. However in the westernmost portion, the shelf was previously a delta and is now a pro delta, which means that it receives fine-grained clays.

As noted earlier, this western portion is more variable, with three distinct sediment types identified:

- (1) the St. Bernard prodelta facies;
- (2) the Chandeleur (sand) facies; and
- (3) the Mississippi prodelta facies.

The St. Bernard prodelta (seaward of the Chandeleur Islands) consists of silty clay; the Chandeleur sediments are sand and the Mississippi River prodelta sediments are terrestrially derived organic-rich clay and silt (Kennicutt et al., 1995).

The sediments of the Chandeleur deposits are chiefly fine-grained, well-sorted sands, being 94% terrigenous sand and 6% carbonate sand. Average median grain-diameter is principally 0.11 mm, with the largest grain size 1.1 mm. The transition zone between this deposit and the St. Bernard prodelta muds represents a mixing of the two deposits, averaging between 5 to 7 km in width. (Ludwick, 1964)

The sediments of the St. Bernard prodelta facies change rapidly eastward as they approach the sand sheet (Doyle and Sparks, 1980). They are mainly mixtures of silt and clay-sized particles. The modal mixture is 1% terrigenous sand, 4% carbonate sand and 95% silt and clay. There is a transition zone to the east between this deposit and the Mississippi-Alabama sand facies, and the contrast between the two deposits is distinct, one being a silty clay and the other sand. The transition zone is a mixture of both sediments. It varies in width, averaging approximately 11 km. (Ludwick, 1965)

The area immediately to the east of the Chandeleur Islands has several small salt diapirs near the shelf edge (USGS Report (1), 1998).

THIS PAGE INTENTIONALLY LEFT BLANK

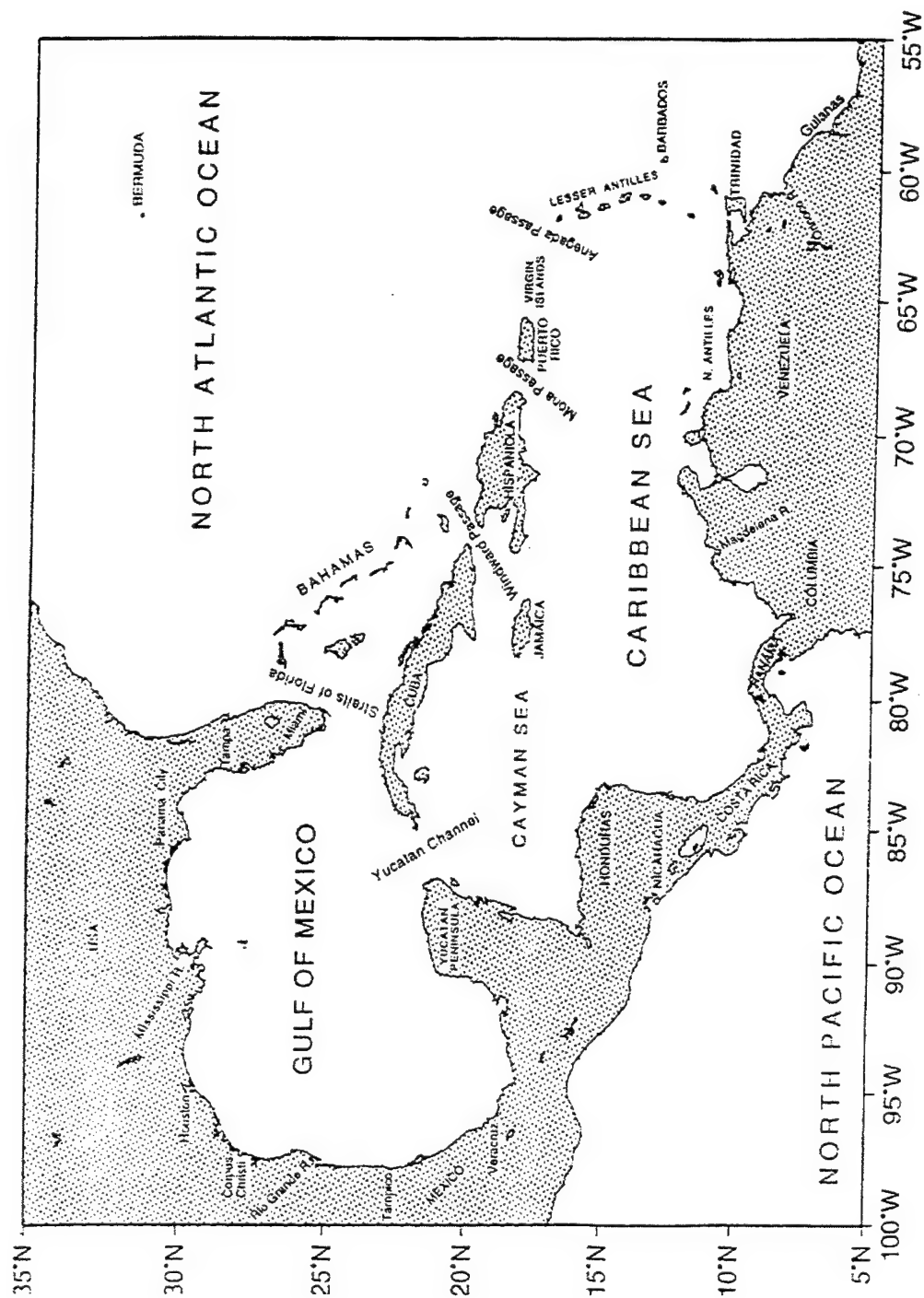


Figure 11. The Intra America Seas (IAS) are the semi-enclosed waters of the western tropical North Atlantic (from Mooers and Maul, 1998).

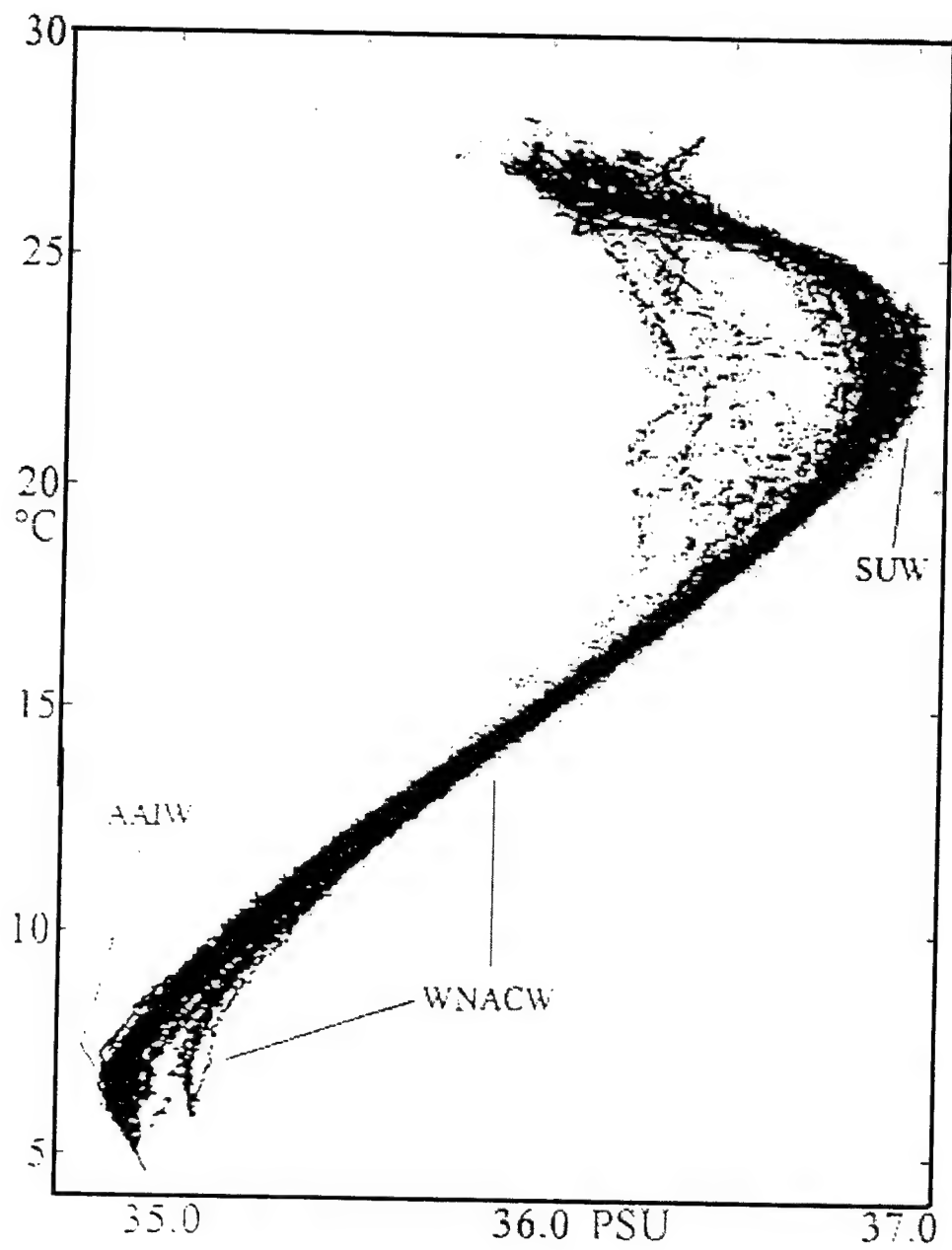


Figure 12. Temperature-salinity diagram that describes the water masses of the IAS (from Mooers and Maul, 1998).

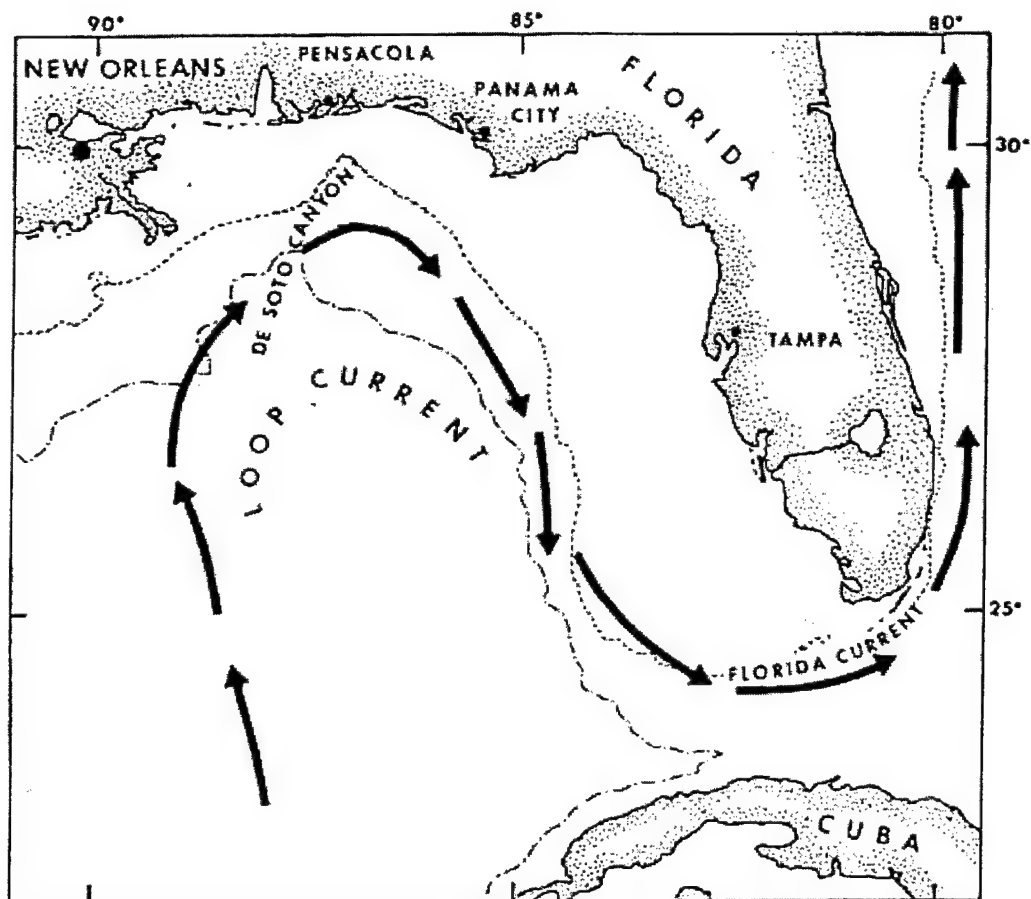


Figure 13. The mean path of the Loop Current is illustrated here. Its northern extent is variable and can in fact intrude onto the continental shelf as occurred in February 1977. (After Huh et al., 1981)



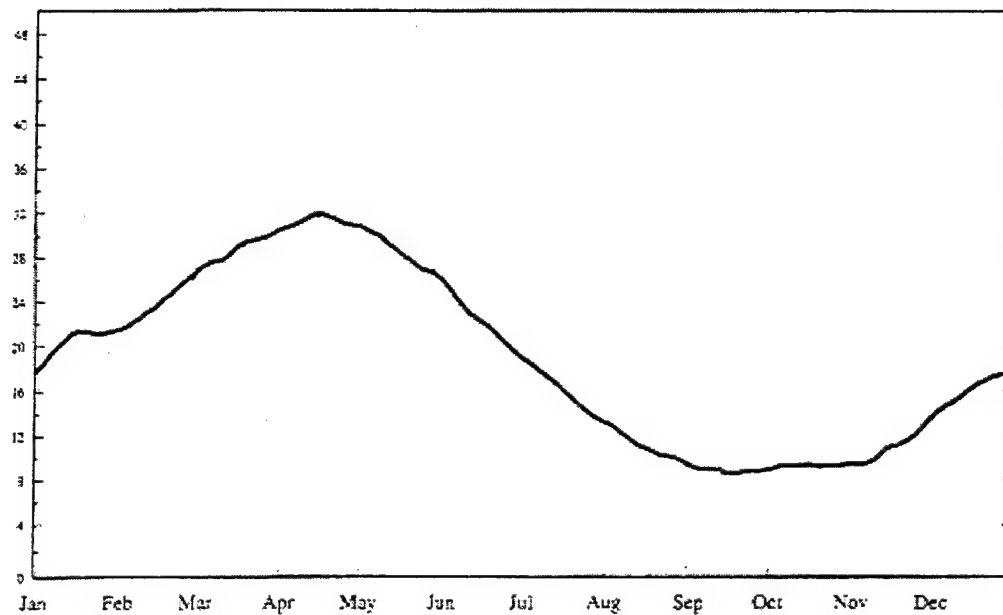


Figure 15. The sixty-four year average river discharge from the Mississippi River is a maximum in spring and a minimum in Fall ( $\times 1000 \text{ m}^3 \text{ s}^{-1}$ ) (after Li et al., 1997).



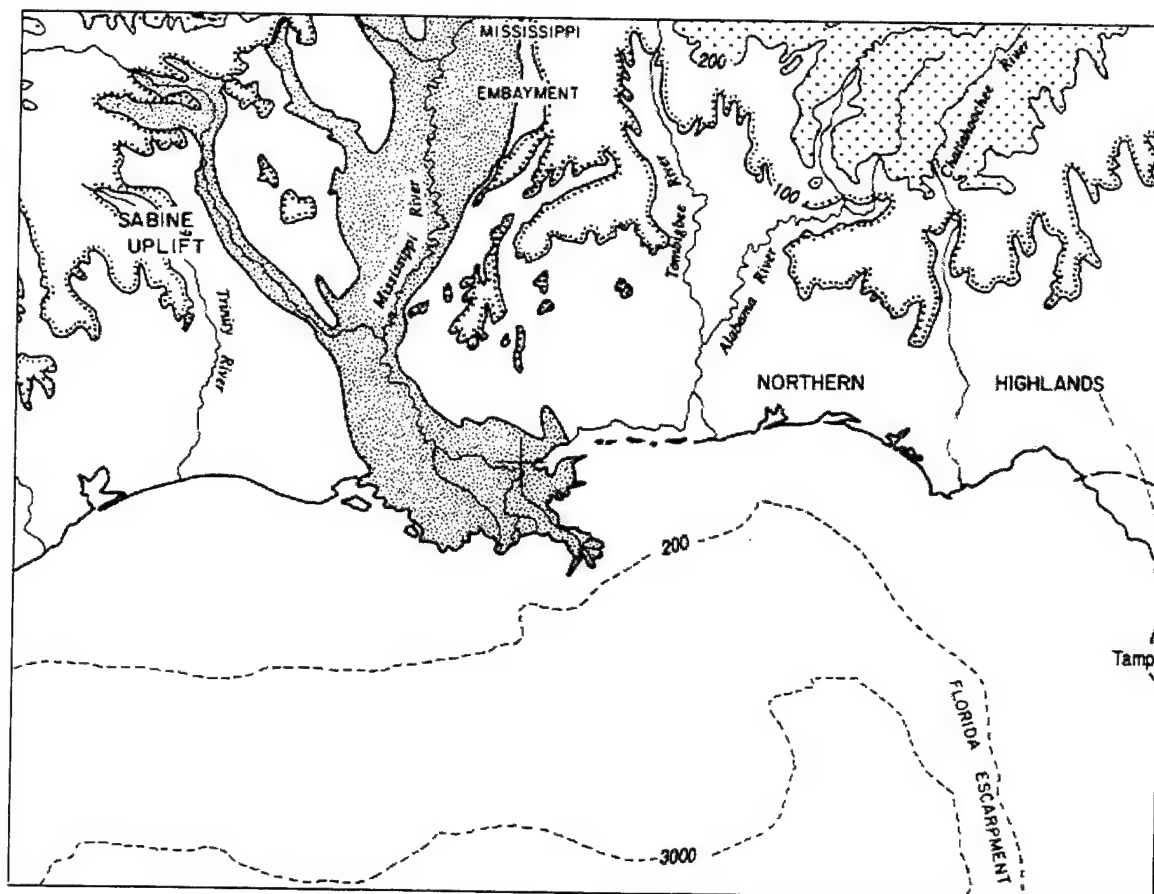


Figure 16. The Mississippi River's outflow is onto the Mississippi-Alabama shelf to the east and the Louisiana-Texas shelf to the west. The shaded region indicates the flood plains of the Mississippi and its tributaries. (After Bryant et al., 1991)

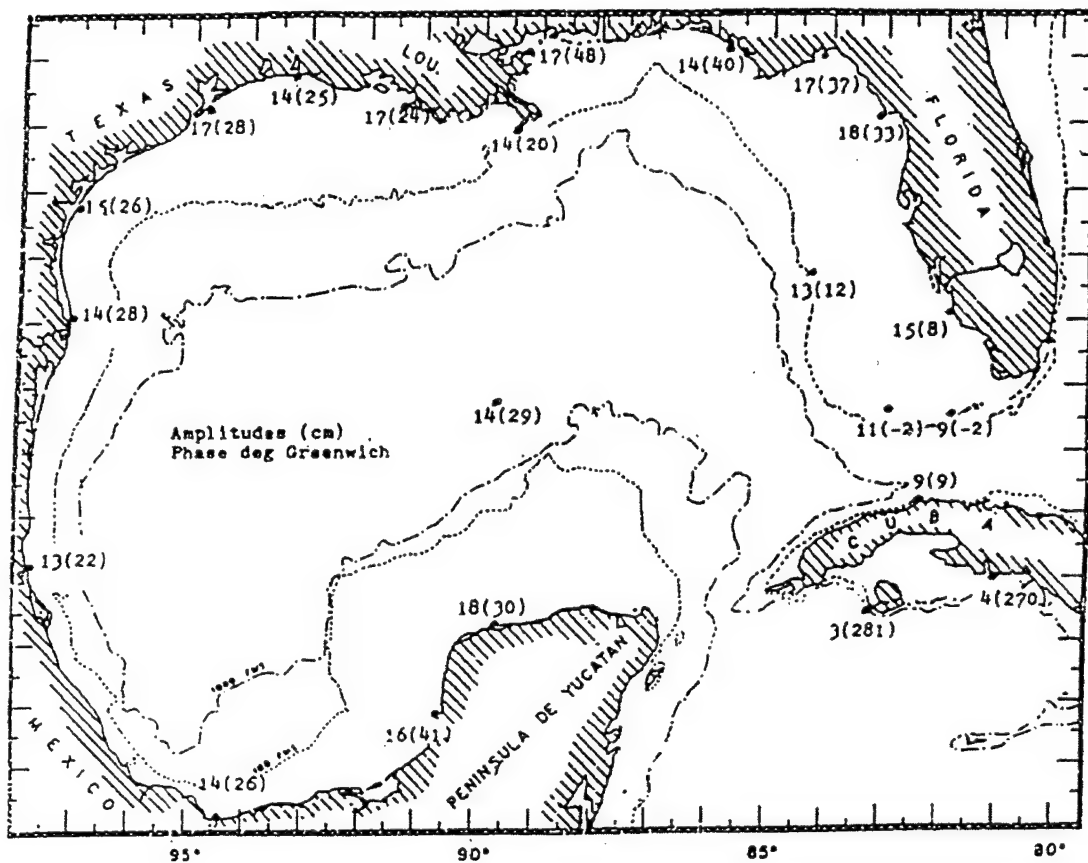


Figure 17. The K1 tide displayed here dominates the diurnal tide along with the O1 constituent. The amplitude is in cm and the Greenwich phase angle in degrees in parentheses (after Clarke, 1994).

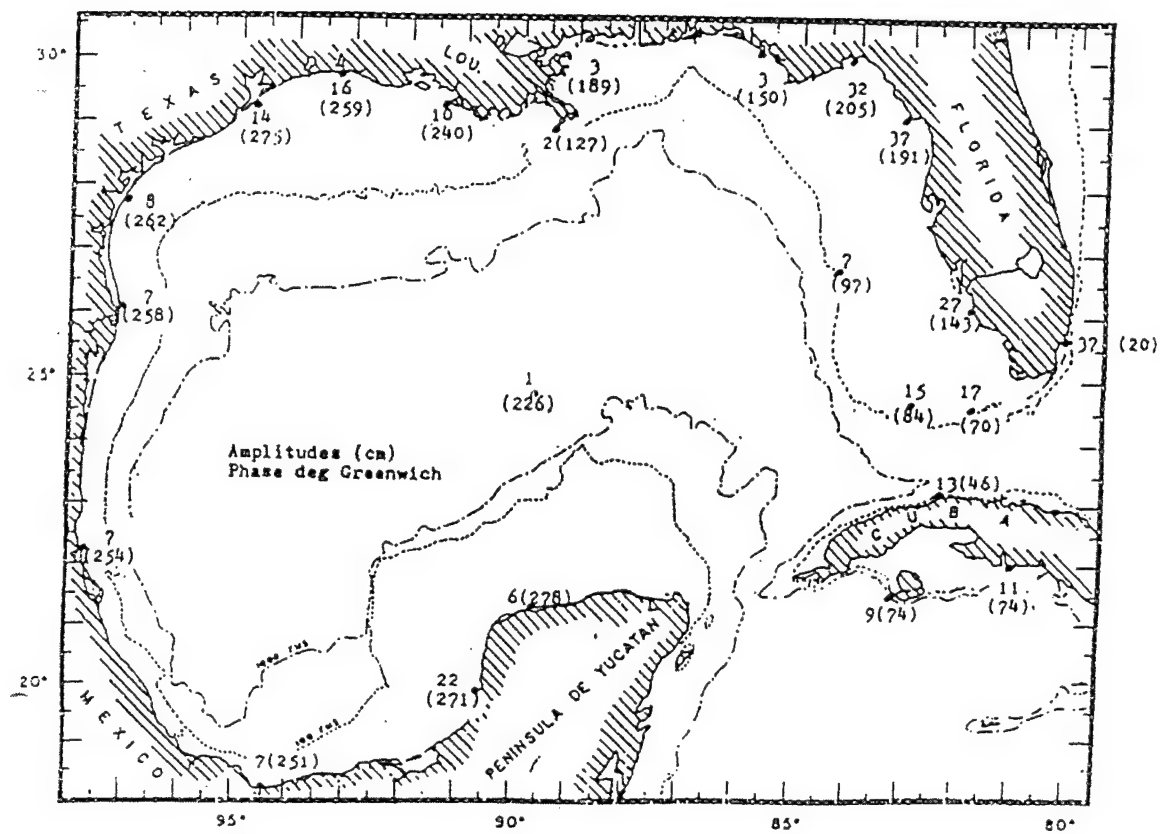


Figure 18. The main semi-diurnal tide is the M2, with amplitude in cm and Greenwich phase angle in degrees in parentheses (after Clarke, 1994).

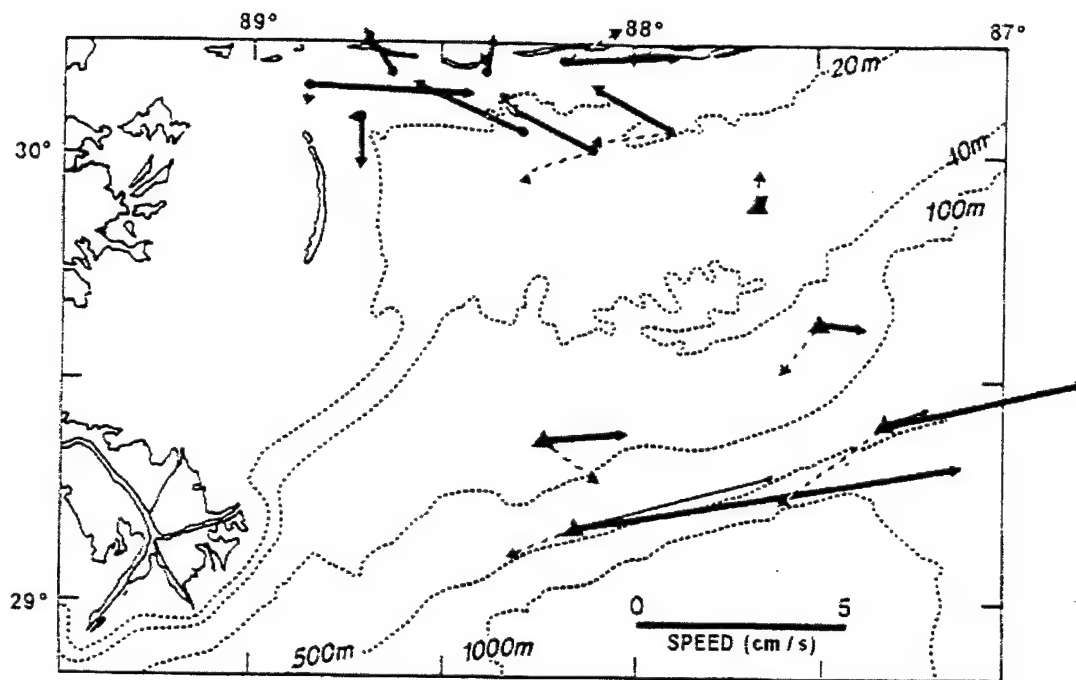


Figure 19. Observed mean current vectors over the Mississippi-Alabama shelf indicate that the mean flow is to the west, most notably on the outer shelf. Thick arrows are near surface currents, thin arrows are mid depth vectors and dashed arrows are near bottom currents, all in cm/s. (After Boicourt et al., 1998)

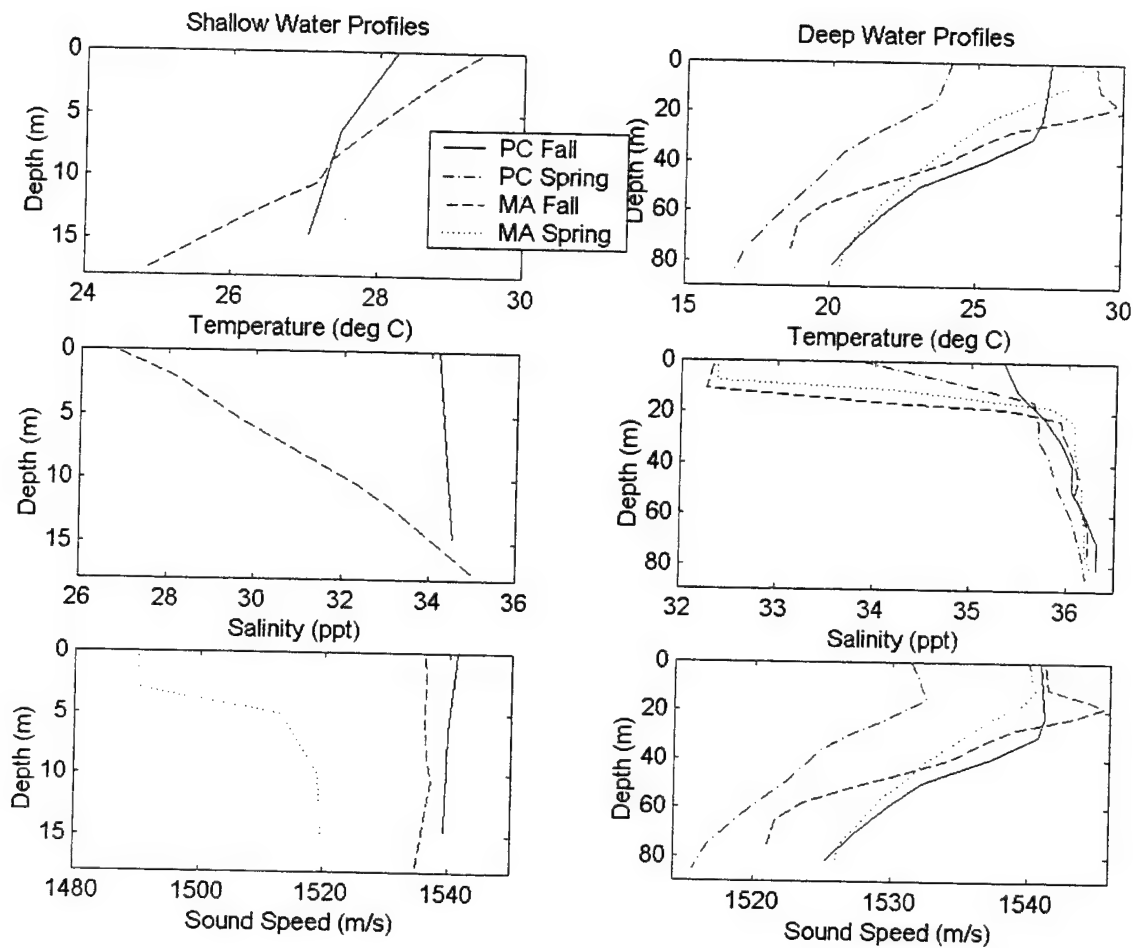


Figure 20. The shallow and deep water profiles for the two regions over the two seasons are displayed here. For the shallow region, temperature, salinity and sound speed profiles for the Panama City Shelf and the Mississippi-Alabama Shelf in fall are displayed, with an additional SSP for Mississippi-Alabama in spring for a flood event. For the deep water region, all three profiles have the Panama City Shelf and the Mississippi-Alabama Shelf in both fall and spring.



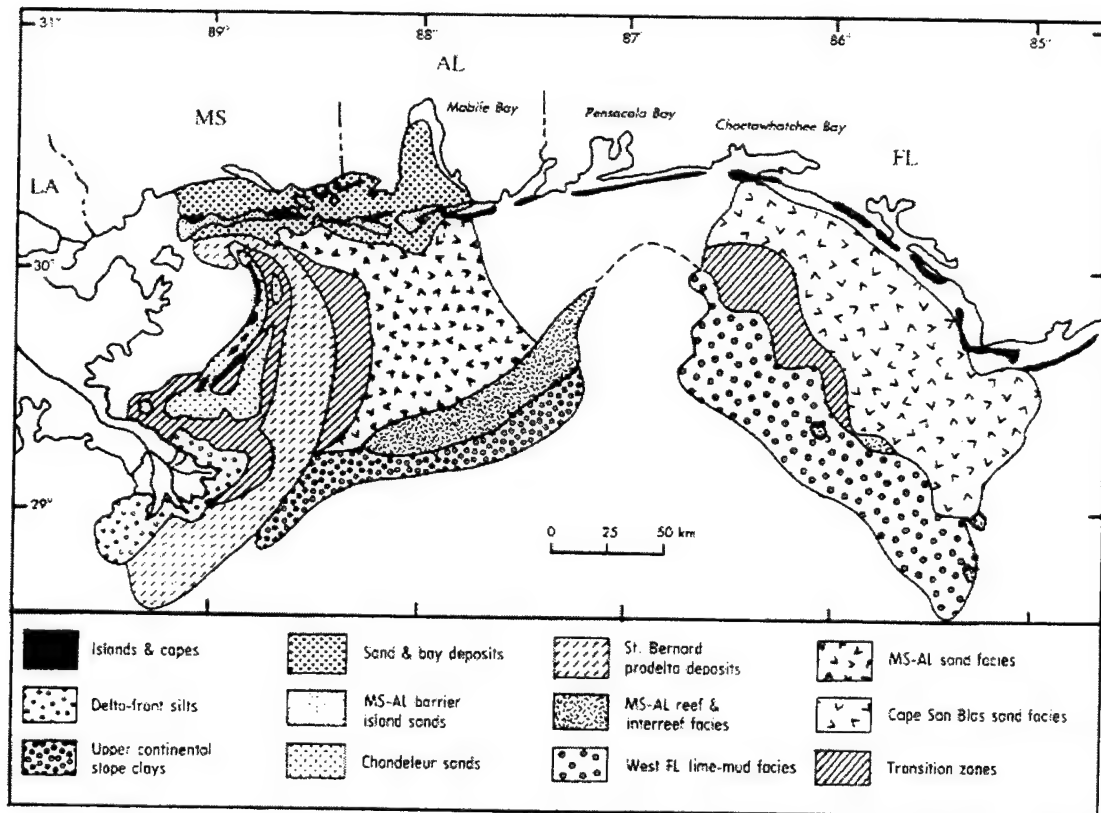


Figure 22. The surficial sediments on the Florida-Mississippi-Alabama shelf are illustrated here. The sediments, from the Mississippi Delta east to Cape San Blas, are described as a number of clastic sand, mud and transitional facies (from Coleman et al., 1991).

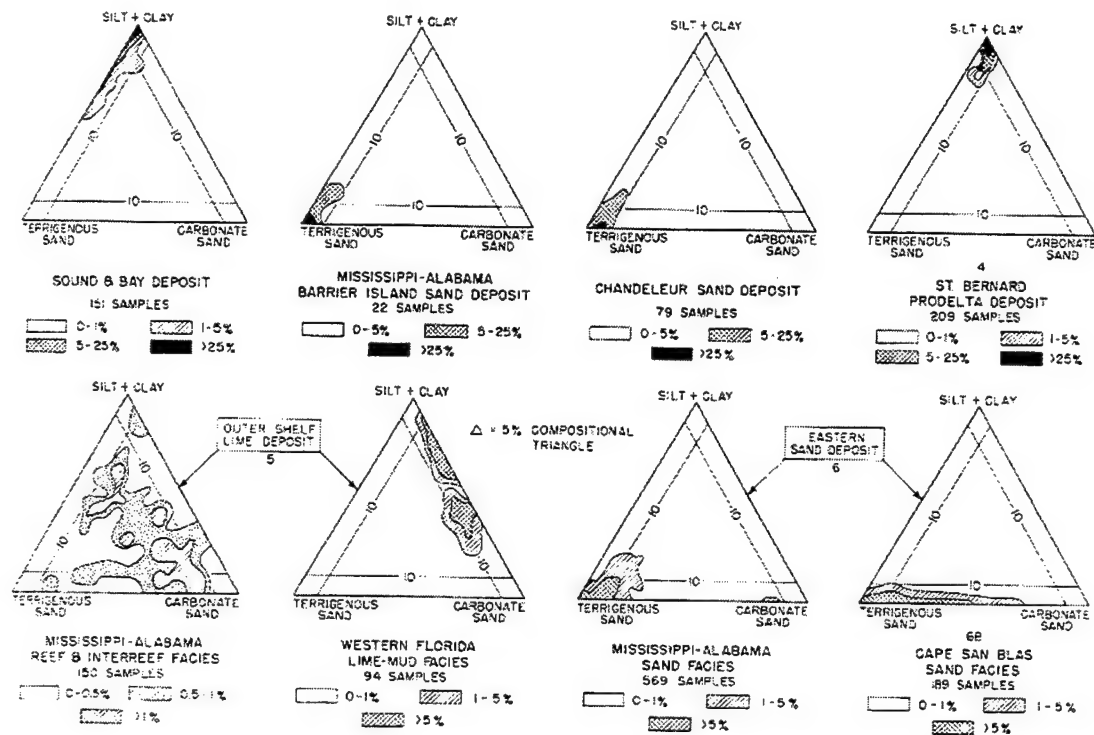


Figure 23. Triangular diagrams for the 8 deposits from Figure 22 are shown here. The three poles are terrigenous sand, carbonate sand, and silt and clay. The frequency of occurrence in percent per 5 percent compositional triangle is illustrated within the shaded region. (After Ludwick, 1964)



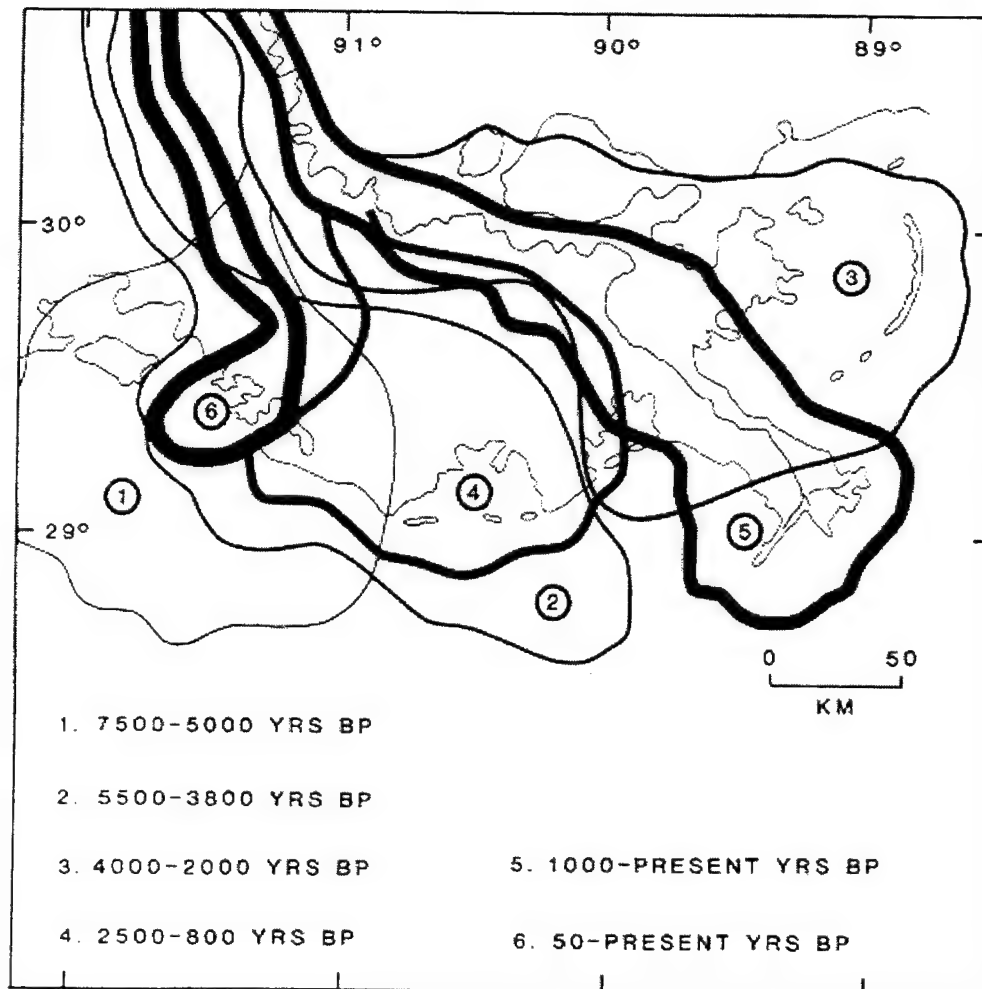


Figure 24. The location of the delta lobes of the Mississippi River delta plain has migrated over time (after Coleman et al., 1991).

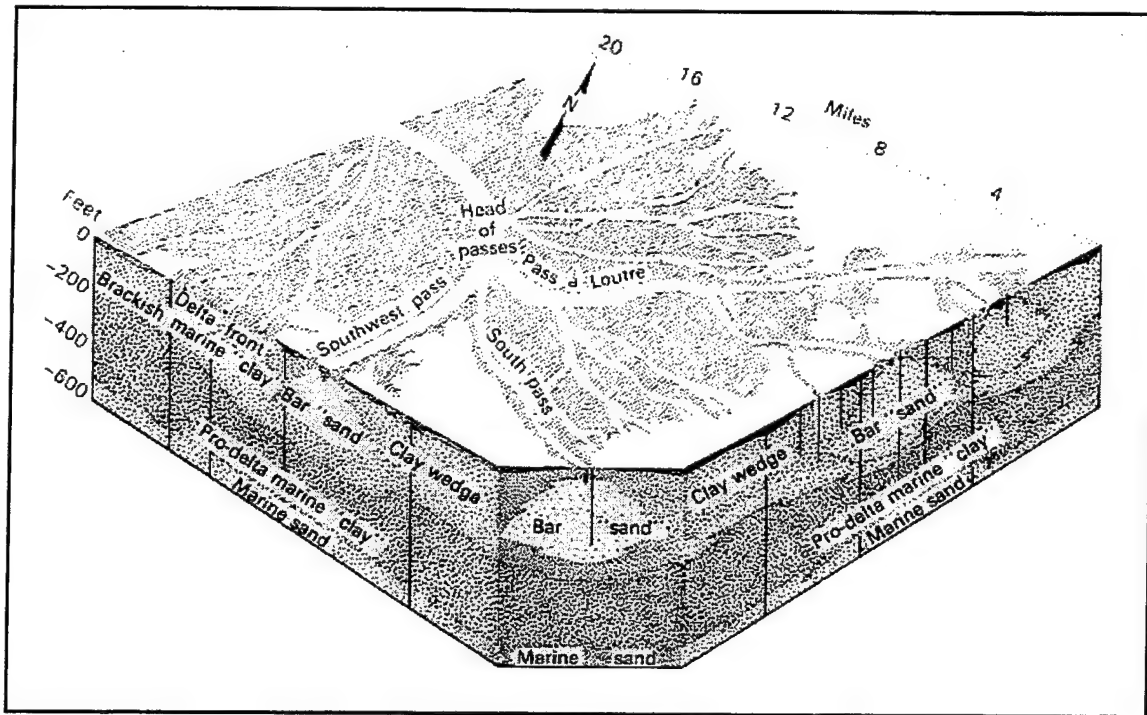


Figure 25. The coarsest material settles out first and nearest to the channel, followed at greater distances by finer and finer material (from Gulluly et al., 1986).

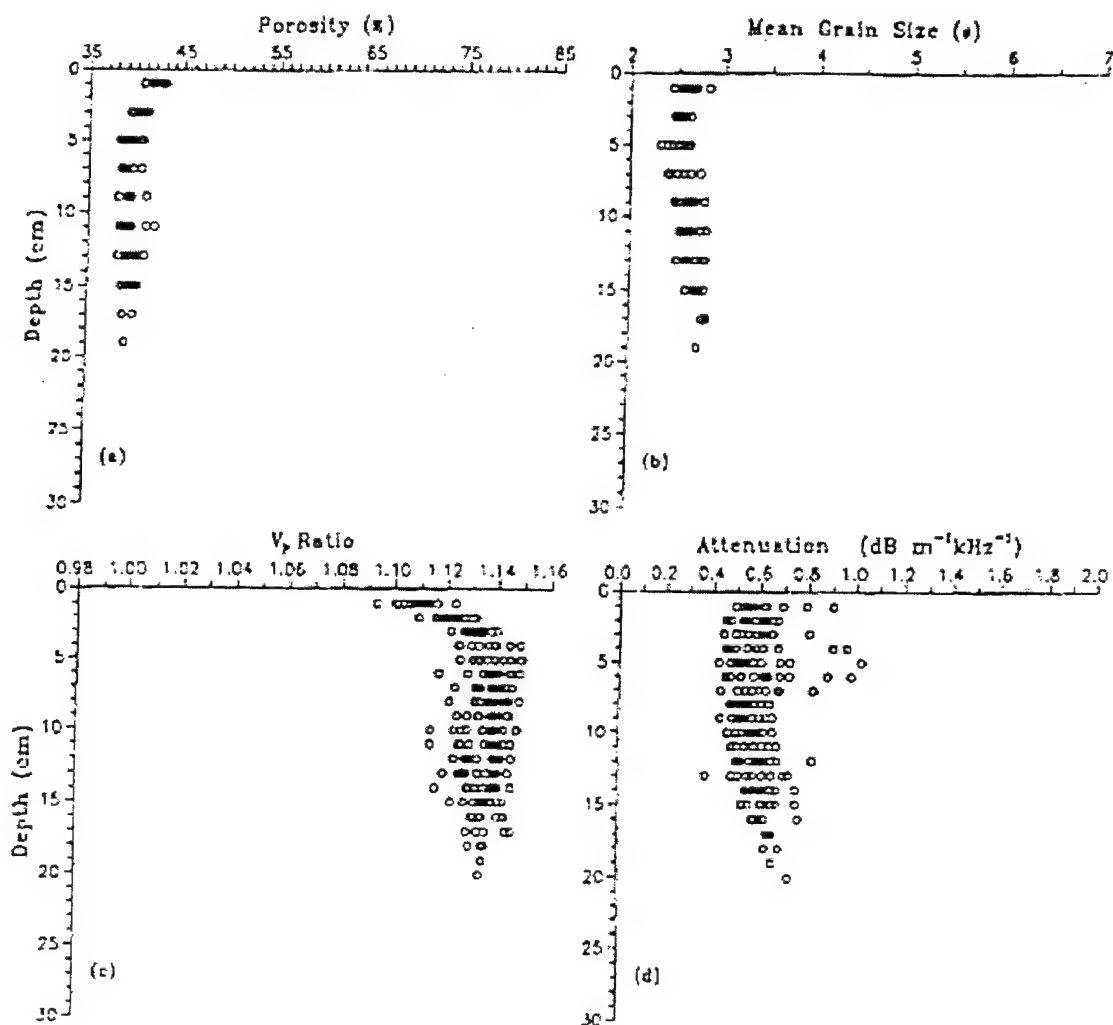


Figure 26. Profiles of geoacoustic properties for a site off Panama City show very little variability with depth. Displayed here are (a) porosity, (b) mean grain size, (c) sound velocity, and (d) attenuation. (From Briggs, 1994)

### **III. MODEL AND SONAR PARAMETERS**

#### **A. SONARS AND MINES**

This study will examine the performance of two sonars; the RAN Type 2093 and a generic USN mine warfare sonar, both discussed below. A comparison between the two sonars (at similar frequencies) will be made using the model PC SWAT.

##### **1. RAN Type 2093**

The parameters and information for the Type 2093 have been provided by Stuart Anstee of the Defence Science and Technology Organization (DSTO), Australia. The frequencies, beamwidths and bandwidths have been modified to permit an unclassified analysis.

The Type 2093 is an active, high frequency, forward-looking sonar. It operates at two different frequencies for search and for classification, denoted VLF and LF for search, HF and VHF for classification. For this study, only the search frequencies are examined. The 2093 was initially intended as a deep-water variable-depth sonar that could find very large anti-submarine mines at long distances. In such cases, detection ranges of over a kilometer might be achieved with the VLF mode, where the closest distance of safe approach to the newer anti-submarine mines was of the order 600 m. The concept of the VLF mode is considered, to some extent, redundant in normal, relatively shallow water minehunting, where the LF mode is the frequency more commonly used.

The sonar can be operated in the hull-mounted mode, where the source depth is 3 m, or at variable depth. The frequencies are 40 kHz (VLF) and 90 kHz (LF) with each

employing a bandwidth of 5 kHz, a pulse length of 0.2 millisecond and a vertical beamwidth of  $50^\circ$ . The 40 kHz mode operates with a source level of 205 dB; for the 90 kHz mode the source level is increased to 210 dB. The sonar parameters to be used are listed in Table 6. The sonar performance at two frequencies will be compared.

## **2. USN Generic MIW Sonar**

The sonar parameters used are representative of a generic MIW sonar proposed to model the performance of USN MIW sonars. It is an active, high frequency, forward-looking sonar. It can be operated in the hull-mounted mode, where the depth of source is 5 m, or at variable depth. The frequency is 35kHz for search with a bandwidth of 5kHz, the source level is 221 dB, the pulse length is 1.0 millisecond and the vertical beamwidth is  $9.8^\circ$ . The parameters to be used are listed in Table 6.

## **3. Mines**

Chapter I outlined the current mine threat. For the purpose of this study, only moored and bottom mines will be considered. The more modern moored mines are generally found in deep water (water which is deeper than 100 m) or in the deeper range of shallow water. Moored mines can be found in shallower waters, however it is less common. More often bottom mines are deployed here as they become less effective as the water depth increases (Lathrop, 1995). Thus, moored mines will not be considered in the shallower regions of the model runs. For bottom mines, the majority of the model runs will be with the bottom mines "proud" on the bottom, not buried, as the hard sand bottom of the Panama City Shelf does not permit the burial of mines. Buried mines will be modelled in regions where clay sediments are found and where burial is likely, i.e., sounds

sounds and bays and the St. Bernard prodelta facies. The dimensions of the target mines modelled are typical of a modern mine and are 1 m in length, 0.3 m in radius with a target strength of -19 dB.

## **B. MODELS**

The primary MIW performance model used for this study is PC SWAT (Personal Computer Shallow Water Acoustic Tool-Set) version 6.0. The performance predictions of this model will be compared to the HODGSON model, which will be used for a smaller number of runs.

Because this study compares two propagation loss models, it is important that intercomparisons are made using the same input parameters and the same algorithms to calculate the results. Keeping things as similar as possible ensures a more legitimate comparison between the models. This was, unfortunately, not entirely achieved in this study, with some of the input parameters differing and the embedded algorithms differing between the two models. To understand these algorithms will assist in the comparison, providing some guidance on the results.

### **1. PC SWAT**

PC SWAT, as its name indicates, is designed for use in shallow water and very shallow water regions. It is intended to simulate the performance of MCM detection sonars, whereas its counterpart SWAT is used for performance analysis of even higher frequency classification sonars. PC SWAT uses a Gaussian beam propagation model

based upon the GRAB (Gaussian Ray Bundle) propagation model to estimate the transmission loss component of the sonar equation.

Weinberg and Keenan (1996) discuss the GRAB model. It is a high frequency, range dependent, propagation loss model for use in shallow ocean environments. The model is based on ray tracing, Gaussian ray bundles and virtual rays. The ray tracing determines ray trajectories inclination angles and losses due to volume attenuation and the ocean boundaries; the Gaussian ray bundle technique replaces the classical spreading loss of geometrical acoustics; and virtual rays are the unfolding of the contributions from the tails of bundles that extend into the ocean bottom.

Weinberg and Keenan (1996) compared propagation loss predictions with those of various standard models at lower frequencies. They assumed that if Gaussian ray bundles compared well at lower frequencies, then they should perform well at higher frequencies as ray approximations improve. In comparison with parabolic equation (PE) models, they found the GRAB method to be valid over a large band of frequencies. In comparison with the Navy standard PE v3.4 at 25 Hz and 10 kHz, unexpectedly good results were achieved for GRAB, which was not designed for frequencies as low as 25 Hz. A second comparison was made with the academic model EFEPE. The comparison conducted was at 1000 Hz, due to the high-frequency computation requirements of EFEPE. The assumption was made that the essential physics at 1000 Hz was the same as at 20 kHz (with differences being attributed to volume and boundary losses whose accuracy is independent of the propagation model). The results showed exceptional agreement between the two models, with tests conducted over a variety of bottom types.

To assess sonar performance PC SWAT employs various options that can be run to represent different types of measures of effectiveness. For the purposes of this study two options from the Global menu were examined, one way TL and SNR (signal to noise ratio). The SNR option calculates the SNR, which takes into account all parameters in the sonar equation including sonar parameters, reverberation, attenuation, noise, and target parameters. In plotting SNR, various parameters can be displayed, including signal level, bottom RL, surface RL, volume RL, ambient noise and the SNR.

Parameters of the model that are to remain constant for all runs are listed in Table 7. Of these parameters, a number of algorithms were chosen to calculate the particular parameter, some of which are outlined in the Users Manual (Sammelmann, 2000). Of most significance to this study are the algorithms for bottom loss and bottom scattering, both are discussed the APL-UW TR 9407 (1994).

For bottom loss, which is a major component in the TL calculations, the APL/UW model is used. The bottom loss model is a relatively simple model designed to estimate the forward reflection loss associated with high frequency propagation. The model does not include gradients or layering of the bottom sediments and, as such, has no explicit frequency dependence. Figure 27 illustrates the bottom loss for a variety of sediment types from silt through rock. It is based on a limited data set from three sites (including a soft clayey bottom and a hard sandy bottom), over a frequency range of 20-30 kHz and a limited number of grazing angles (5-30° and 90°). The bottom loss curves indicate that TL increases with decreasing grain size, in agreement with the principle that small grain



sizes (i.e., mud and silts) result in increased penetration of acoustic energy into the bottom where it is attenuated and contributes little to forward propagation

For bottom backscattering, APL/UW's bistatic bottom scattering model is used. When the monostatic option is selected, as it is here, the average of the incident and scattered grazing angles is used to compute the bottom reverberation. APL/UW's bistatic bottom scattering model treats scattering as a function of two components, interface roughness and sediment volume inhomogeneity. It is a generalisation of an earlier APL/UW backscattering model updated to include more angular variables for volume scattering. In the bistatic model calculations, interface roughness dominates sediment volume scattering away from specular directions for hard (sandy) bottoms, whereas the opposite is true for soft (silt and clay) bottoms. Additionally, the scattering strength shows a peak where the angle is near incident for both bottom types due to coherent scattering occurring.

The updated model produces results similar to the earlier backscattering model and is consistent with available data for backscattering from sea floors exhibiting small to moderate roughnesses (e.g., clay, silt, sand.) Figure 28 is an example of the bottom scattering strengths for generic bottom types at 30 kHz based on the earlier backscattering model. It illustrates an increase in scattering strength with increasing grazing angle and with increasing sediment grain size or roughness scale, grading from silt to rough rock. Additionally, an increase in backscattering strength with increasing frequency is noted, a feature appropriate for sediments exhibiting small to moderate roughnesses. For the same

grazing angle and bottom type a difference of up to 3.5 dB exists between 30 and 40 kHz and up to 7 dB between 40 and 100 kHz.

## **2. HODGSON**

The HODGSON<sup>®</sup> model is the embedded range prediction and propagation loss model in WADER<sup>®</sup>, a United Kingdom (UK) program that provides global bathymetric and hydrographic data sets amongst other features to support acoustic propagation loss models.

HODGSON, as described in the WADER user guide (HODGSON, 2000), is a range-dependent acoustic ray trace propagation loss model designed for use at frequencies above 150 Hz in varying environmental conditions and does range prediction (solving the sonar equation) for active sonars. It is designed for use in both shallow and deep water.

For bottom loss in transmission loss calculations, HODGSON uses data based on the Navy standard high frequency bottom loss (HFBL) curves as displayed in Figure 29. In comparing the bottom loss predicted here with that for PC SWAT, as displayed in Figure 27, it can be seen that there are similarities in the predicted values. For example, for bottom loss curve 3 in the Navy HFBL curves compares well with the bottom loss in Figure 27 for a fine sand bottom at 50° grazing angle; both values are close to 11 dB. Similarly for the higher loss curves, the Navy HFBL curve 7 displays bottom loss of near 22 dB at 50° grazing angle and the curves in Figure 27 displays losses of 22 to 24 dB at a grazing angle of 50° for the two curves representing the smaller grain sizes, silt and sandy silt.

The following discussion outlines the method that HODGSON uses to calculate bottom reverberation as provided by John Hodgson (2000). In calculating bottom reverberation, HODGSON provides backscattering estimates for five bottom types, these being mud, sand, gravel, rock and very rough (HODGSON Engine User Guide, 2000). The first four are considered to represent acoustically smooth bottoms and, as discussed in Chapter I, a variation with frequency is expected. The algorithm used to determine the backscattering coefficient ( $S_b$ ) as a function of grazing angle ( $\theta$ , in radians) and frequency (Hz) is as follows:

$$S_b = C \times (Freq^{3.2-0.8 \times Type}) \times (10^{2.8 \times Type-12}) \times (2.53) + 10^{-4.5}$$

$$C = B \times (\sin(\theta) + 0.19)^D$$

$$B = 1 + 125 \times \exp(E)$$

$$D = Type \times \cos(\theta)^{16}$$

$$E = -2.65 \times (Type - 1.75)^2 - 50 \times (\cot^2(\theta) / Type)$$

Type = 1 – Mud

2 – Sand

3 – Gravel

4 – Rock

This algorithm is based on data gathered in the frequency range of 12.5 to 290 kHz (which covers frequencies for this study), but can be applied to a broader range, 1 kHz to 500 kHz. The fifth bottom type for reverberation is very rough, where no

frequency dependence is expected. For this case Lambert's Law is used, with the bottom roughness constant of -27 dB selected:

$$S_B = -27 + 10 \log \sin^2 \theta$$

This equation results in a similar curve but with lower backscattering values to those displayed in Figure 28 for PC SWAT bottom backscattering, for rough rock, rock and cobble strata. Values of -36 dB for a grazing angle of 20°, and -33 dB for a grazing angle of 30° determined from Lambert's Law correlate more closely with the smaller grainsize sediments in Figure 28, however this result does not impact this study as very rough bottoms are not examined.

For the four HODGSON runs using the two modes of the 2093 sonar (VLF and LF operating with a frequencies of 40 and 90 kHz, respectively), the parameters used were taken from Table 6 as applicable. Several extra or changed parameters are required for HODGSON and they are outlined in Table 8. The maximum and minimum ray angles are based on the depression angle (10° down) and the vertical receiver beamwidth (50°) for both frequencies. The pulse length is 0.01 seconds, not the much shorter pulse length used in PC SWAT, as this is the lowest value that HODGSON will accept. For the spike filter the default is on, however, it is recommended to be off for short ranges and shallow receiver depths in the WADER User Guide (HODGSON, 2000). This corresponded to PC SWAT as there is no spike filter in that model. This filter in HODGSON was developed to reduce the incidences of positive spikes on propagation loss curves, caused when the program samples the acoustic field very near a caustic. For the Figure of Merit

(FOM) calculator, the maximum frequency is 10 kHz, thus this is chosen. System Gain equals the directivity index minus recognition differential minus bandwidth correction. The recognition differential was taken as 12 dB, bandwidth correction was zero (due to being a narrowband system) and the directivity index, as defined in Urick (1983), is equal to:

$$10 \log (4*\pi/\text{solid angle}),$$

where the solid angle is the product of the horizontal and vertical beamwidths of the receiver.

### **3. Model Parameters**

Table 9 outlines the format for the series of model runs performed, displaying an entire set of runs, thirteen in all. The basis for this list is to intercompare a variety of sonar and environmental parameters to determine those variables that are most sensitive in the estimation of sonar performance. Such a study will provide guidelines governing the accuracy that input parameters such as SSP or bottom characterization must be known or measured.

The two study areas divide the runs clearly into bottom types. The Panama City Shelf sediments modelled are fine sand inshore grading to coarse sand offshore. On the Mississippi-Alabama Shelf the clay inshore transitions to the sandy outer shelf. Thus, for the purposes of the model runs, a clay bottom was used to represent the shallow depth region and in the transition zone, muddy sand was selected for the deep-water regimes. The other dominant sediment in the Mississippi-Alabama region is sand and similar results can be anticipated for the sandy regions off Panama City. The depths chosen for

the shallow water and deep water regimes are approximately the two extremes of the Shallow Water Zone.

The environment determined the depths of the sonar, with guidelines given that the Type 2093 must remain 30 m above the bottom. As such, in shallow water the hull mounted mode was selected (source depths of 3 m for the 2093 and 5 m for the US sonar), whilst in deeper water the variability in SSP and bottom type are used to determine the depth for optimum sonar performance. After some analysis of PC SWAT, a depth of 40 m was chosen, approximately mid depth in the water column. This provided best performance for both moored and bottom mines and ensured the sonar was below the mixed layer in all cases, avoiding surface features or cross-layer situations that could deteriorate performance.

Because FBE-H was conducted from mid August to mid September, the majority of the model runs were conducted using SSPs indicative of the region in fall. To determine the seasonal influence of the SSP on sonar performance, the deeper runs were conducted using a spring profile. This is the season that varies the most from the fall time frame, with the deep water runs only chosen as the shallow water profiles remained well mixed year round. The summer and winter profiles are remarkably similar in shape to the fall profiles, only being altered in their absolute temperature values. Additionally, to model the effects of high river runoff (most common in spring), the runs on the Mississippi-Alabama Shelf in the shallow region were conducted with a SSP indicative of these conditions. All SSPs are displayed in Figure 20.

The mine targets modelled are as defined previously, with bottom mines examined in all regions, moored mines only in the deeper regions and buried mines in the clay regions where burial is likely.

From these options, a total of thirty-nine model runs were made. From the entire set of runs outlined in Table 9, runs 1 to 11 were conducted for all three sonar options, i.e., the US sonar and the Type 2093 at both frequencies, for a total of thirty-three runs. This permitted a comparison of the two sonars under varying conditions and also for two frequencies of the Type 2093, under varying conditions. Two additional runs were made using the 2093 VLF option for high river runoff conditions (12 and 13), one with the sonar in the hullmounted position, as would be used in this shallow water environment, and the second with the sonar at 10 m, below the thermocline.

A further four runs were conducted using the HODGSON model to allow comparison between the two models. These are run numbers 1, and 6 for both frequencies of the 2093 sonar.

Run numbers are of the format **model\_sonar\_number**. The variables are defined as follows:

- Model: S = PC SWAT; H = HODGSON
- Sonar: U35 = US sonar at 35 kHz;  
A40 = Australian sonar at 40 kHz;  
A90 = Australian sonar at 90 kHz
- Number: the run number listed in Table 9.

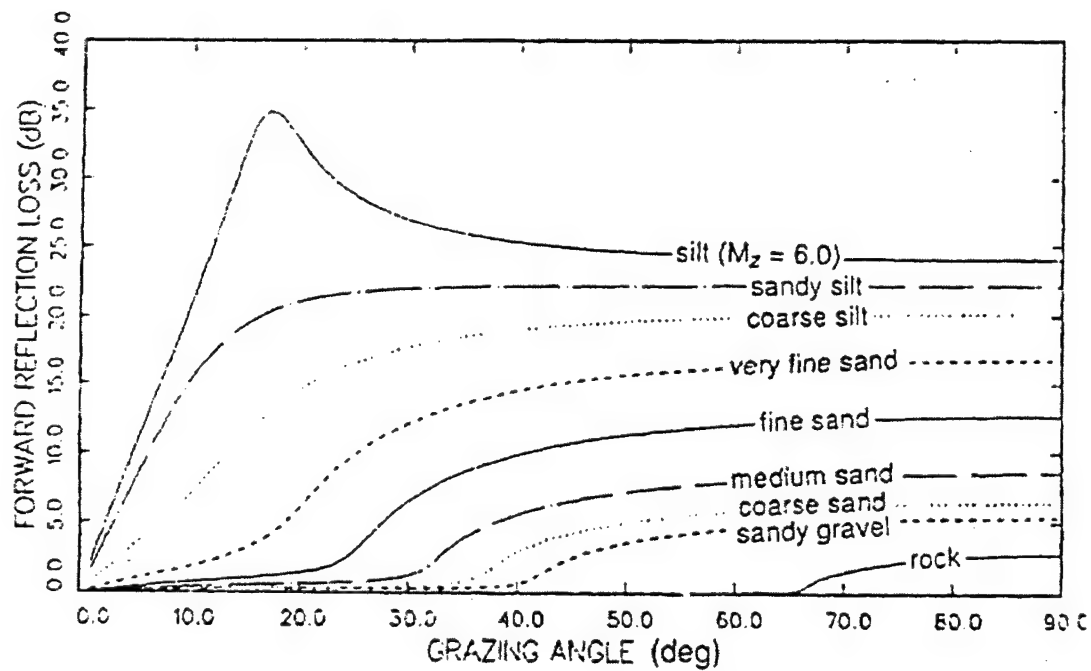


Figure 27. Curves for the bottom loss model in PC SWAT for a variety of bottom types and valid over the frequency range 20 to 30 kHz, as a function of grazing angle.  $M_z$  is grain size in logarithmic units. (From APL-UW, 1994)



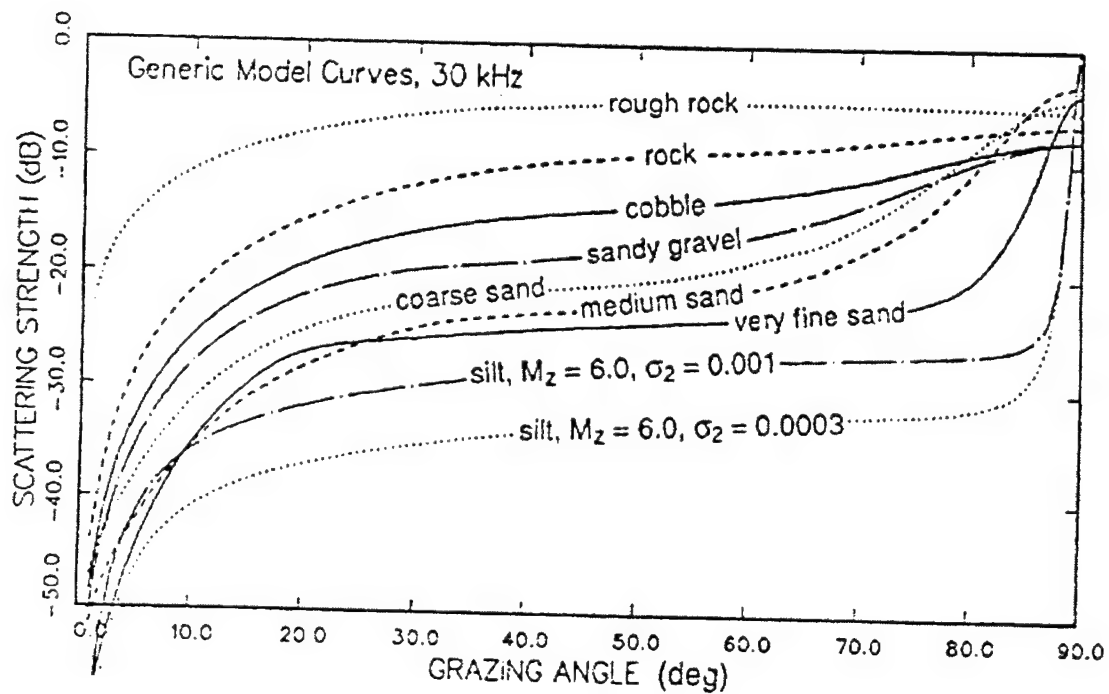


Figure 28. Model curves for backscattering strength at 30 kHz for a variety of bottom types. Data is available for frequencies in the range of 10 to 100 kHz. (From APL/UW, 1994)

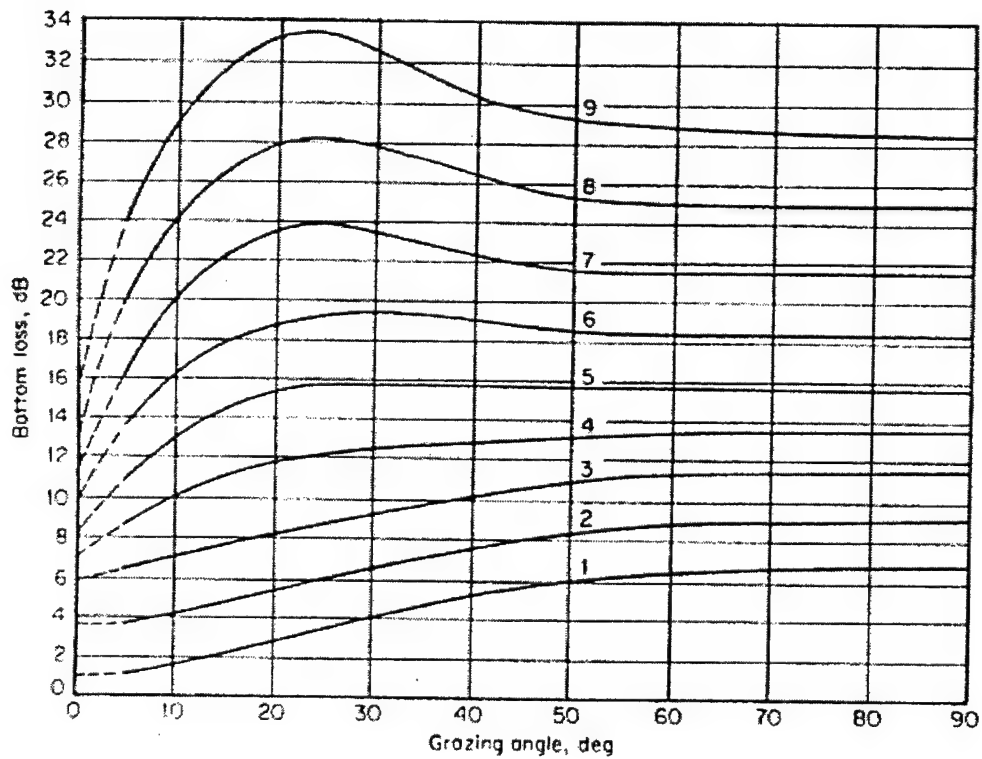


Figure 29. Navy standard high frequency bottom loss (HFBL) curves as a function of grazing angle for the frequency band 1-4 kHz (from Urick, 1983).

Parameters		Sonars		
		US	Aus – VLF	Aus - LF
Sonar Projector	Source Level (dB)	221	205	210
	Frequency (kHz)	35	40	90
	Band Width (kHz)	5	5	5
	Pulse Length (milliseconds)	1.0	0.2	0.2
	Number of Sub-bands	1	1	1
	D/E Range (“-” up, “+” down), (°)	-4, 0, 4, 8, 12	-30 to +30	-30 to +30
	D/E Angle (°)	4	10	10
	Hull Mounted Sonar Depth (m)	5	3	3
	Beam Width (°)	H V	60 60	60 40
	Side Lobe Levels (dB)	H V	13 13	13 13
	Orientation of Array	Horizontal	Horizontal	Horizontal
	Array Type Radius (m)	Circular 0.9	Circular 0.5	Circular 1.0
Sonar Receiver	Bandwidth (kHz)	5	6	6
	Number of Vertical Beams	1	1	1
	Angular Spacing Between Beams (°)	2.5	4	2.1
	D/E Range (“-” up, “+” down), (°)	-4, 0, 4, 8, 12	-30 to +30	-30 to +30
	D/E Angle (°)	4	10	10
	Beam Width (°)	H V	4 50	2.1 50
	Side Lobe Levels (dB)	H V	20 13	13 13

Table 6. Sonar Parameters

<b>Position</b>	
Max Range / Range to Receiver	1300
Range Increment	1
X source, Y source	0
Z receiver depth	same as source (using monostatic sonar)
Bearing from source to receiver	0
Bearing projector, Bearing receiver	0
<b>Options (long)</b>	
Dimension of grid	1D or 2D as applicable
# of sub bands	1
DI Computations	Taylor Shading
Angle between test rays	0.1
Max/Min angle of test rays	±85
Surface Roughness Model	Pierson Moskowitz
Surface / Bottom Loss Model	APL/UW
Surface / Bottom Scattering Model	Monostatic
Volume Scattering Model	APL/UW Direct path
# Surface / Bottom bounces	10
# Upper/lower vertexes	10
# Bounces to target	10
# Bounces reverb	10
SNR type	Max SNR
<b>Options (bool)</b>	
Enable Surface reverb	All listed here are the options that are checked. All others are unchecked
Enable bottom reverb	
Enable volume reverb	
Enable ambient noise	
Enable DO prj	
Enable DI Rec	
Enable frequency spreading	
Enable shadow contrast	
Sum active SNR	
Sum Passive SNR	
<b>Isovelocity 1D environment</b>	Disabled
<b>Doppler and PD/PC</b>	Left as default as not being used
<b>Batch</b>	DE angles applicable to sonar
<b>Environment</b>	
Wind Speed (m/s)	4
Rain Rate (mm/hr)	0
Wind Direction (deg)	135
Air-Sea Temperature Difference (°C)	0

Table 7. PC SWAT Input Parameters

Menu Option	Parameter
<b>Sonar Type</b>	
Active CW Pulse	(selected)
Max Ray Angle	15
Min Ray Angle	-35
Pulse Length	0.01
<b>Run Options</b>	
Plot Left	Off
Plot Right	On
Spike Filter	Off
Shadow Detector	On
Variable Ray Step	On
Coherent Mode	Off
Calculate Reverbs	On
Range Scale	Km
SSP smoothing	Off
Fast Profile	Off
<b>Seabed Loss</b>	HF3 (Panama City Shelf) HF7 (Mississippi-Alabama Shelf)
<b>Proploss Curves</b>	
Show reverbs / Show FOM	Yes
FOM Calculator	
Frequency (Hz)	10000
System Gain	-24 (Type 2093, VLF) -21 (Type 2093, LF)
FOM	134 (Type 2093, VLF) 142 (Type 2093, LF)

Table 8. HODGSON Additional Parameters

Area	VARIABLE					Run No.
	Bottom Type / Region	Water Depth (m)	Depth of Sonar (m)	Season	Target	
Panama City Shelf	Fine Sand / Inshore	15	Hull mount	Fall	Bottom	01
	Coarse Sand / Offshore	80	40	Fall	Moored	02
					Bottom	03
				Spring	Moored	04
					Bottom	05
Mississippi-Alabama Shelf	Clay / Sounds & Bays and St. Bernard Pro Delta	15	Hull mount	Fall	Bottom	06
					Buried	07
				Spring	Bottom	12
		15	10	Spring	Bottom	13
	Muddy Sand / Transition Zones	80	40	Fall	Moored	08
					Bottom	09
				Spring	Moored	10
					Bottom	11

Table 9. Matrix of Model Runs

THIS PAGE INTENTIONALLY LEFT BLANK

## IV. RESULTS

### A. OVERVIEW

This chapter discusses the various parameters that were compared for this study and their effect on sonar performance. The output of all model runs (PC SWAT and HODGSON) are plotted in Appendix A but a series of the comparison plots are included in this chapter. The HODGSON figures in Appendix A display two way TL, bottom RL, surface RL and the FOM. The PC SWAT figures in Appendix A consist of three plots over a one-way transmission range of 1300 m, the SNR, RL (bottom and surface) and TL. The SNR and RL curves commence at 80 m as this value corresponds with the arrival time of the first credible signal. On the SNR plot of each figure, three values are displayed. They are:

- a. the first zero crossing, (m)
- b. the maximum and minimum range for the signal above the threshold value of 5 dB (m), and
- c. the cumulative sum of the SNR over the range in b (dB).

These values are also summarised in Table 10 for both sonars and for both frequencies for the Type 2093. For the first run in each set, the coherent TL was plotted in addition to the incoherent TL, which is plotted all other plots. This was done to illustrate, more closely, the fluctuations inherent in real time data.



## **B. COMPARISONS**

The parameters compared were bottom type, SSP (season), water depth/sonar depth, target location, frequency, sonars and models. As PC SWAT is considered the baseline model for this study, all runs were conducted using this model, except for the four runs in the model comparison section. As such, the numbering format outlined in Chapter III is abbreviated, leaving off the "model" for all comparisons except the model comparison. The first three parameters are essentially the environmental parameters for this study, with the aim to determine which parameters affect sonar performance the greatest, and also to examine the relative importance of bottom RL versus TL. In the comparisons between target location and between the two sonars, a simple comparison of the expected detection for both options was made. When comparing the different frequencies of the Type 2093, the aim was to determine which parameters resulted in the greatest change in performance between the two frequencies. The final comparison was between the two models, with the aim of comparing expected sonar performance from both models with varying bottom type, water depth and frequency, and from this determine which sonar parameters had the most influence in their respective models.

### **1. Bottom Type**

In comparing bottom types, two comparisons were made. The first comparison was between the shallow water regions of the two study areas, comparing clay to fine sand. The second comparison was between the deep-water regions of the two areas, comparing coarse sand with muddy sand.

To compare the bottom types in shallow water run 1 was compared with run 6 for both sonars and frequencies. The comparison of A40\_01 with A40\_06 is plotted in Figure 30. The range at which detection could be expected was similar between the sandy bottom and the clay bottom, at approximately 600 m for all three sets of sonar parameters. For the 2093 sonar, the two different frequencies had a number of common features. Firstly, the strength of the return was higher for the clay bottom in the short and mid range. From 150 – 500 m the strength of the SNR was typically 10 dB higher than for the sand bottom for both frequencies of the 2093 sonar, which resulted in the cumulative sum of the SNR over the threshold range (value c) to be approximately 3000 dB higher. The strength of the SNR for the clay runs was almost constant for the entire range out to approximately 600 m when there was a steep gradient in the SNR, decreasing through zero at 700 m. At a range of 600 to 700 m the surface RL becomes the limiting factor for the clay bottom, with bottom RL being higher than surface RL for shorter ranges before the curves cross and the surface RL being higher. TL is much higher for the mud bottom, 15 dB higher over the range of 600 – 1300 m, thus reducing the signal resulting in a reduction in bottom RL.

For the sandy bottom, although the strength of return was lower over the detection range of 600 m, the SNR showed a gradual decrease rather than a sharp drop off, with the zero crossing at greater range than for the mud bottom.

For the US sonar, there were some similarities and some differences to this pattern and the comparison for U35\_01 and U35\_06 is displayed in Figure 31. The clay bottom run had a similar shape to that in Figure 30

Figure 30, of relatively constant performance over the range and a sharp decrease at 600 m when the surface RL dominated. However, a difference occurred over the sandy bottom, which displayed a higher SNR than for the clay bottom in the very close range (the first 200m). Similar SNR strengths are noted to approximately 600 m, after which the clay curve decreased to zero and the sandy curve continued with a more gradual decrease in performance out to 1200 m with no zero crossing.

The bottom RL was consistently higher for the sandy (more reflective) bottom for all three sonars (U35, A40 and A90), as would be expected in contrast to a more absorptive clay bottom. The clay bottom RL curves initially showed similar results to the sand bottom, but the RL for the more absorptive bottom decreased at a much steeper rate over the entire range, with the two curves differing by 15 to 25 dB at 1000 m. The surface RL was lower than bottom RL and showed a gradual decrease over range for the sandy bottom, however it showed a vastly different result for the clay bottom. At a range of 600 – 700 m the surface RL increased, crossing above the bottom RL. The increase in surface RL is the result of increased ray density due to the interaction of refracted and reflected rays at selected ranges (multipath summation) as observed in various ray traces. One such ray trace is displayed in the top panel of Figure 32, which is the ray trace for A40\_06, where a concentration of rays is noted at 600 m, coinciding with the increase in surface RL for this run.

The one way TL was higher for the clay (more absorptive) bottom as expected, with the differences between the two curves for all three cases being 15 – 20 dB. As

stated, this higher TL for clay bottom resulted in the lowering of the bottom RL over range allowing the surface RL to dominate the SNR.

The second comparison with bottom types was for bottom mines in the deeper water environment. For this comparison run 3 was compared with run 9, and run 5 was compared with run 11 for both sonars and both frequencies of the 2093 sonar. The comparison for runs A40\_03 with A40\_09 is displayed in Figure 33, which is representative for the runs of this comparison. The results observed in the shallow water cases were again seen in the deeper water comparisons, during both seasons, with a few differences. The muddy sand bottom demonstrated a consistently higher SNR of 6 to 10 dB over the entire range, as observed in the shallow water cases. Additionally, the cumulative sum of SNR above the 5 dB threshold was 3000 to 4000 dB higher for the muddy sand bottom compared to the sand bottom. In contrast to the shallow water case, a sharp decrease in SNR was not evident, with the range of detection being greater for muddy sand (900 m) than for sand (400 m). This is clearly due to the fact that we are dealing with a muddy sand bottom and not a purely mud or clay bottom where the TL is very high. For the muddy sand bottom, the TL was almost identical in magnitude to the sand bottom.

As seen in the shallow water cases, bottom RL was higher for the sandy bottom by approximately 10 dB in all cases. Surface RL (not shown) was lower than bottom RL for all cases, and was similar for both bottom types with no instances of the surface RL becoming greater than bottom RL. The main difference from the shallow water cases was that the TL was almost identical between both bottom types, explained by the large

percentage of sand in the muddy sand bottom. When considering the contribution of TL and RL to SNR, sonars operating over the muddy sand bottom clearly performed better than when operating over a sand bottom due to the inherent lower bottom RL associated with sediments containing a substantial fine grain (mud) component. As the TL doesn't differ between the two bottom types, the sharp decrease in SNR observed in the clay bottom, shallow water scenarios is not seen here, with the muddy sand bottom also having greater range before the zero crossing.

The difference due to bottom composition must be noted here, because in shallow water the two bottom types being compared are fine sand and clay and as expected their performance differences are greater. For the deeper water, the bottom types are coarse sand and muddy sand. A small difference is detected in the RL curve due to the presence of mud in the sediment, however the TL is very similar due to the similarities in the bottom type.

In both the shallow water and the deep-water cases, the change in bottom sediment type was found to be more sensitive to magnitude and shape of the bottom RL than the TL curve.

## **2. Season and SSP**

Similar to the investigation concerning sensitivity to bottom type variation, two comparisons relative to the sensitivity of SSP on performance are made in this section, one case for shallow water and one for deep water.

In shallow water, only one seasonal comparison was made, a comparison between run A40\_06 and A40\_12 in Figure 34, as the profiles remained similar year round. The

one comparison was between typical August/September conditions along the Mississippi-Alabama shelf in contrast with conditions when a significant influx of fresh water occurs from river flooding, typically occurring in the spring. Note, however, that extensive flooding has been recorded in all seasons. SSPs for both cases are shown in Figure 20. During the flooding condition, a significant positive sound speed gradient is observed due to the fresh water layer on the surface. These conditions are typical of conditions that would be expected in waters adjacent to rivers or estuaries where freshwater input affects the SSP. The ray trace diagrams for these two SSPs are illustrated in Figure 32 with the ray trace for a centre beam depression angle of  $10^\circ$ , with beam width of  $\pm 25^\circ$  and rays plotted at  $3^\circ$  intervals. The upper figure is the August/September SSP and the middle figure is the flooding conditions in spring, with the sonar at 3m. The positive sound speed gradient causes significant refraction of the rays toward the surface, illustrated in the middle panel. Because acoustic energy is trapped in the upper layer, below layer or near bottom targets are poorly illuminated and performance is significantly degraded over the entire range.

For the fall conditions, the signal remained above the threshold of 5 dB out to 600 m, with consistently good performance over this range. For the spring conditions, intermittent detection is observed over the first 500 m with the peaks approximately 20 dB above and the troughs between 0 and 10 dB below, due to the multipath nature of the propagation. Beyond 500 m detection goes below zero. These results can be explained by the RL and TL curves. For spring conditions with the sonar located in the mixed layer, the surface RL is higher than the bottom RL by 25 dB, and is higher than the surface RL

for fall conditions by 30 dB over the range to 700 m. At this range and beyond, the model shows that surface RL values increase for fall conditions, as seen in the previous section, and the surface RL values become similar for the two seasons. The TL curves are similar for both seasons out to 700 m whereafter they diverge and TL becomes higher for the fall conditions. The two TL curves continue to diverge with 10 dB difference at 1200 m, due to more bottom interaction for the fall case causing higher bottom loss. The TL curve for the spring conditions shows a flattening in the range 1000 – 1300 m. The bottom RL curves have a similar magnitude out to 1000 m after which they diverge. This is as a result of the higher TL in the fall causing the bottom RL to decrease and the spring TL curve to flatten out causing a similar plateau in the bottom RL. The difference in the bottom RL curves for the two seasons is 10 dB higher for the spring case than for the fall case at the extended ranges.

A further comparison during spring flood conditions was conducted to examine the performance when the sonar was hull mounted, as is usual for shallow water conditions, and at 10 m, below the thermocline. This is a comparison between runs A40\_12 and A40\_12, and plotted together in Figure 35. With the sonar at 10 m a significant improvement in performance is noted, as is displayed in the bottom panel of ray trace diagrams in Figure 32. As the sonar is below the thermocline, it does not exhibit such strong upward refraction. Good performance is seen over the entire 1300 m range with the SNR well above the threshold value of 5 dB, and the cumulative sum of SNR over the threshold range increased from 2500 dB to 31500 dB, indicative of the increase in performance. The bottom RL increased by approximately 15 dB when the sonar was

placed at the deeper depth, as expected as the sonar is nearer the bottom thus causing higher reverberation. Both TL and surface RL are significantly reduced when the sonar is below the thermocline, by approximately 10 dB and 30 dB, respectively, thus accounting for the exceptional performance of the 10 m source depth.

The second seasonal comparison was for the deeper water regions of both areas, between runs 3 and 5 and between runs 9 and 11 for both sonars and both frequencies. Very little difference in performance was noted between the fall and spring SSPs, with a representative comparison, between U35\_09 with U35\_11, displayed in Figure 36.

Over the Panama City shelf in deeper water, the changing season had little effect on sonar performance. The sound speed profiles differed in that the thermocline was shallower in the spring than the fall, approximately 39 m in the fall and 15 m in the spring, and the absolute value of the SSP was higher in the fall. Because the sonar was placed at 40 m, below the mixed layer for both seasons, the seasonal difference in SSP was minimised and a similar performance was seen.

Over the Mississippi-Alabama shelf in fall a slightly cooler surface layer was present causing a shallow positive temperature gradient above 20 m. This feature exerted little effect on performance as the sonar was below this feature at 40 m. The performance was slightly better in the spring when the thermocline was shallow and weak due to convective mixing, most notably in the US sonar.

### **3. Water Depth and Sonar Depth**

The investigation of the influence of water depth on sonar performance was restricted to the runs at a single location, the Panama City Shelf. The sediments on the



Mississippi-Alabama Shelf differed significantly from the shallow region to the deep region and this difference in bottom sediments affected the results, thus invalidating any meaningful comparison investigating performance solely as a function of water depth.

The comparison here is between runs 1 and 3 for the two sonars and two frequencies of the 2093 sonar. Sonar performance was markedly better in the shallow water environment. For both frequencies of the 2093, as displayed in Figure 37 by the comparison between A40\_01 with A40\_03, bottom RL was initially of very similar magnitude for both shallow and deep water. However the curves diverged, differing by 20 dB at 1300 m, with the deep water curves exhibiting greater backscatter. Additionally, TL was lower in shallow water by 5 to 10 dB.

In shallow water, the surface RL was initially 10 dB lower than the bottom RL, however with a steeper decrease in bottom RL, surface and bottom RL were of similar magnitude beyond a range of 700 m. In deep water, the surface RL was 20 dB lower than bottom RL over the entire range. In comparing surface RL between deep and shallow water, it was higher in shallow water at short range, by 10 to 15 dB.

For the US sonar, shallow water performance was better than deep-water performance by approximately 7 dB, as displayed by the comparison of U35\_01 with U35\_03 in Figure 38. The bottom RL curves were almost identical, and the surface RL was higher for the shallow case by almost 15 dB at shorter range, decreasing to a difference of 5 dB at 1200 m. The TL was higher in deep water by 8 dB, which clearly contributed to the lower SNR in deep water. The poorer performance in deep water appears to arise principally from TL considerations.

In comparisons in the previous section for SSPs, it was clearly seen that sonar depth is important. Placing the sonar in the same layer as the target, i.e., below the thermocline for bottom or deeper moored mines, increases performance dramatically. If the sonar is placed in a position where a cross layer scenario is encountered, performance is exceptionally poor.

#### **4. Target**

The performance assessment based on mine types considers a comparison between moored and bottom mines and a comparison between bottom and buried mines in the clay bottom.

As a comparison for the moored mines has not been discussed thus far, a brief comparison will be made here. These comparisons were between runs 2 and 8, and runs 4 and 10 for both sonars and both frequencies of the 2093 sonar. Figure 39 displays A40\_02 and A40\_08. Moored mines generally displayed poor detection capability at closer ranges over a sand bottom, showing improved detection at greater ranges of 10 dB. Over the muddy sand bottom, the detection of moored mines was improved for all sonars, with SNR again increasing with range. In the case of the muddy sand bottom, the bottom RL was 10 dB lower than for the sand bottom, and this was reflected in the improved SNR curve, with the SNR being higher by approximately 10 dB. Very little difference is seen in the TL curves for the two bottom types, again suggesting that bottom RL is the most sensitive parameter affecting sonar performance. The improved detection of moored mines at distance is due to multipath returns, when sound is reflected into the main water column, allowing for the detection of mines within the water column.

When comparing detection of moored mines versus bottom mines, the runs examined are 2 versus 3, 4 versus 5, 8 versus 9 and 10 versus 11 for both sonars and both frequencies of the 2093 sonar. A representative plot is displayed in Figure 40, a comparison between A40\_08 and A40\_09. In this comparison better detection occurs for bottom mines for ranges less than 500 m due to the downward orientation of the sonar beams. Beyond this range, detection of moored mines increases substantially as the number of multipath returns increases with range. This is manifested in a reduced TL for the moored mines at ranges in excess of 1000 m, whereas the bottom and surface RL curves showed no substantial change in slope with increased range.

A point of note here is that no false targets were injected in this study. In an actual situation false targets would likely be encountered on the bottom, which would complicate the picture when searching for bottom mines. Thus, although the performance at short range was poorer for moored mines, in reality it might be closer to that for the bottom mine as there would not be the added complexity of other factors such as false targets, which must be dealt with when searching for bottom mines.

The second mine comparison was between bottom and buried mines, comparing runs 6 and 7 for both sonars and both frequencies of the 2093 sonar. A comparison is displayed in Figure 41, of A40\_06 versus A40\_07. As expected, performance is much poorer for buried mines than proud bottom mines. When the mine is buried, much of the high frequency energy is rapidly attenuated upon transmission into the sediment, thus the returned signal is significantly weakened. It must be noted that on the comparison plot (Figure 41), the TL curves for both buried and bottom mines are identical. This is,

obviously inaccurate as TL should not be identical in this situation. When running TL on PC SWAT separate from SNR, the option for modelling the TL for a buried mine is not possible, thus it generates an inaccurate curve indicative of a proud, bottom mine.

## **5. Frequency**

The frequency comparison examined all runs, 1 through 11, comparing each one at the two frequencies of the 2093 sonar, 40 kHz and 90 kHz.

For the frequency comparison, the RL was consistently higher for the lower frequency and the TL was consistently higher for the higher frequency. This behaviour of RL is not as expected. Scattering strength from the sea surface and ocean floor is expected to increase with frequency, however, one must consider the influence of TL on RL. The TL increases with increasing frequency due to absorption and boundary interaction thus mitigating the increase in scattering strength and reducing the total RL, a feature observed in all model runs.

A comparison for the sand bottoms for the Panama City shelf sediments is displayed in Figure 42, between A40\_01 and A90\_01. When searching over a sandy bottom, performance was marginally better at higher frequency out to a range of 700 m at which point the cumulative effect of high TL for higher frequencies was manifested and the performance of the lower frequency sonar mode was better. In shallow water, the higher frequency was expected to provide better detection in close ranges, with deteriorating performance at greater ranges, as this is why a high frequency mode was designed into the sonar. However, better performance at short ranges was also noted for the deep water runs, for both moored and bottom mines.

When searching over a muddy bottom, the contribution of increased TL at higher frequency was an important factor, as displayed by the comparison between A40\_06 and A90\_06 in Figure 43. In the shallow water with a clay bottom, searching for a bottom mine, the high frequency mode performed slightly better ( $< 5$  dB) but at a shorter detection range (approximately 400 m) than when operating over a sandy sea floor. Beyond 400 m range, the TL at higher frequency increased rapidly, permitting the lower frequency to perform better, with detection out to 600 m. The buried mine was barely detected by the higher frequency due to its strong attenuation in the sediment; the lower frequency mode suggests detections out to 300 m are possible. For the deep-water mines over the muddy sand, a similar result was seen as with the sand bottom, with the higher frequency performing better in the short range out to 600m, beyond which the lower frequency performed better.

When considering frequency as a factor in sonar performance, TL was the most sensitive parameter. At shorter ranges the increased TL associated with high frequency propagation reduces the reverberation thus increasing the performance of the high frequency mode. With increased range (beyond 400 to 600 m) the cumulative increase in TL exceeds the reduction in RL and at this point the curves cross and the lower frequency mode shows better detection performance. Thus the higher frequency mode provides better detection at shorter ranges. The initial detection range is expected to be greater at low frequency than at high frequency.

## 6. Sonars

The sonar comparison investigates the relative performance of the US sonar at 35 kHz and the 2093 sonar at 40 kHz, thus all runs 1 through 11 were intercompared.

Over either a sandy bottom or a muddy sand bottom, the US sonar displayed better performance than the 2093 VLF sonar. Figure 44 is a typical comparison for this case, comparing A40\_01 with U35\_01. The SNR of the US sonar was approximately 5 dB higher and initial detection ranges were approximately 200m greater. The TL curves were very similar for both sonars implying sonar performance was dependent on the slope and magnitude of the RL curves. The RL was consistently lower for the 2093 sonar by 5 to 10 dB over either bottom type, which would imply that the performance (SNR) for the 2093 sonar should be better than for the US sonar. Hence, the difference in performance must be caused by differences in sonar parameters such as SL, beam pattern or pulse duration.

A comparison for the sonars over a clay bottom is displayed in Figure 45. For the clay bottom in shallow water, the bottom RL is lower by 15 to 20 db for the 2093 sonar as compared with the US sonar. This RL difference is much greater than for the sandy bottoms and resulted in a stronger SNR for the 2093 sonar over the range to 600 m, with both curves dropping off sharply at 600 m as discussed previously.

Several parameters differ between these two sonars, with the source level being 16 dB higher for the US sonar, the receiver vertical bandwidth being much larger for the Australian sonar and the pulse length being an order of magnitude different, smaller for the Australian sonar. Figure 46 illustrates how these three parameters affect performance

(SNR), RL and TL, which in turn accounts for the differences in the intercomparison between the two sonars. In Figure 46, the curve for the US sonar with the baseline sonar parameters used for the runs of this study is plotted. The other curves plotted are for comparison with this baseline, changing only the one particular parameter for each case to the value used for the 2093 sonar at 40 kHz. When the source level is decreased from 221 dB to 205 dB, negligible difference in the SNR results. This is due to the compensating decrease in bottom RL for the decreased signal strength. When the vertical receive beamwidth is changed from  $9.8^\circ$  to  $50^\circ$ , a noticeable change is detected, with SNR decreasing by 10 dB and both bottom and surface RL increasing with increased beamwidth, i.e., reverberation is received over a wider area. When the pulse length is decreased from 1 ms to 0.2 ms, an increase in performance is seen, again with the change in bottom and surface RL (both decreasing as the reverberant area is reduced) being the affected parameters.

For the comparison for the sandy bottom (Figure 44), the 2093 sonar displays lower bottom RL due to a lower signal level. However, as the 2093 has a wider vertical receive beamwidth, this bottom RL amount was only slightly lower and was insufficient to offset the 16 dB increase in SL for the US sonar. However, over a clay bottom significantly lower RL is expected than over a sand bottom, and the reduction in this parameter would effect the performance of the 2093 sonar even with its wider vertical beamwidth. In this case, the bottom RL of the 2093 sonar was substantially lower than for the US sonar and resulted in better performance of the 2093 sonar.

Additionally, when modelling the detection of moored mines, the performance of the US sonar was better than that for the 2093 sonar. This could be attributed to the fact that the US sonar has a shallow depression angle ( $4^\circ$ ) permitting more acoustic energy to avoid bottom interactions in contrast to the 2093 sonar which has a depression angle of  $10^\circ$ .

## **7. Models**

The model comparison will examine how differences in frequency and bottom type affect the estimates of sonar performance of the 2093 sonar. The four runs are A40\_01, A40\_06, A90\_01 and A90\_06 and are all in Appendix A, Figures A1,A6,A14 and A19 for the runs on PC SWAT and Figures A36-A39 for HODGSON model runs.

For these two comparisons, the PC SWAT and HODGSON models showed many similarities in the shape and behaviour of the bottom RL and TL curves for both frequencies.

An examination of the predicted bottom RL for the 2093 sonar at 40 kHz indicates that both models showed agreement. For the shallow water sandy bottom (A40\_01), the bottom RL showed a decrease of approximately 60 dB over 1300 m for SWAT (Figure A 1) and 80 dB for HODGSON (Figure A 36). Also, a small peak evident at approximately 1220 m on the bottom RL curve for SWAT was replicated by HODGSON at 1200 m, though the magnitude was greater for HODGSON. When comparing the HODGSON bottom RL curve for the sandy bottom to the mud bottom, the pattern reflected that modelled by SWAT. For the mud bottom, the RL curve decreased much more than for the sandy bottom over the same range, being almost 90 dB for



SWAT (Figure A 6) and almost 100 dB for HODGSON (Figure A 37). Thus for the varying bottom types a similar pattern was seen for the two models, with steeper bottom RL slope change over the clay bottom compared with the sand bottom, i.e., lower bottom RL over the clay bottom. The values of the change in bottom RL were within 10 to 20 dB for both cases, with HODGSON being consistently higher.

TL curves displayed on the HODGSON runs are two way, and for this discussion they are divided by two to equate to one way TL for ease when comparing with the TL from PC SWAT. When considering the TL curves for the VLF option of the 2093 sonar, there were a number of similarities. For the shallow water sandy bottom, both models showed similar curves, with one-way TL increasing by approximately 30 dB for the SWAT run (Figure A 1) and by 50 dB for the HODGSON run over 1200 m (Figure A 36). For the clay bottom, both TL curves showed and increase in magnitude of the TL curve over the 1200 m. The TL for the SWAT run increased by 40 dB (Figure A 6) and the HODGSON run (Figure A 37) increased by 55 dB over the range of 1200m. Thus, TL curves also showed a similar pattern for the two models, with one way TL loss differing by 10 to 20 dB for the two models for both cases, with HODGSON again being higher. As expected, the TL was higher for over the clay bottom compared with sand bottoms.

The third parameter is surface RL, which again showed similar behaviour between the two models. Of particular importance was the treatment of surface RL at mid range (approximately 600 m) for the clay bottom when PC SWAT displayed increased surface RL with it becoming greater than bottom RL. The HODGSON model replicated this pattern between 600 and 700 m, with surface RL becoming greater than bottom RL.

The final comparison for the models is between the two frequencies of the 2093 sonar, looking at bottom RL and TL. For bottom RL a clear similarity is noted in the pattern for both models, with the bottom RL curve decreasing significantly more at the higher frequency than at the lower frequency. This is displayed in the shallow water case on the Panama City shelf. The bottom RL curve for SWAT showed a decrease in RL over 1000 m of 50 dB for the lower frequency (Figure A 1) and 90 dB for the higher frequency (Figure A 14). Similarly for the HODGSON model over 1000 m, the lower frequency showed a decrease of RL of 70 dB (Figure A 36), and 120 dB for the higher frequency (Figure A 38).

For the TL curves, both models demonstrated an increase in TL at higher frequencies. This occurs for shallow water areas with either clay or sand sediments. The largest change in TL occurred for the clay bottom runs. For one-way TL over 600 m, PC SWAT predicted an increase of 20 dB for the 40 kHz (Figure A 6) and 45 dB for the 90 kHz, whereas the HODGSON model predicted an increase of 45 dB and 70 dB for the lower frequency (Figure A 37) and higher frequencies (Figure A 39) respectively.

In summary, even though it was not designed for high frequency mine hunting sonar applications, the HODGSON model compared well with the PC SWAT model. HODGSON displayed decreased bottom RL and increased TL for propagation over clay sediments compared to sandy sediments. A correct response was noted when the frequency was changed from 40 to 90 kHz with a higher TL and lower RL observed for higher frequencies. Additionally, the initial detection ranges of both models showed some similarities. For the 40 kHz sonar over the clay bottom (A40\_06) and the 90 kHz

over the clay bottom (A90\_01), the two models predicted similar values. The zero crossing for PC SWAT for A40\_06 was 660 m and was 590 m for HODGSON, and for A90\_01 PC SWAT predicted 680 m and HODGSON predicted 620 m. However, for the 40 kHz sonar over a sandy bottom (A40\_01) and the 90 kHz over a clay bottom (A90\_06), there were some differences with HODGSON predicting shorter ranges than PC SWAT.

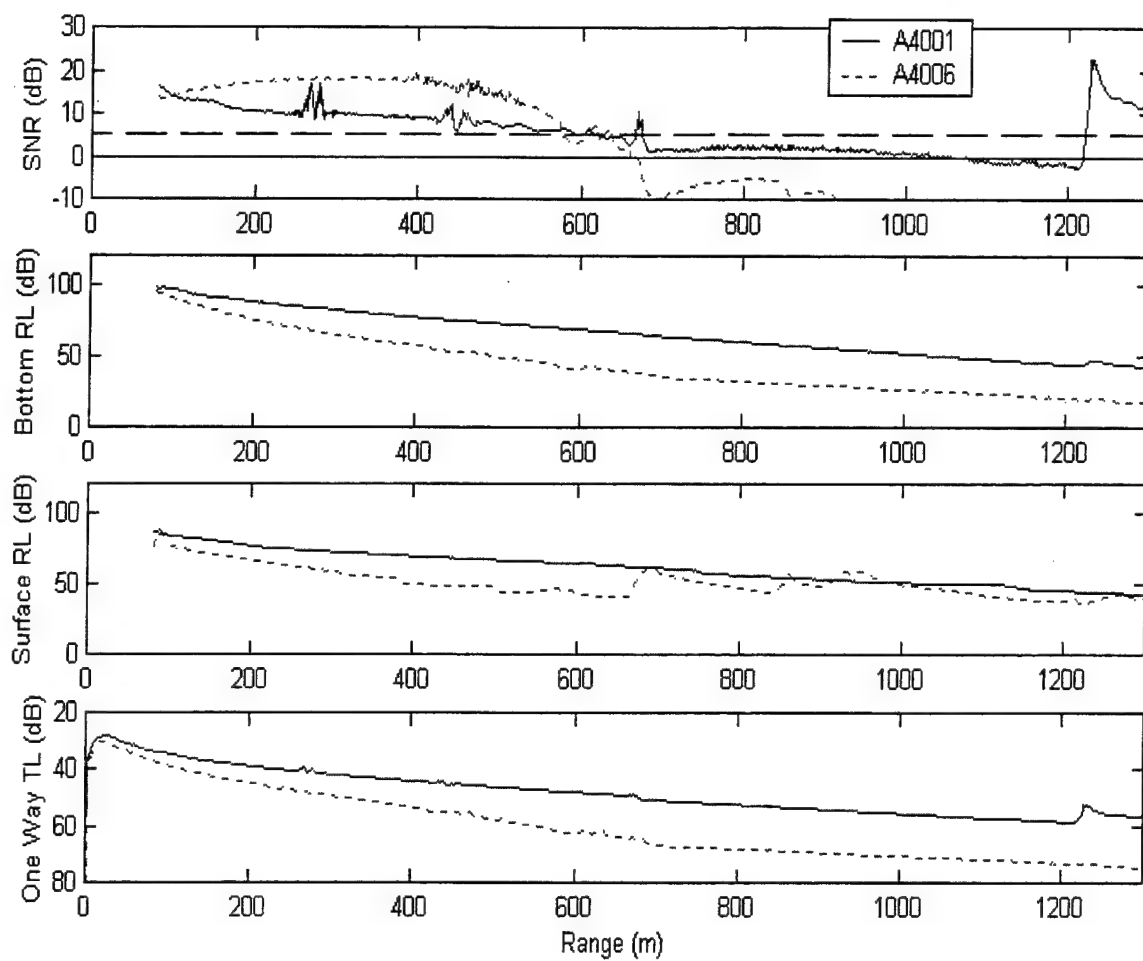


Figure 30. Comparison of sand (—) and clay (---) bottoms for the 2093 sonar operating in shallow water at 40 kHz.

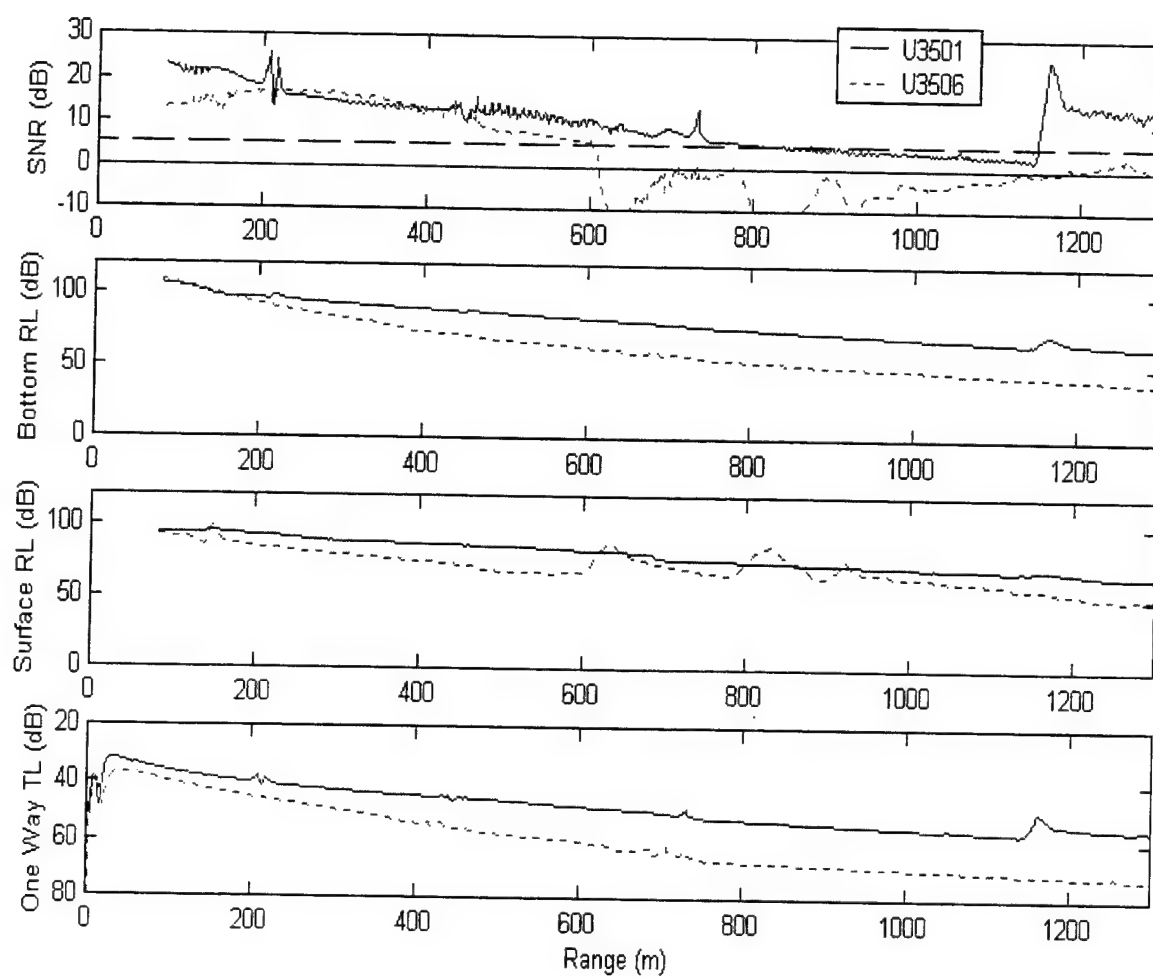


Figure 31. Comparison of sand (—) and clay (---) bottoms for the US sonar operating in shallow water at 35 kHz.

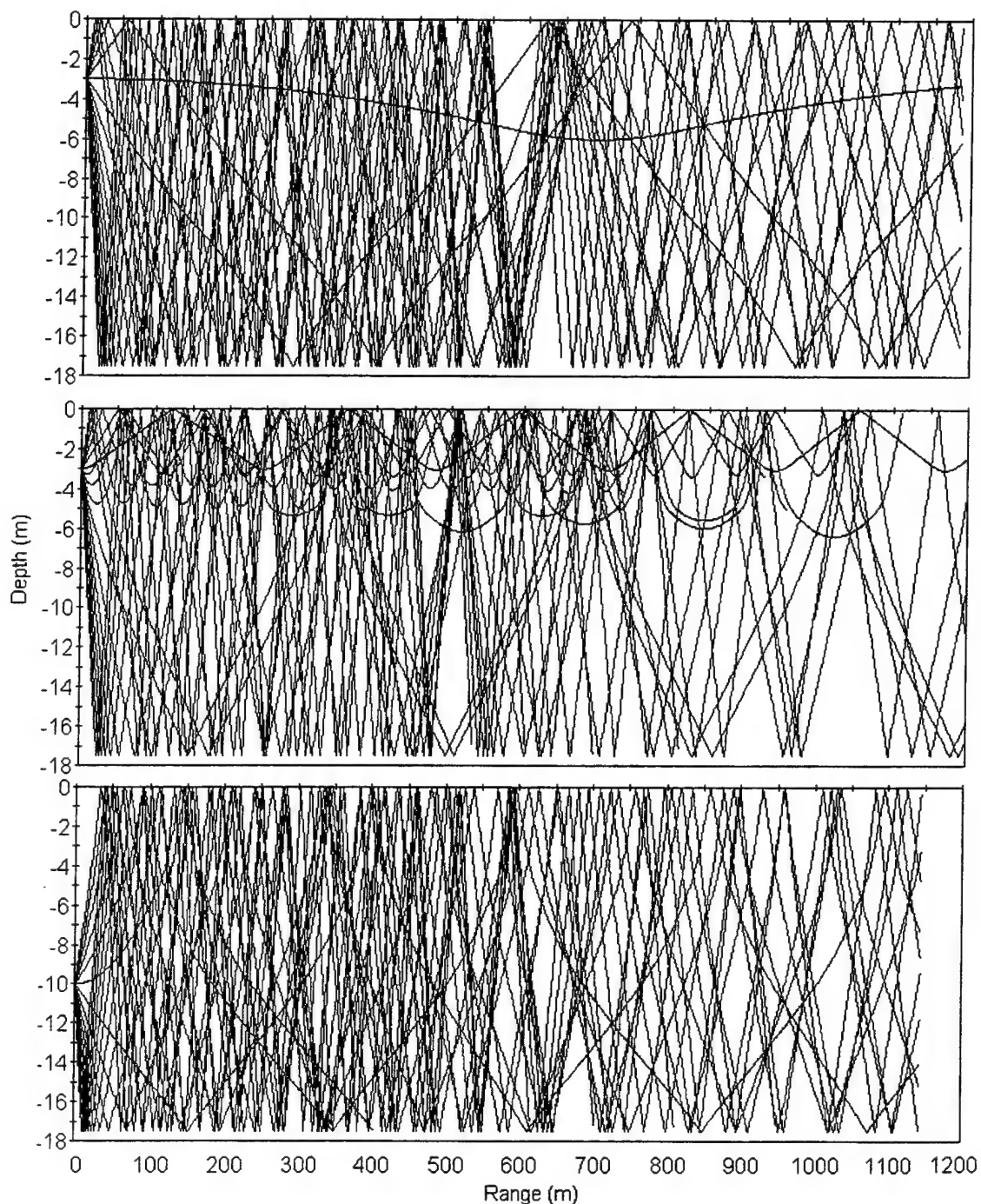


Figure 32. Ray trace diagram for the shallow water environment on the Mississippi-Alabama shelf. The top figure is for August-September (A40\_06) and the middle figure is for a flood event in spring (A40\_12) when there is a strong positive sound speed gradient with the sonar at 3 m for both cases. The bottom figure is for a flood event in spring with the sonar at 10 m (A40\_13).

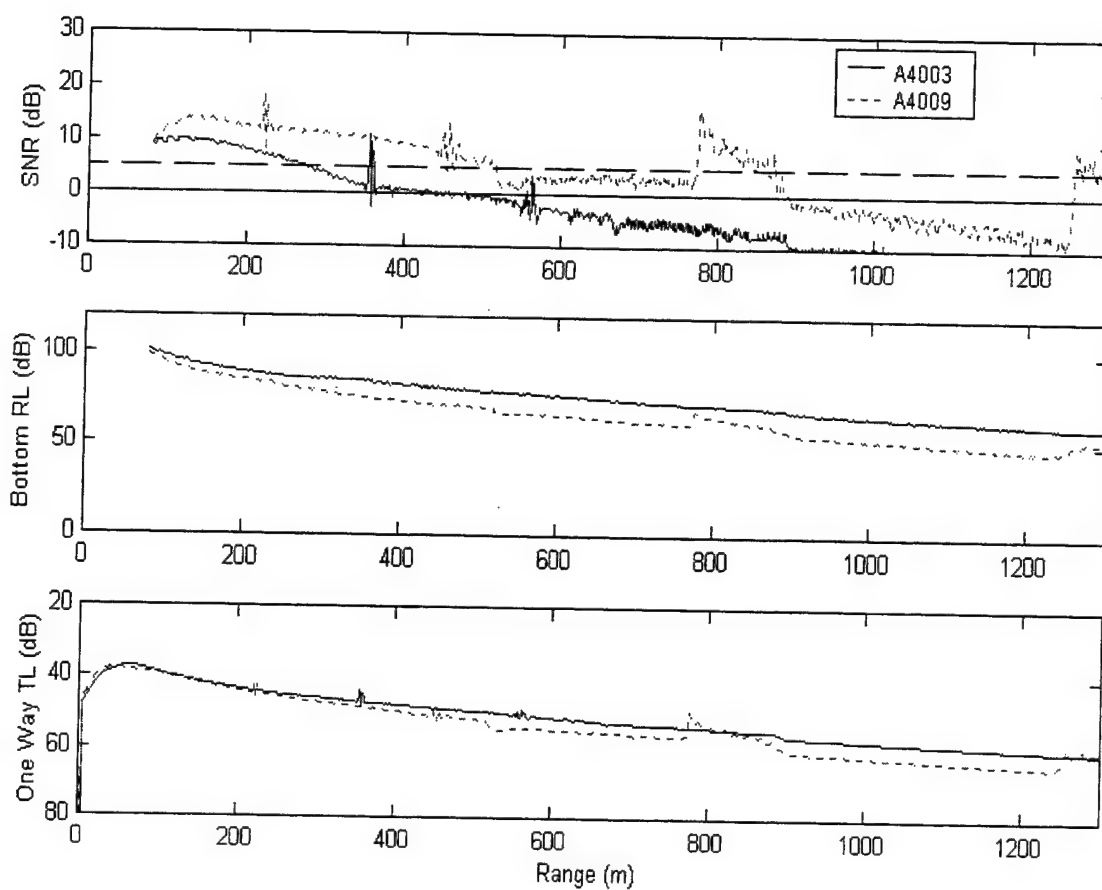


Figure 33. Comparison of sand (—) and muddy sand (--) bottoms for the 2093 sonar operating in deep water at 40 kHz.

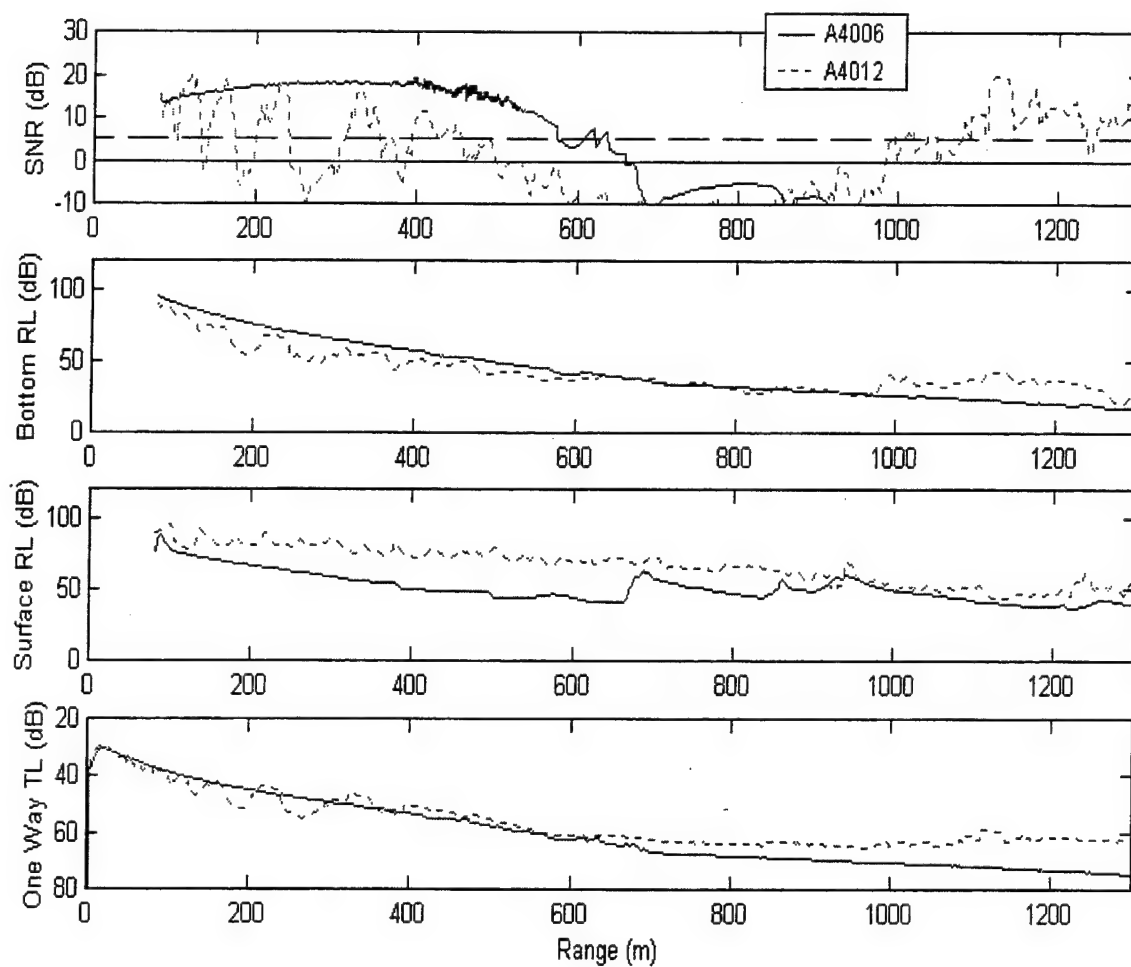


Figure 34. Comparison of the fall (—) and spring flood (---) SSPs in shallow water for the 2093 sonar at 40 kHz.



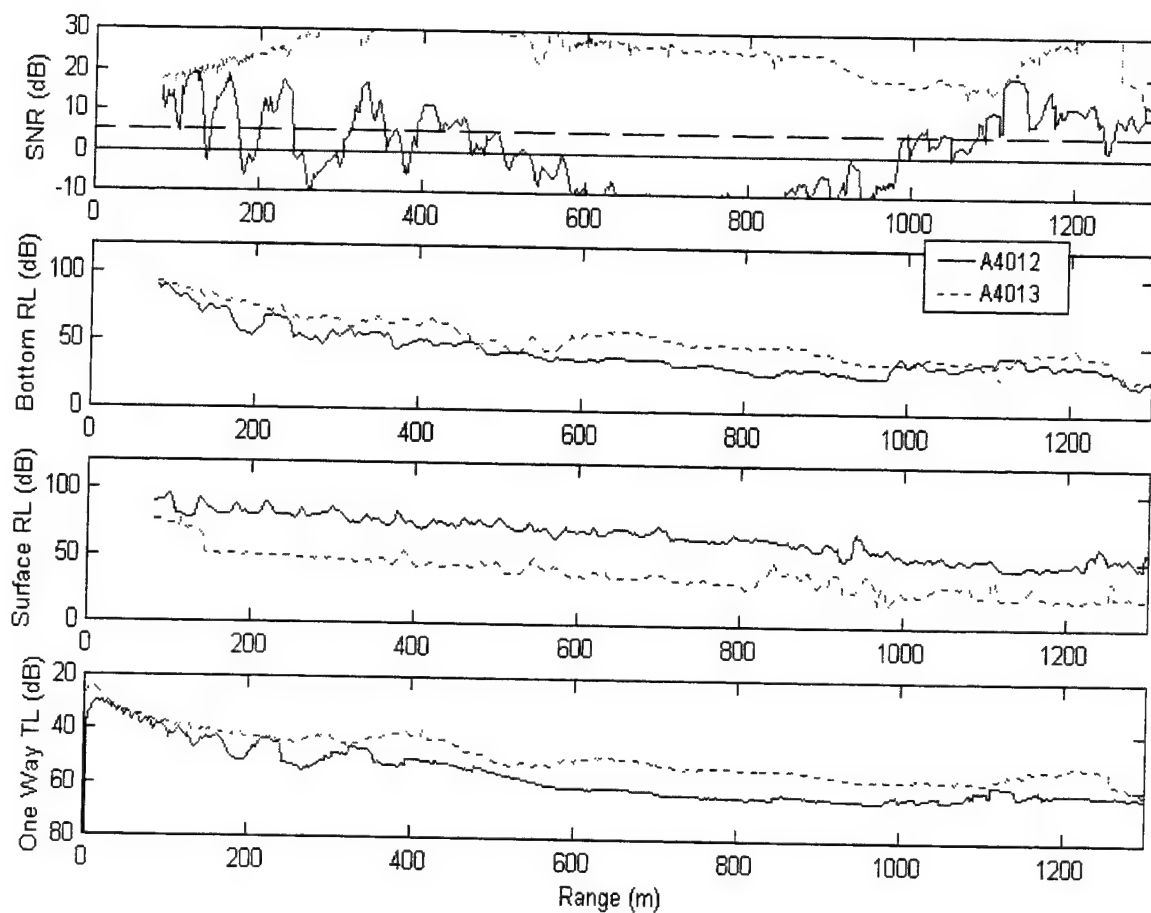


Figure 35. Comparison of the spring SSP with the source above the layer (—) and below (---) the layer when searching for a bottom target.

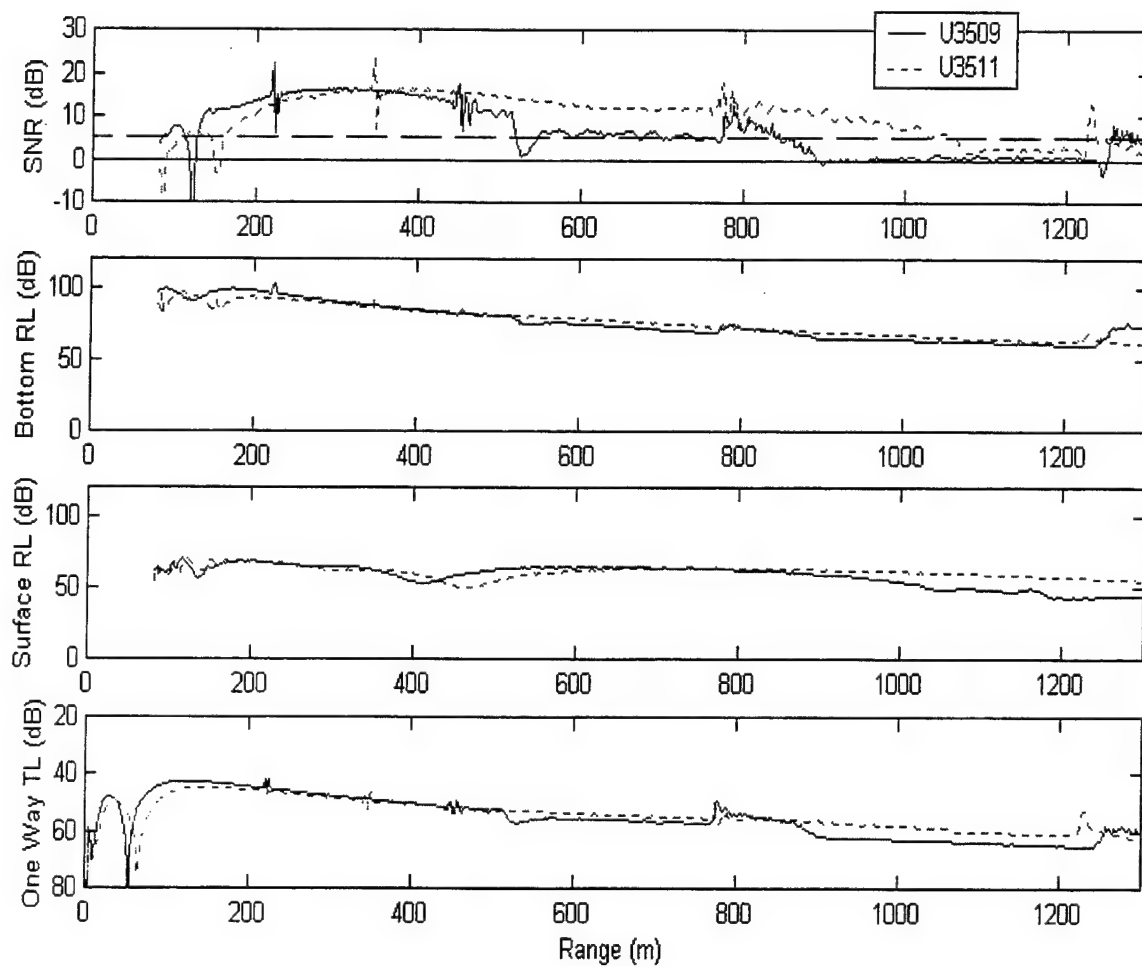


Figure 36. Comparison of the fall (—) and spring (---) SSPs in deep water for the US sonar.

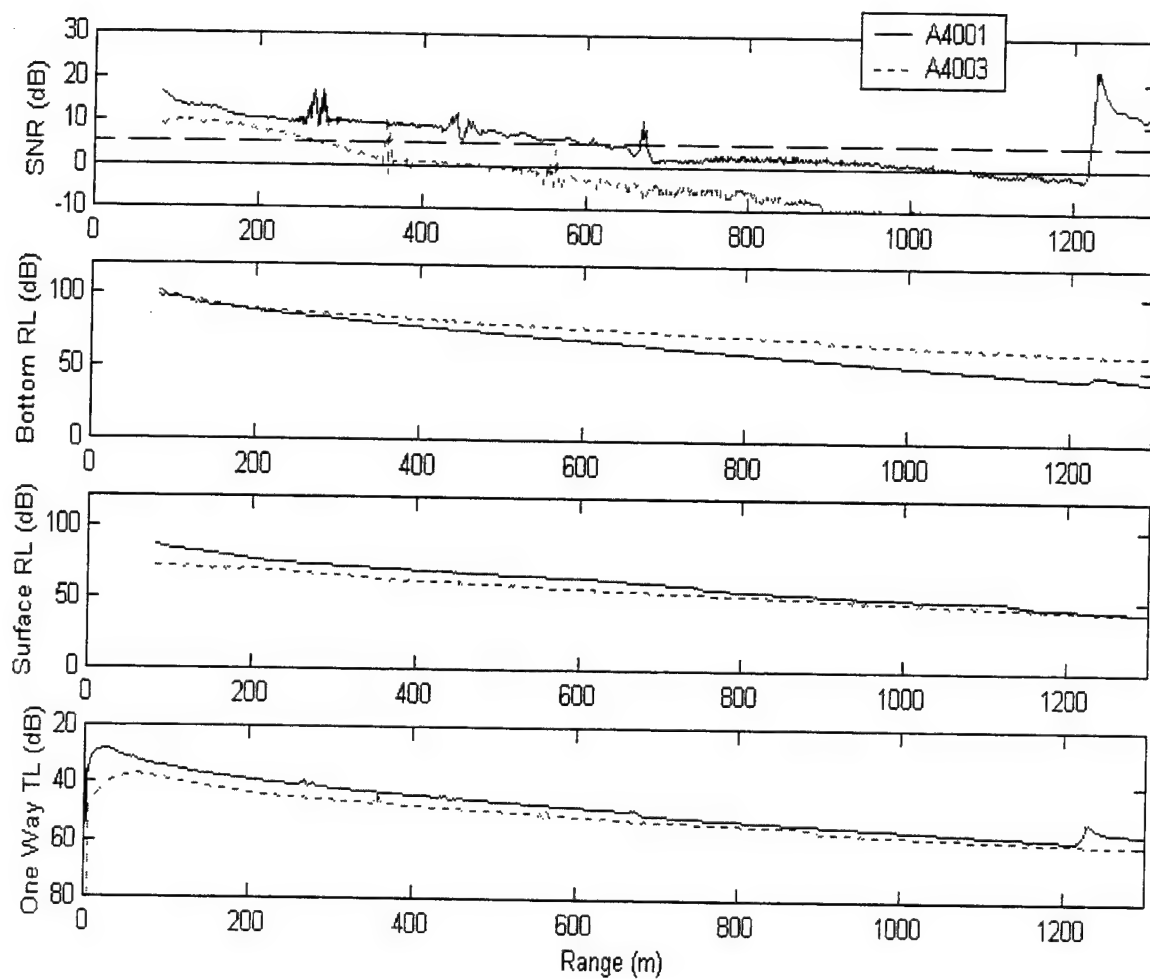


Figure 37. Comparison of shallow (—) and deep (---) water conditions on the Panama City shelf for the 2093 sonar at 40 kHz.

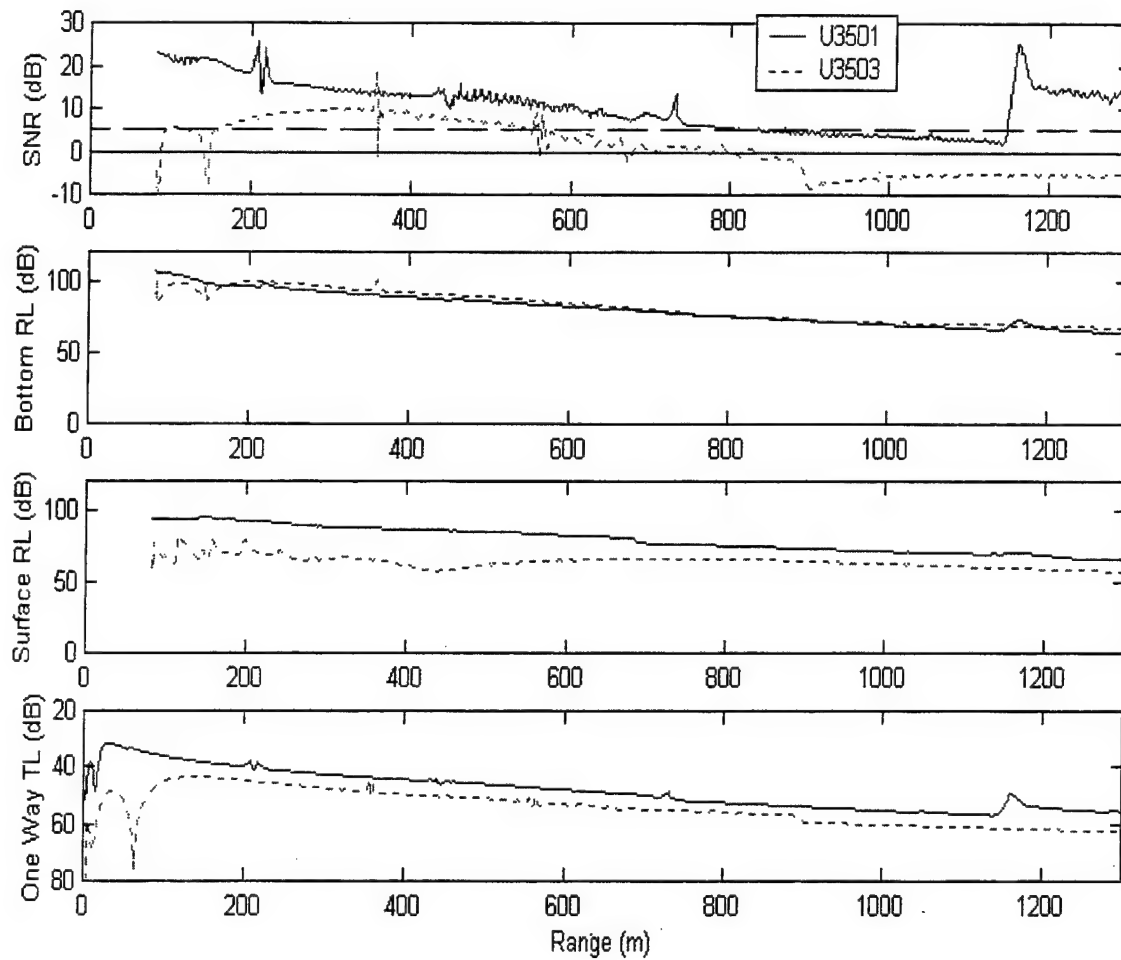


Figure 38. Comparison of shallow (—) and deep (---) water conditions on the Panama City shelf for the US sonar.

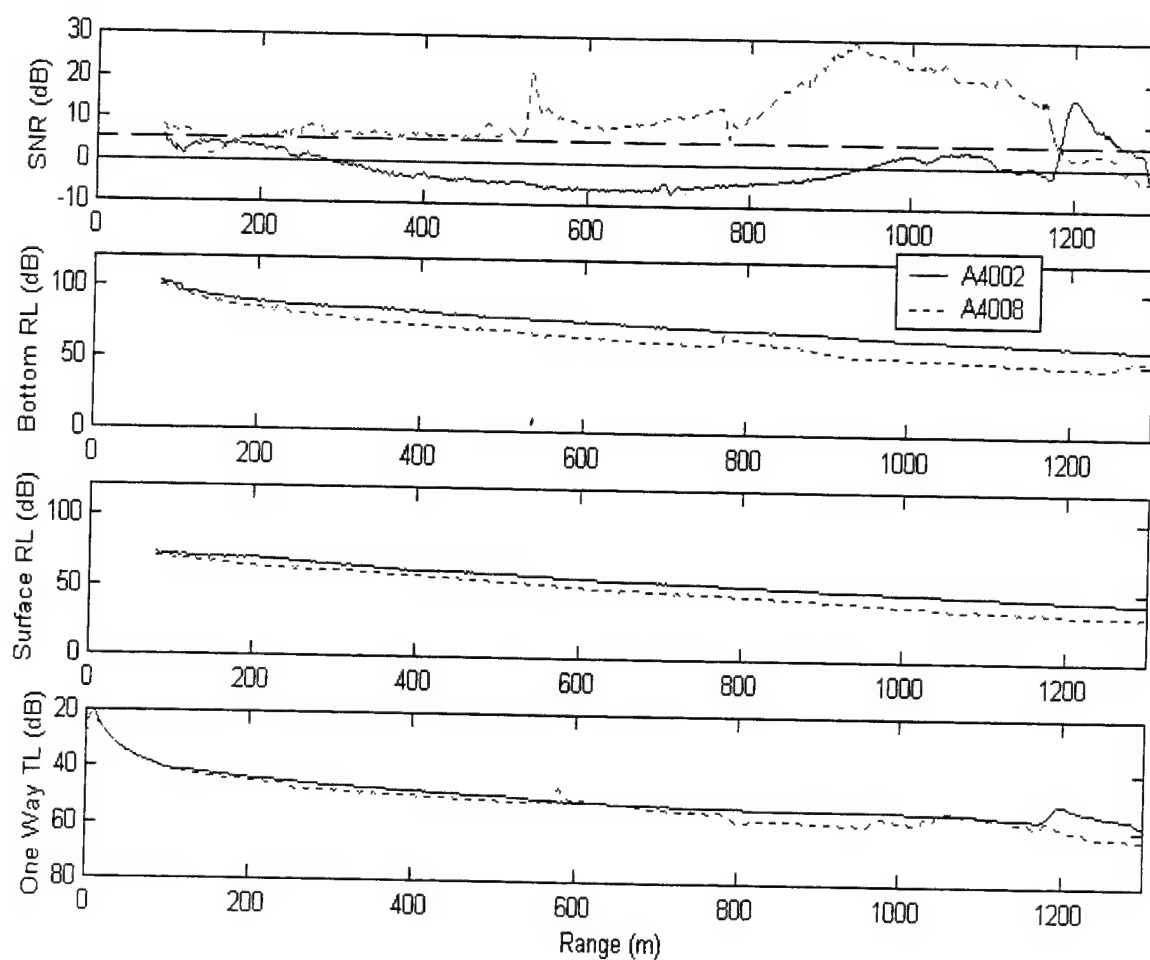


Figure 39. Comparison of moored mines over a sand (—) bottom and a muddy sand (---) bottom for the 2093 sonar at 40 kHz.

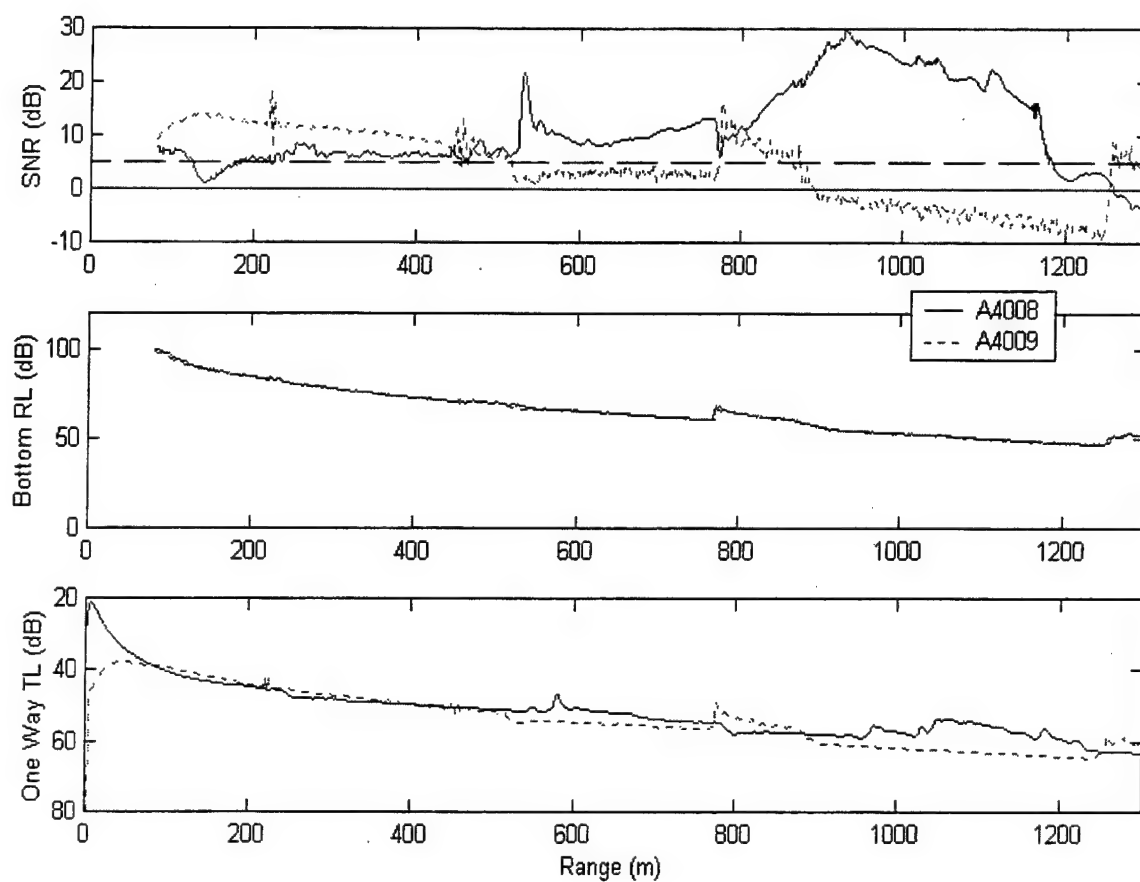


Figure 40. Comparison of moored (—) and bottom (---) mines over a muddy sand bottom for the 2093 sonar at 40 kHz.

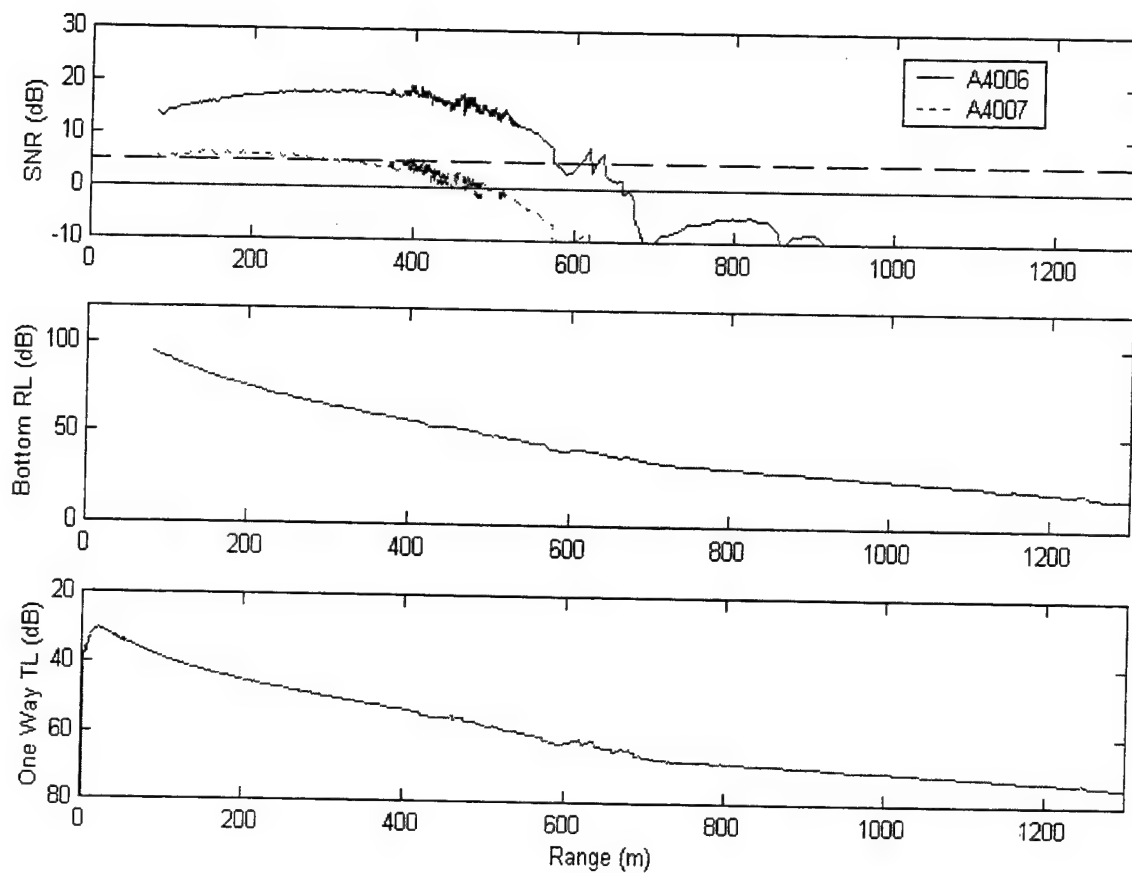


Figure 41. Comparison of bottom (—) and buried (---) mines on the Mississippi-Alabama shelf (clay bottom) for the 2093 sonar at 40 kHz.

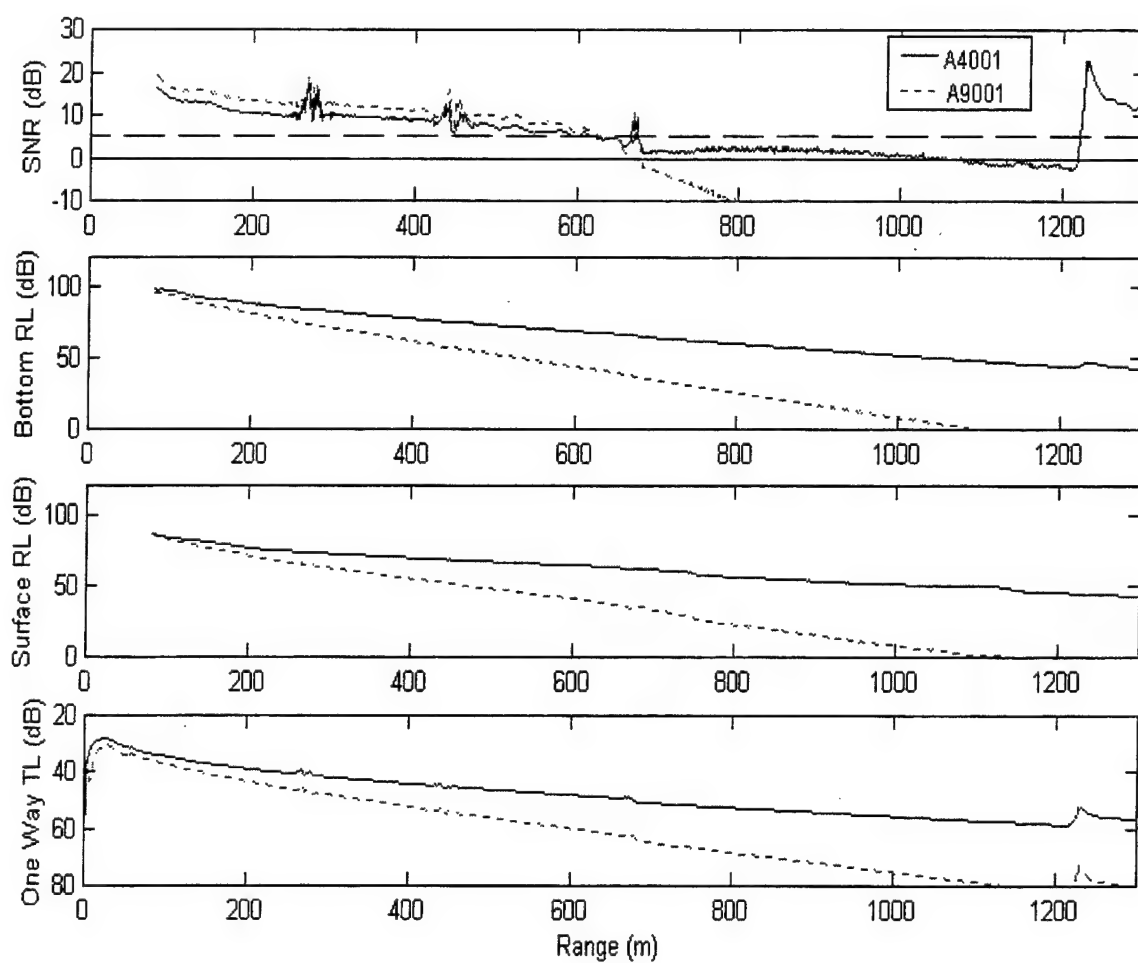


Figure 42. Comparison of the 2093 sonar at 40 kHz (—) and at 90 kHz (---) over a sandy bottom in shallow water.



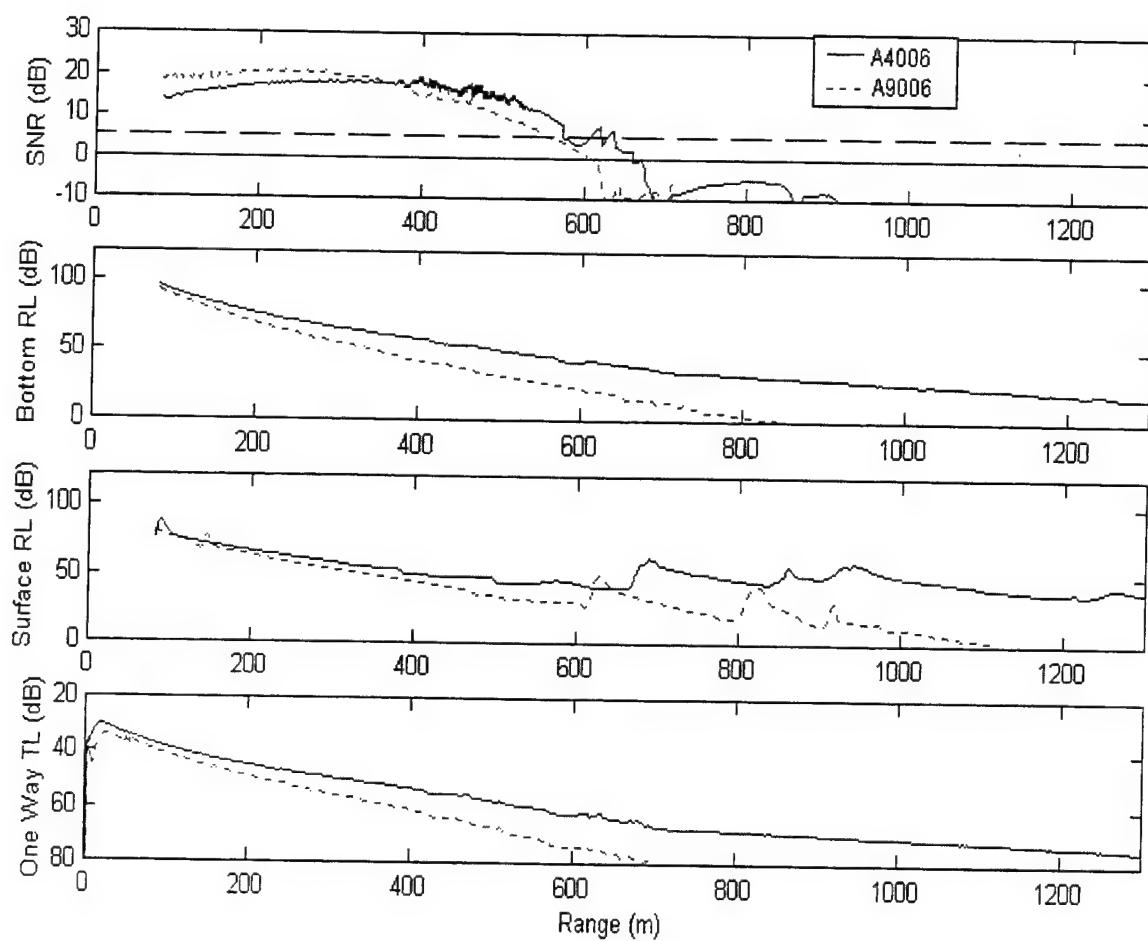


Figure 43. Comparison of the 2093 sonar at 40 kHz (—) and at 90 kHz (---) over a clay bottom in shallow water.

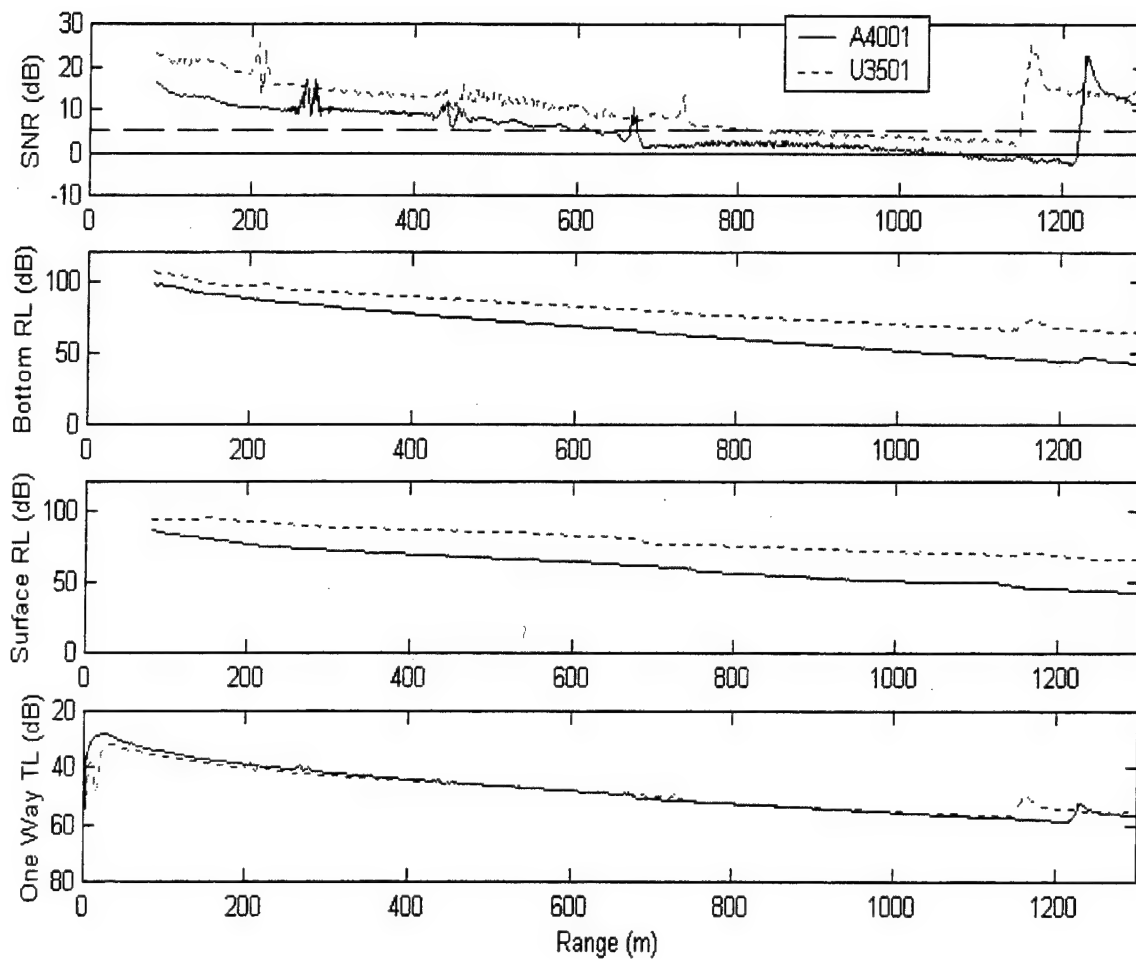


Figure 44. Comparison of the Australian Type 2093 sonar (—) and the US sonar (---) over a sandy bottom.

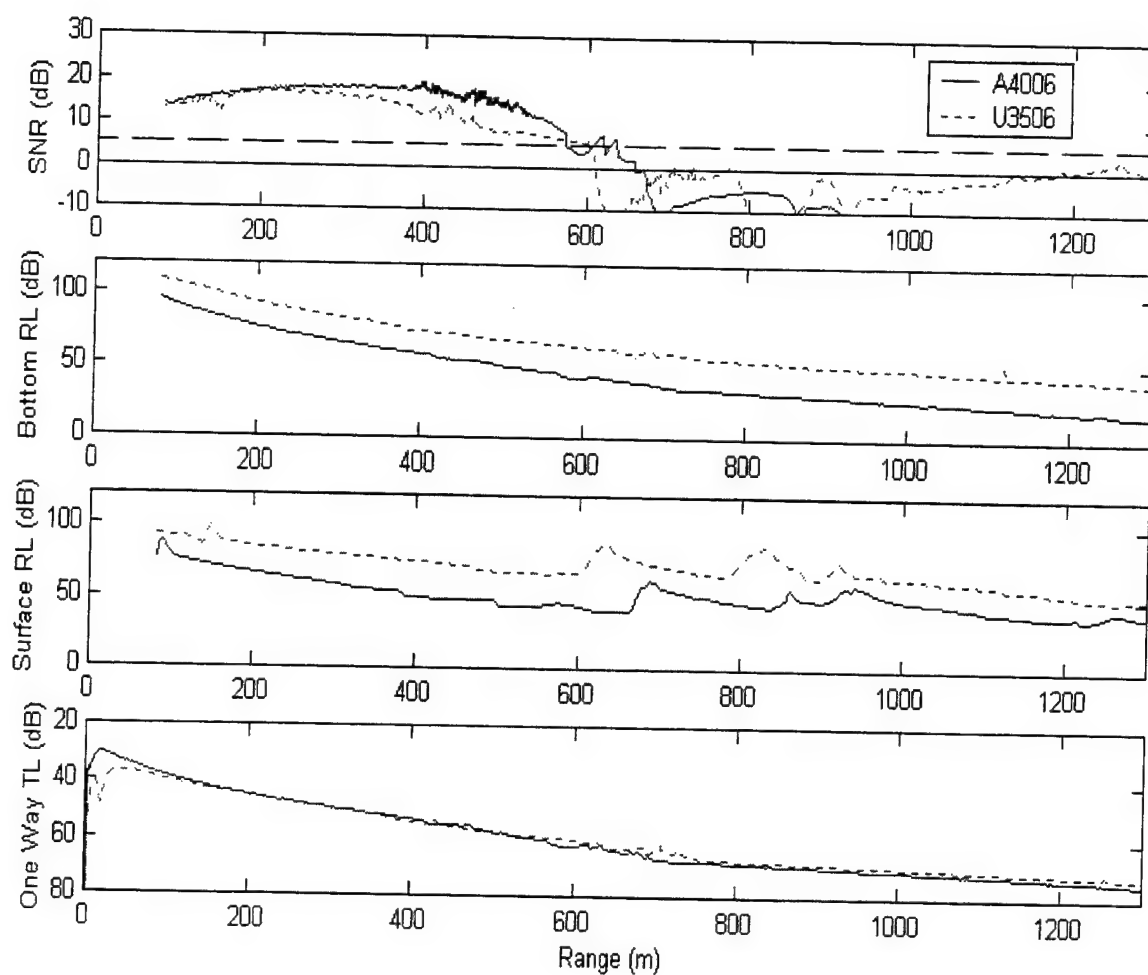


Figure 45. Comparison of the Australian Type 2093 sonar (—) and the US sonar (---) over a clay bottom.

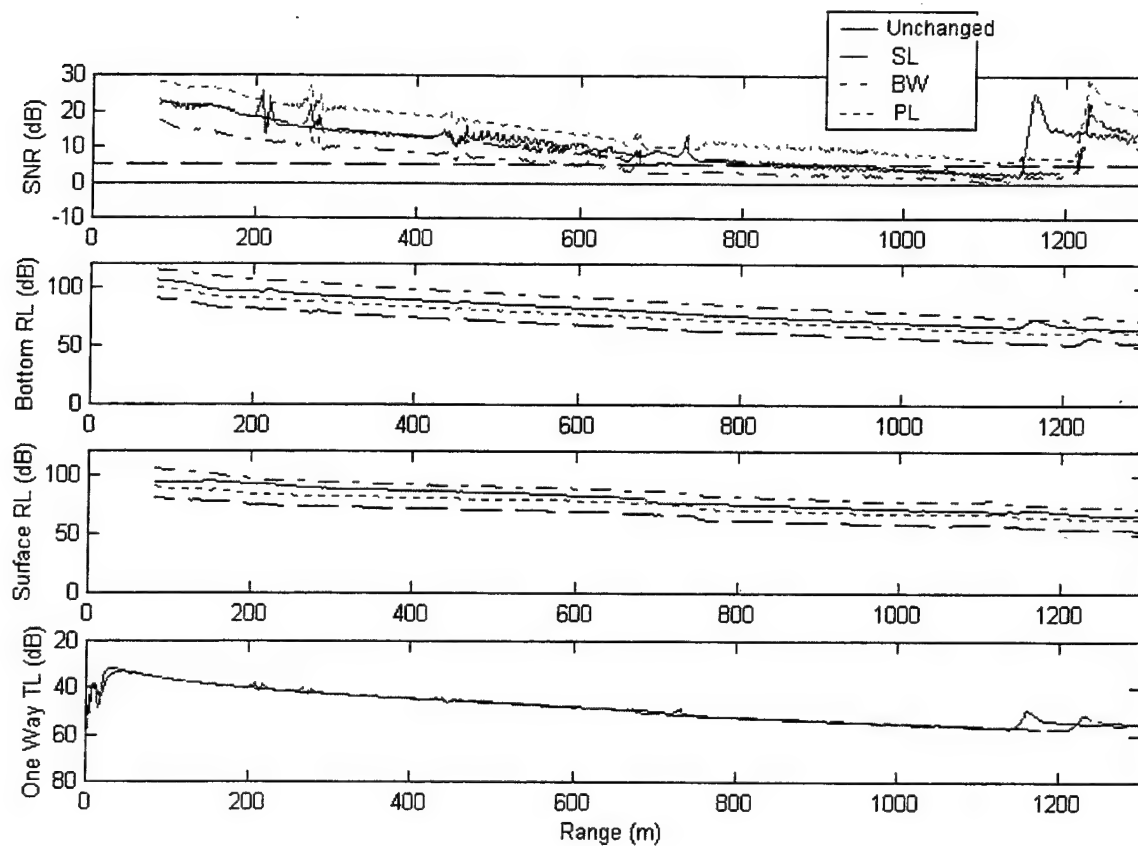


Figure 46. Analysis of the US sonar over a sandy bottom, comparing the three sonar parameters of source level, beamwidth and pulse length against the baseline parameters listed in Table 6.

Run No.	U35			A40			A90		
	a.	b.	c.	a.	b.	c.	a.	b.	c.
1	-	80/827	9660	1032	80/677	5399	680	80/674	6577
2	-	629/1300	8136	281	-	-	328	80/231	672
3	560	153/581	3351	357	80/303	1719	357	80/365	2446
4	350	-	-	307	80/189	500	345	80/303	1142
5	821	189/638	3438	340	80/285	1610	495	80/356	2377
6	612	80/602	6663	660	80/638	8225	604	80/554	7858
7	383	-	-	460	80/416	1770	266	-	-
8	1258	326/1255	18749	1259	80/1180	13602	1004	80/968	7872
9	892	126/854	7391	891	80/518	4680	672	80/524	6674
10	-	80/1300	12772	1224	80/542	2947	658	80/593	4584
11	-	159/1060	11038	1073	80/1057	8018	753	80/677	7827
12	-	-	-	134	80/461	2504	-	-	-
12	-	-	-	-	80/1300	31454	-	-	-

Table 10. The Results from the SWAT Runs.

## **V. CONCLUSIONS AND RECOMMENDATIONS**

### **A. CONCLUSIONS**

The ocean environment impacts mine warfare sonar performance to such a high degree that having detailed information on its temporal and spatial variability for a given location is a distinct advantage. Thus the aim of this thesis was to investigate a shallow coastal region to compile a detailed environmental picture of its sediment composition and water characteristics and from this model sonar performance as a means to determine what parameters (both sonar and environmental parameters) exerted the greatest effect on performance.

The region examined was the shelf adjacent to Panama City, referred to as the Panama City shelf, where the MIW component of FBE-H was conducted during August-September, 2000. Sediments in the region where MCM was conducted are comprised of well-sorted sand, grading from fine sand inshore to coarse sand offshore. In contrast to this shelf of relatively uniform sediments, the nearby Mississippi-Alabama shelf shows high variability in sediment composition, with clay, sand and regions of mixed sediments (clay and silt with sand) present. This allowed a comparison of the Panama City fine sand with clay in shallow depth regions, and coarse sand on the Panama City shelf with muddy sand. The sound speed profiles for both regions typically display a near isospeed character or a weak negative sound speed gradient in shallow regions year round. A shallow mixed layer, extending to 30 to 40 m in the fall, is frequently observed to shoal to 20 m in the spring. The proximity of the Mississippi River and the rivers feeding into

Mobile Bay provide a source of low salinity water to the Mississippi-Alabama shelf year round, affecting the SSP most notably in the spring when high precipitation or flood conditions cause a significant increase in the freshwater input onto the shelf.

Two water depths were considered, 15 m and 80 m, both contained in the Shallow Water region as defined in MCM depth regimes. Mines typical for these water depths are either moored above the seafloor at various depths in the water column, or located on the sea bottom, both proud and buried, all of which were modelled for this study.

The performance of two mine hunting sonars was compared, allowing for an investigation of which sonar parameters had an influence on sonar performance under varying environmental conditions. These sonars were the RAN Type 2093 and a USN generic MIW sonar. Of these parameters, frequency was examined closely with a comparison of the two search frequencies of the 2093 sonar, these being 40 kHz and 90 kHz.

The primary model employed to investigate the sonar performance was PC SWAT, a model designed to simulate MCM acoustic detection. A secondary model, the UK HODGSON model designed for ASW performance estimations, was selected to determine how well it could perform in an MCM scenario.

Performance was assessed using several measures of effectiveness including the signal to noise ratio (SNR) and initial detection range. Variations in these measures were analysed by investigating how TL and surface and bottom RL responded to changing environmental parameters.

From all the above options, seven sets of comparisons were undertaken, specifically examining the influence of bottom type, SSP (season), water depth/sonar depth, target location, frequency, sonars and models on performance estimates of mine detection.

No one clear parameter was identified that affected sonar performance significantly above all others. Of the environmental parameters considered, variations in bottom type exerted the most influence on TL and RL and ultimately on sonar performance.

When conducting the model runs over sediments of different grain size (clay versus sand) the resulting sonar parameters showed a complicated response. At short ranges, less than 600 m, the high bottom RL associated with the coarser grained sediments resulted in poor performance. For ranges beyond this, the high TL of the smaller grain size sediments exerted the greatest impact, with the higher TL reducing both the SNR and the RL levels for this run. For sediments that show less differences (e.g., coarse sand versus muddy sand) the bottom RL displays differences between the two bottom types whereas little difference is detected in the TL curves. From these comparisons bottom RL is seen as the more sensitive term over the wider range of bottom types. However TL is clearly a significant factor when the bottom type is comprised of absorptive, fine-grained material which limits the range of detection.

When the water column is not under the influence of significant freshwater input, the near spatial homogeneity of the SSP throughout the year causes sonar performance to



be essentially invariant between seasons, achieving an initial detection range of 660 m over a clay bottom. With the introduction of a freshwater layer at the surface, often due to spring flooding, the resulting sonar performance is seriously degraded with a cross layer situation restricting detection, reducing the initial detection range to 460 m and resulting in a weaker returned signal. The limiting factors are surface RL and the concentration of acoustic energy in the upper layer, with less energy penetrating into the lower layer where the mine is located.

Sonar performance was better in shallow water (15 m) than deep water (80 m). Both TL and RL were seen to be higher in deep water, restricting detection ranges to approximately one third of that in shallow water. The depth of the source is an important factor as a thermocline or halocline is often present causing a cross layer situation to arise when the sonar is hull mounted. When the sonar is placed below the thermocline (or in the same layer as the target) performance improves dramatically, from fluctuating detections over a short range of 500 m to strong continuous detection over 1300 m.

The detection of moored mines was rather poor at short ranges (<500 m) due to the downward orientation of the sonar beams, with TL and RL similar to that for bottom mines. At ranges greater than 500 m, the detection of moored mines became substantially better than that for bottom mines, as the number of multi-path returns resulted in more energy in the water column (less TL), permitting detection of mines moored at depths substantially above the seafloor. As expected, the detection of buried mines was substantially poorer than for unburied bottom mines. The attenuation of these high

frequency signals upon penetration into the sediment is high and is the limiting factor to detection of buried mines.

When comparing the effect of search frequencies of 40 kHz and 90 kHz on performance, TL appeared to be the most sensitive term. For MCM sonars it is expected that both TL and RL should increase with frequency and this was observed for TL. However, bottom RL was lower at the higher frequency, explained by the fact that the higher TL reduced the signal level and consequently reduced the bottom RL. The higher frequency displayed a stronger SNR than the lower frequency over short ranges, however the higher frequency was limited by TL at greater ranges with the lower frequency achieving greater initial detection ranges.

The sonar comparisons allowed the determination of which parameters associated with the source (source level, beamwidth or pulse length) affected performance. A higher source level does not necessarily result in increased performance, as the resulting increased reverberation resulted in no change in performance. Most of the differences appeared to be attributed to the increased vertical receiver beamwidth of the 2093 sonar. For runs over highly reflecting sediments such as sand, the 2093 showed poorer performance; however over an absorptive muddy bottom where the RL was lower, this sonar performed better.

The PC SWAT and HODGSON models showed similar patterns in their treatment of the input parameters, although the absolute values differed in most cases. Both models demonstrated a steeper decrease in bottom RL and an increase in TL over clay sediments

compared to sand. Consistency was also seen for changing frequency, with higher TL and a steeper decrease in bottom RL for higher frequency. These results impart confidence in the use of HODGSON for MCM performance assessments. However, as no ground truth was available to compare these two models, there is no way to determine which model provides the most accurate predictions.

## **B. RECOMMENDATIONS**

From these results it can be clearly seen that the environment dictates sonar performance. Using knowledge of the SSP to determine the depth to position the sonar provides a definite improvement in detection and thus collection and analysis of in situ SSPs remains important. Secondly, and possibly more importantly, knowledge of the bottom composition is crucial for planning operations and the collection of such information to create extensive data bases will provide future exercises and, ultimately, operations with a tactical advantage.

As can be seen from this study, one can not assume that the sediment composition is homogeneous over large areas as in deep water. Over distances as small as 1 km sediments can change from highly reverberant coarse-grained sediments with lower transmission loss to fine grained sediments with lower reverberation levels and significantly increased transmission loss. Two recommendations result from the fine-scale resolution of the sediment distribution in shallow water. Firstly, range dependent models must be used to determine sonar performance. Secondly, the environment must govern the search plan in mine hunting, in contrast to current methods where all areas are searched with a constant width regardless of sediment composition.

Finally, to further this study, two additional recommendations are made. The model comparison should be extended to regions of bottom types not examined in this thesis. The second and more important recommendation is that the results achieved here should be compared with ground truth information to assess the absolute performance of the models used. Ideally this would occur with results achieved during FBE-H to compare actual detection ranges. However, to compare with any ground truth information of similar sediment characteristics would begin to provide validation of these results.

THIS PAGE INTENTIONALLY LEFT BLANK

## LIST OF REFERENCES

- Anstee, S., Defence Science and Technology Organisation, Australia, email correspondence with the author, May – September 2000.
- Antoine, J. W., "Structure of the Gulf of Mexico", in *Contributions on the Geological and Geophysical Oceanography of the Gulf of Mexico*, Rezak, R., and Henry, V. J., editors, Gulf Publishing Company, Houston, 1972.
- Applied Oceanography and Meteorology Center (AOMC), Royal Navy. *Training Publication in Oceanography and Acoustics for Mine Warfare*, 1999.
- Blanton, J., "US Southeast Continental Shelf Inner Shelf Processes Relevant to the Northeastern Gulf of Mexico Inner Shelf", in *Northeastern Gulf of Mexico Physical Oceanography Workshop. Proceedings of a Workshop held in Tallahassee, Florida*, Clarke A. J., editor, 131-137, 5-7 April 1994.
- Boehme, H., Chotiros, N. P., Rolleigh, L. D., Pitt, S. P., Garcia, A. L., Goldsberry, T. G., and Lamb, R. A., "Acoustic Backscattering at Low Grazing Angles from the Ocean Bottom. Part I. Bottom Backscattering Strength." *J. Acoust. Soc. Am.*, 77, 962-974, 1985.
- Boicourt, W. C., Wiseman, W. J., Valle-Levinson, A. and Atkinson, L. P., "Continental Shelf of the Southeastern United States and the Gulf of Mexico: in the shadow of the Western Boundary Current", Chap. 6. in *The Sea, Vol. 11, The Global Coastal Ocean: Regional Studies and Syntheses*, Robinson, A. R., and Brink, K. H., editors, Wiley, New York, 1998.
- Briggs, K. B., "High-Frequency Acoustic Scattering from Sediment Interface Roughness and Volume Inhomogeneities." Naval Research Laboratory, Mississippi, Report no. NRL/FR/7431- -94-9617, December 1994.
- Brink, K. H., "Report of the Mid-Shelf Working Group", in *Northeastern Gulf of Mexico Physical Oceanography Workshop. Proceedings of a Workshop held in Tallahassee, Florida*, Clarke A. J., editor, 187-190, 5-7 April 1994.
- Brown, L. K., "Mine Countermeasures and Amphibious Operations, A Line in the Sea?" unpublished paper submitted to the Department of Operations, Newport, June 1991.
- Bryant, W. R., Lugo, J., Cordova, C. and Salvador, A., "Physiography and Bathymetry", in *The Geology of North America, Vol. J, The Gulf of Mexico Basin*, Salvador, A., editor, 13-28, The Geological Society of America, Austin, 1991.

- Bunchuk, A. V., and Zhitkovskii, Y. Y., "Sound Scattering by the Ocean Bottom in Shallow-Water Regions", *Soviet Physics - Acoustics*, 26, 363-370, 1980.
- Chapman, R. P., Bluy, O. Z., and Hines, P. C., "Backscattering From Rough Surfaces and Inhomogeneous Volumes", in *Encyclopedia of Acoustics*, Crocker, M. J., editor, Vol. 1, Chapter 40, John Wiley & Sons, Inc., New York, 1997.
- Clarke, A. J., "Overview of the Physical Oceanography of the Florida Shelf in the Study Region", in *Northeastern Gulf of Mexico Physical Oceanography Workshop. Proceedings of a Workshop held in Tallahassee, Florida*, Clarke, A. J., editor, Minerals Management Service Report OCMMS94-0044, 17-33, 5-7 April 1994.
- Coleman, J. M., Roberts, H. H., and Bryant, W. R., "Late Quarternary Sedimentation", in *The Geology of North America, Vol. J, The Gulf of Mexico Basin*, Salvador, A., editor, The Geological Society of America, Austin, 1991.
- COMINEWARCOM TACMEMO MZ6000-01-99, *Mine Warfare Campaign Plan Route Survey Databases*, 1999.
- Dinnel, S.P., Wiseman, W.J., and Rouse, L.J., *Coastal Currents in the Northern Gulf of Mexico: Dixie Country, Florida to the US - Mexico Border*, Minerals Management Service Report OCMMS97-0005, April 1997.
- Department of the Navy, *U.S. Naval Mine Warfare Plan, Fourth Edition*, Programs for the New Millennium, Department of the Navy, Washington, DC, January 2000.
- Doyle, L. J. and Sparks, T. N., "Sediments of the Mississippi, Alabama and Florida (MAFLA) Continental Shelf." *J. Sedimentary Petrol.*, 50, 3, 905-916, 1980.
- Elliot, B. A., "Anticyclonic Rings in the Gulf of Mexico", *J. Phys. Oceanogr.*, 12, 1292-1309, 1982.
- Fleischer, P. and Sawyer, W. B., "Environmental Characterization of Proposed Experiment Site off Panama City Beach, Florida" in *High Frequency Sound Interaction in Ocean Sediments*.  
[<http://www.apl.washington.edu/hfsa-dri/Fleischer.html>] 2 July 1999.
- Friedman, N., *The Naval Institute Guide to World Naval Weapon Systems*, p 331, U.S. Naval Institute, Annapolis, Maryland, 1997
- Garvine, R. W., "Report of the Inner-Shelf Working", in *Northeastern Gulf of Mexico Physical Oceanography Workshop. Proceedings of a Workshop held in Tallahassee, Florida*, Clarke A. J., editor, 179-183, 5-7 April 1994.

- Gerken, L. C., *Mine Warfare Technology*, 220-222, American Scientific Corp., Chula Vista, 1989,
- Gill, A. E., *Atmosphere – Ocean Dynamics*, Vol. 30, Academic Press, San Diego, 1982.
- Gilluly, J., Waters, A. C., and Woodford, A. O., *Principles of Geology*, Third Edition, W.H. Freeman and Company, San Francisco, California, 1968.
- Hamilton, E. L., "Geoacoustic Modelling of the Sea Floor". *J. Acoust. Soc. Am.*, 68, 5, 1980.
- Hamilton, E. L., "Geoacoustic Model of the Sea Floor", in *Physics of Sound in Marine Sediments*, Hampton, L., editor, Plenum Press, New York, 1974 (a).
- Hamilton, E. L., "Prediction of Deep-Sea Sediment Properties: State of the Art", in *Deep Sea Sediments, Physical and Mechanical Properties*, Inderbitzen, A. L., editor, Plenum Press, New York, 1974 (b).
- Hinge, A., *Mine Warfare in Australia's First Line of Defence*, 111-114, Australian National University, Canberra, Australia, 1992.
- Hodgson, J. and Hodgson, D., *Wader User Manual*, Version 5.82, Ocean Acoustic Developments Ltd, United Kingdom, January 2000.
- Hodgson, J. and Hodgson, D., *Hodgson Engine User Guide – Annex H – 32-Bit Version*, Ocean Acoustic Developments Ltd, United Kingdom, January 2000.
- Hodgson, J., Ocean Acoustic Development Ltd, email correspondence with the author September 2000.
- Huh, O. K., Wiseman, W. J., and Rouse, L. J., "Intrusion of Loop Current Waters onto the West Florida Continental Shelf" *J. Geophys. Res.*, 86, 4186-4192, 1981.
- Jackson, D. R., Baird, A. M., Crisp, J. J., and Thomson, P. A. G., "High Frequency Bottom Backscatter Measurements in Shallow Water", *J. Acoust. Soc. Am.*, 80, 4, 1188-1199, 1986.
- Jane's Underwater Warfare Systems, Watts, A. J., editor, 12<sup>th</sup> ed., Jane's Information Group, Virginia, 2000.
- Johns, M. W., "Geotechnical Properties of Mississippi River Delta Sediments Utilizing in situ Pressure Sampling Techniques", in *Handbook of Geophysical Exploration at Sea*, 2<sup>nd</sup> Edition Hydrocarbons, Geyer, R. A., editor, 353, CRC Press Inc., Texas, 1992.



- Kelly, F. J., and Vastano, A. C., "A Census of Loop Current Related Intrusions onto the Mississippi-Alabama Continental Slope and Shelf", in *Northeastern Gulf of Mexico Physical Oceanography Workshop. Proceedings of a Workshop held in Tallahassee, Florida*, Clarke A. J., editor, Minerals Management Service Report OCMMS94-0044, 87-93, 5-7 April 1994.
- Kelly, F. J., "Monitoring the Frequency and Structure of Loop Current Related Intrusions onto the Slope and Shelf in the Northwestern Gulf of Mexico", in *Northeastern Gulf of Mexico Physical Oceanography Workshop. Proceedings of a Workshop held in Tallahassee, Florida*, Clarke A. J., editor, Minerals Management Service Report OCMMS94-0044, 221-222, 5-7 April 1994.
- Kennicutt, M. C., Schroeder, W. W., and Brooks, J. M., "Temporal and Spatial Variations in Sediment Characteristics on the Mississippi-Alabama Continental Shelf", *Continental Shelf Res.*, 15, 1, 1-18, 1995.
- Komar, P. D., *Beach Processes and Sedimentation*, Second Edition, p 53, Prentice Hall Inc., New Jersey, 1998.
- Laswell, J. S., Sager, W. W., Schroeder, W. W., Davis, K. S., and Rezak, R., "High Resolution Geophysical Mapping of the Mississippi-Alabama Outer Continental Shelf", in *Handbook of Geophysical Exploration at Sea*, 2<sup>nd</sup> Edition, Hard Minerals, Geyer, R. A., editor, 167-171, CRC Press, Inc., Texas, 1992.
- Lathrop, J. D., "High Area Rate Reconnaissance (HARR) and Mine Reconnaissance/Hunter (MR/H)." [http://www.ncsc.navy.mil/CSS/papers/harrmrhspie.htm]
- Levie, H. S., *Mine Warfare at Sea*, pp. 9, Kluwer Academic Publishers, Massachusetts, 1992.
- Li, Y., Nowlin, W. D., and Reid, R. O., "Mean Hydrographic Fields and their Interannual Variability over the Texas-Louisiana Continental Shelf in Spring, Summer and Fall", *J. Geophys. Res.*, 102, C1, 1027-1049, 1997.
- Ludwick, J. C., "Sediments in Northeastern Gulf of Mexico", in *Papers in Marine Geology*, Miller, R. L., editor, 204-238, Macmillan Company, New York, 1964.
- Malley, G., Naval Oceanographic Office, email correspondence with the author, July 2000.
- McKinney, C. M., and Anderson, C. D., "Measurements of Backscattering of Sound from the Ocean Bottom", *J. Acoust. Soc. Am.*, 36, 1, 158-163, 1964.

Mooers, C. N. K., and Maul G. A., "Intra-Americas Sea Circulation", in *The Sea, Vol. 11, The Global Coastal Ocean: Regional Studies and Syntheses*, Robinson, A. R., and Brink, K. H., editors, 183-204, Wiley, New York, 1998.

National Research Council, Ocean Studies Board, *Oceanography and Mine Warfare*, National Academy Press, Washington DC, 1999.

Naval Warfare Development Command (NWDC) "Fleet Battle Experiments"  
[<http://www.nwdc.navy.mil/navigation/mbc.htm>] August 2000.

Niiler, P., "Surface Circulation of the Eastern Gulf Shelf", in *Northeastern Gulf of Mexico Physical Oceanography Workshop. Proceedings of a Workshop held in Tallahassee, Florida*, Clarke A. J., editor, Minerals Management Service Report OCMMS94-0044, 254, 5-7 April 1994.

Null, M., *Fleet Battle Experiment Hotel Sensor Data Integration*, Neptune Sciences, Inc., San Diego, 2000.

Ortner, P. B., Lee, T. N., Milne, P. J., Zika, R. G., Clarke, M. E., Podesta, G. P., Swart, P. K., Tester, P. A., Atkinson, L. P. and Johnson, W., R., "Mississippi River Flood Waters that Reached the Gulf Stream", *J. Geophys. Res.*, 100, C7, 13595-13601, 1995.

"Physics of Sound in the Sea" Summary Technical Report of Division 6, National Defense Research Committee, Volume 8, pp. 137-157, 240-243, 308-323, Washington DC, 1946.

Ruscher, P. H., "Overview of the Meteorology of the Gulf of Mexico", in *Northeastern Gulf of Mexico Physical Oceanography Workshop. Proceedings of a Workshop held in Tallahassee, Florida*, Clarke A. J., editor, Minerals Management Service Report OCMMS94-0044, 37-40, 5-7 April 1994.

Salsman, G. G., and Ciesluk, A. J., *Environmental Conditions in Coastal Waters Near Panama City Florida*, Naval Coastal Systems Center Report NCSC-TR-337-78, August 1978.

Sammelmann, G. S., *PC SWAT 6.0: Users Manual, CSS Draft Report*, Coastal Systems Station, Panama City, Florida, May 2000.

Sammelmann, G.S., Coastal Systems Station Panama City, telephone conversation with the author, 13 September 2000.

- Scanlon, G. A., Estimation of Bottom Scattering Strength from Measured and Modeled AN/SQS-53C Reverberation Levels, Master's Thesis, Naval Postgraduate School, Monterey, June 1995.
- Schalm, D. A., Inversion of Shallow Water Bottom Sediment Properties using AN/SQS-53C Reverberation Level Data from Exercise LWAD 99-1, Master's Thesis, Naval Postgraduate School, Monterey, September 1999.
- Schroeder W. W., "Buoyancy Driven Exchange and the Fate of Fresh Water Discharged onto the Mississippi-Alabama Continental Shelf: Inner to Mid Shelf Experiment", in *Northeastern Gulf of Mexico Physical Oceanography Workshop. Proceedings of a Workshop held in Tallahassee, Florida*, Clarke A. J., editor, Minerals Management Service Report OCMMS94-0044, 224-225, 5-7 April 1994.
- Schroeder W. W., Dinnel S. P., Kelly F. J., and Wiseman W. J., "Overview of the Physical Oceanography of the Louisiana-Mississippi-Alabama Continental Shelf", in *Northeastern Gulf of Mexico Physical Oceanography Workshop. Proceedings of a Workshop held in Tallahassee, Florida*, Clarke A. J., editor, Minerals Management Service Report OCMMS94-0044, 13-16, 5-7 April 1994.
- Stannic, S., Briggs, K. B., Fleischer, P., Ray, R. I., and Sawyer, W. B., "Shallow-water High-frequency Bottom Scattering off Panama City, Florida", *J. Acoust. Soc. Am.*, 83, 6, 2134-2144, 1988.
- Stannic, S., Briggs, K. B., Fleischer, P., Sawyer, W. B., and Ray, R. I., "High-frequency Acoustic Back Scattering From a Coarse Shell Ocean Bottom", *J. Acoust. Soc. Am.*, 85, 1, 125-136, 1989.
- Tomas, C. R., "Coastal Production Program and Dynamics on the West Florida Shelf", in *Northeastern Gulf of Mexico Physical Oceanography Workshop. Proceedings of a Workshop held in Tallahassee, Florida*, Clarke A. J., editor, Minerals Management Service Report OCMMS94-0044, 79-82, 5-7 April 1994.
- Tomczak, M. and J.S. Godfrey, *Regional Oceanography: An Introduction*. 1st ed. Pergamon Press, Oxford, England, 1994.
- United States Geological Survey, Report USGS/BRD/CR-1997-0008, *Northeastern Gulf of Mexico Coastal and Marine Ecosystem Program: Ecosystem Monitoring, Mississippi/Alabama Shelf; First Annual Interim Report*, January 1998.
- United States Geological Survey, Report USGS/BRD/CR-1998-0002, *Northeastern Gulf of Mexico Coastal and Marine Ecosystem Program: Ecosystem Monitoring, Mississippi/Alabama Shelf; Second Annual Interim Report*, December 1998.

- Urick, R. F., *Principles of Underwater Sound*, 3d ed., p. 19, McGraw-Hill Inc, 1983.
- Vukovich, F. M., Crissman B. W., Bushman M., and King W. J., "Some Aspects of the Oceanography of the Gulf of Mexico Using Satellite and In Situ Data." *J. Geophys. Res.*, 84, 7749-7768, 1979.
- University of Washington, *APL-UW High-Frequency Ocean Environment Acoustic Models Handbook*, Applied Physics Laboratory, Report APL-UW-TR-9407, Seattle, October 1994.
- Weinberg, H., and Keenan, R. E., "Gaussian Ray Bundles For Modeling High-frequency Propagation Loss Under Shallow Water Conditions", *J. Acoust. Soc. Am.*, 1421-1431, 100 (3), 1996.
- Winn, K., Becker, G., and Theilen, F., "The Relationship Between Sediment Parameters and the Acoustic Reflectivity of the Seabed" in *Acoustics and the Sea-Bed*, Conference Proceedings, Pace, N. G., editor, 31-38, Bath University Press, Bath UK, 1983.
- Winn, K., and Becker, G., "The influence of the Sedimentary Succession Upon the Acoustic Penetration in the Western Baltic" in *Acoustics and the Sea-Bed*, Conference Proceedings, Pace, N. G., editor, 107-113, Bath University Press, Bath UK, 1983.
- Wong, H. K., and Chesterman, W. D., "Bottom Backscattering near Grazing Incidence in Shallow Water", *J. Acoust. Soc. Am.*, 44, 1713-1718, 1968.
- Zhitkovskii, Y. Y., and Lysanov, Y. P., "Reflection and Scattering of Sound from the Ocean Bottom", *Soviet Physics - Acoustics*, 13, 1, 1-13, 1967.

THIS PAGE INTENTIONALLY LEFT BLANK

## APPENDIX A. MODEL RUNS

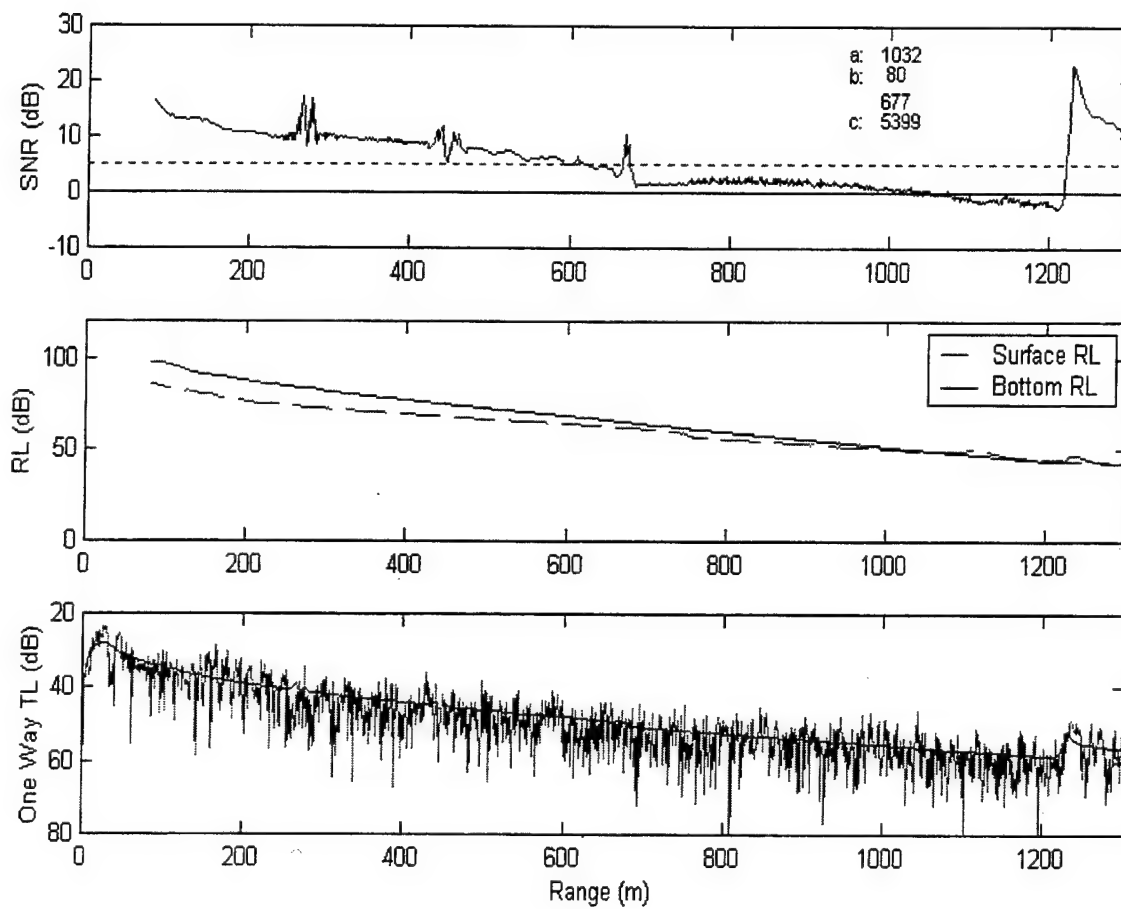


Figure A 1. S\_A40\_01

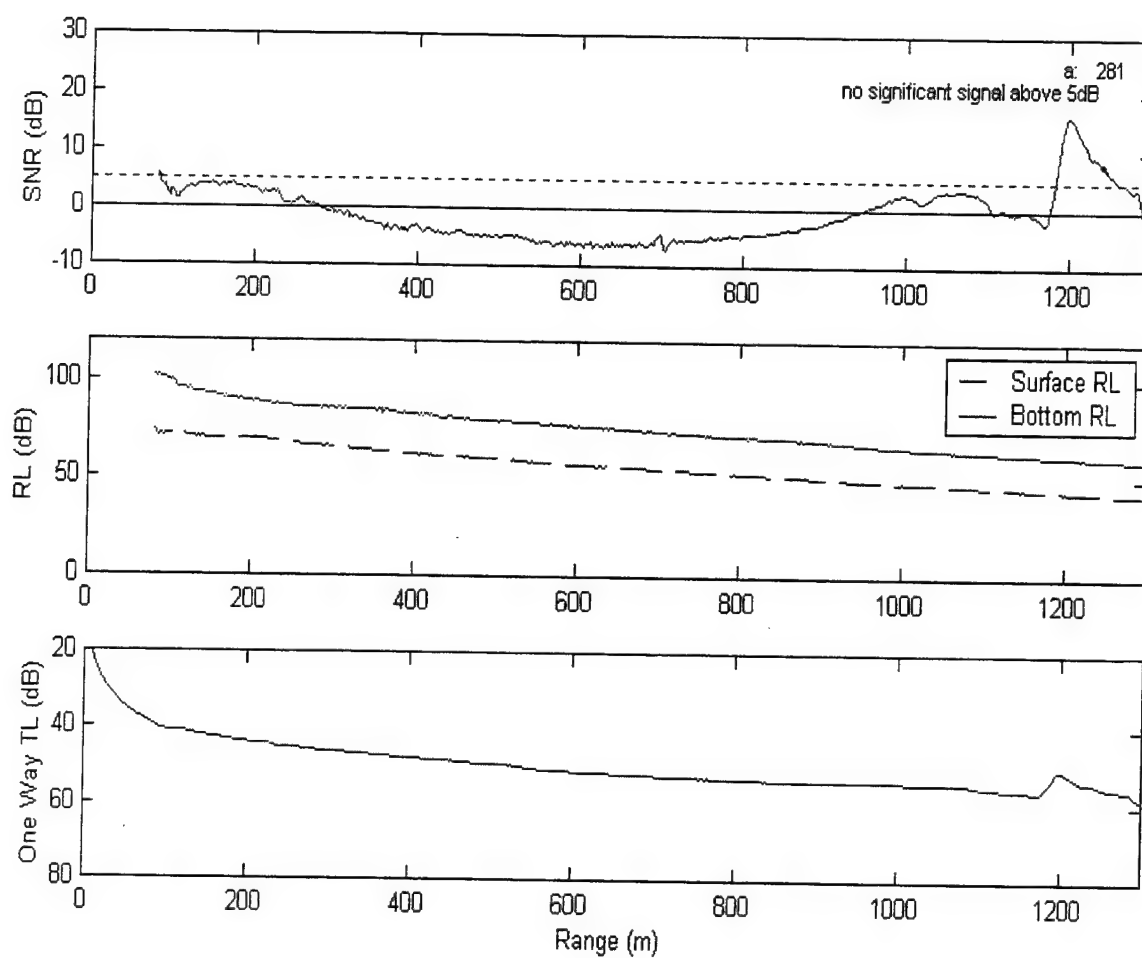


Figure A 2. S\_A40\_02

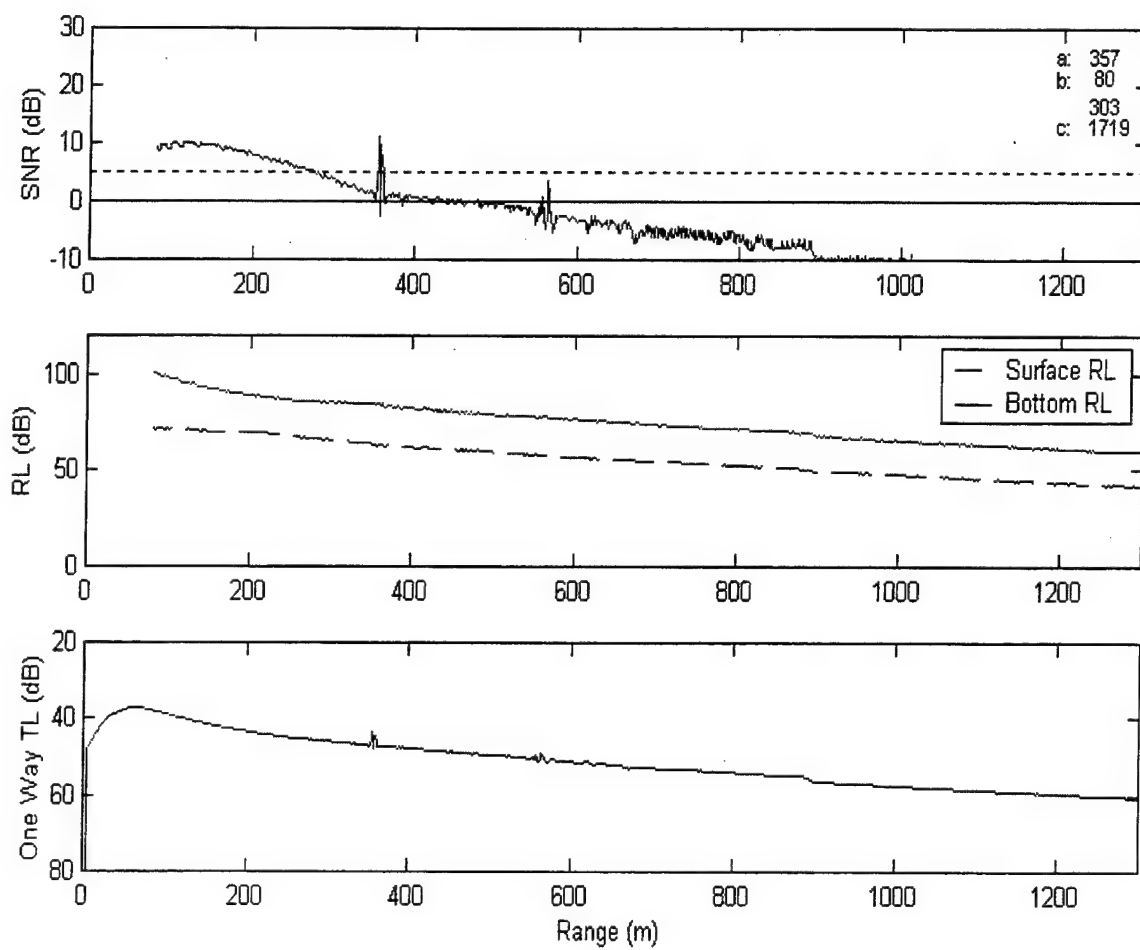


Figure A 3. S\_A40\_03



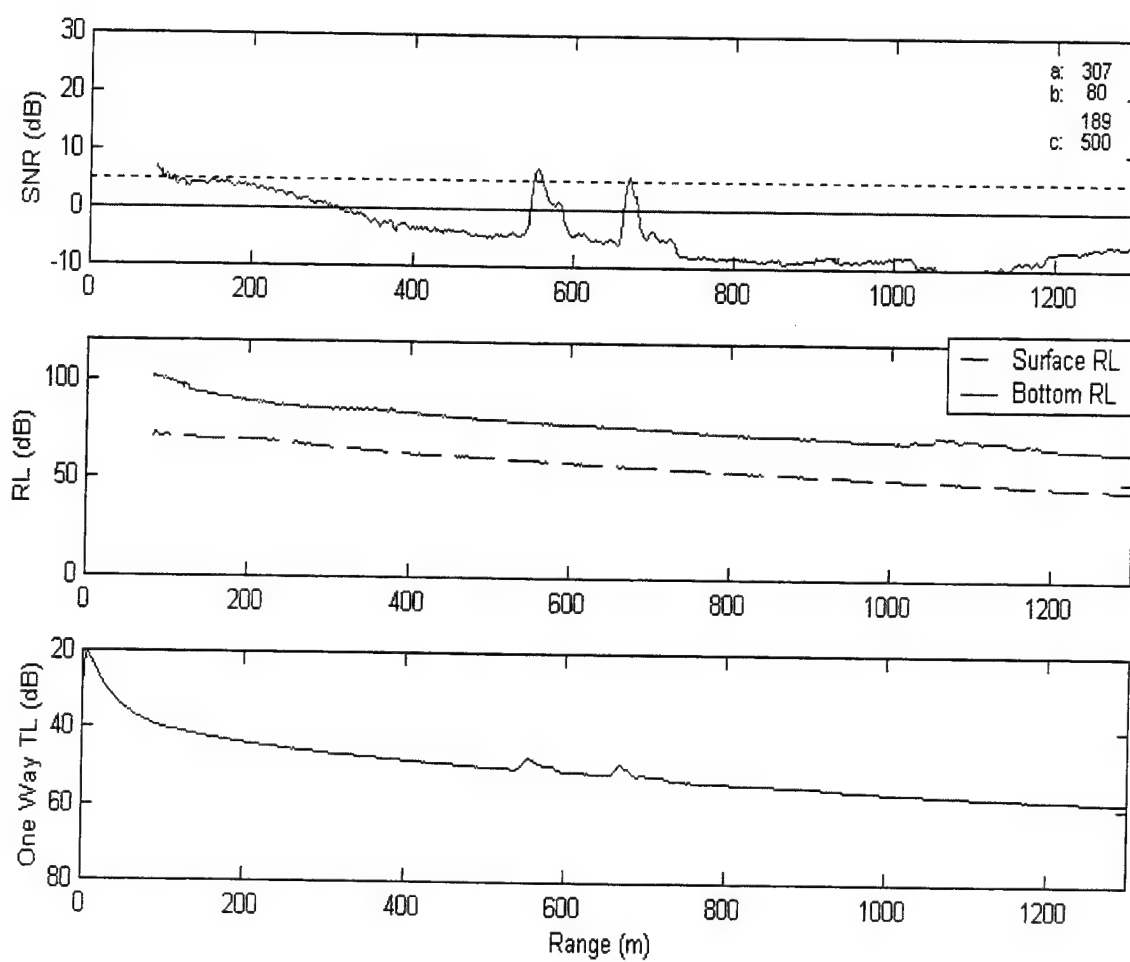


Figure A 4. S\_A40\_04

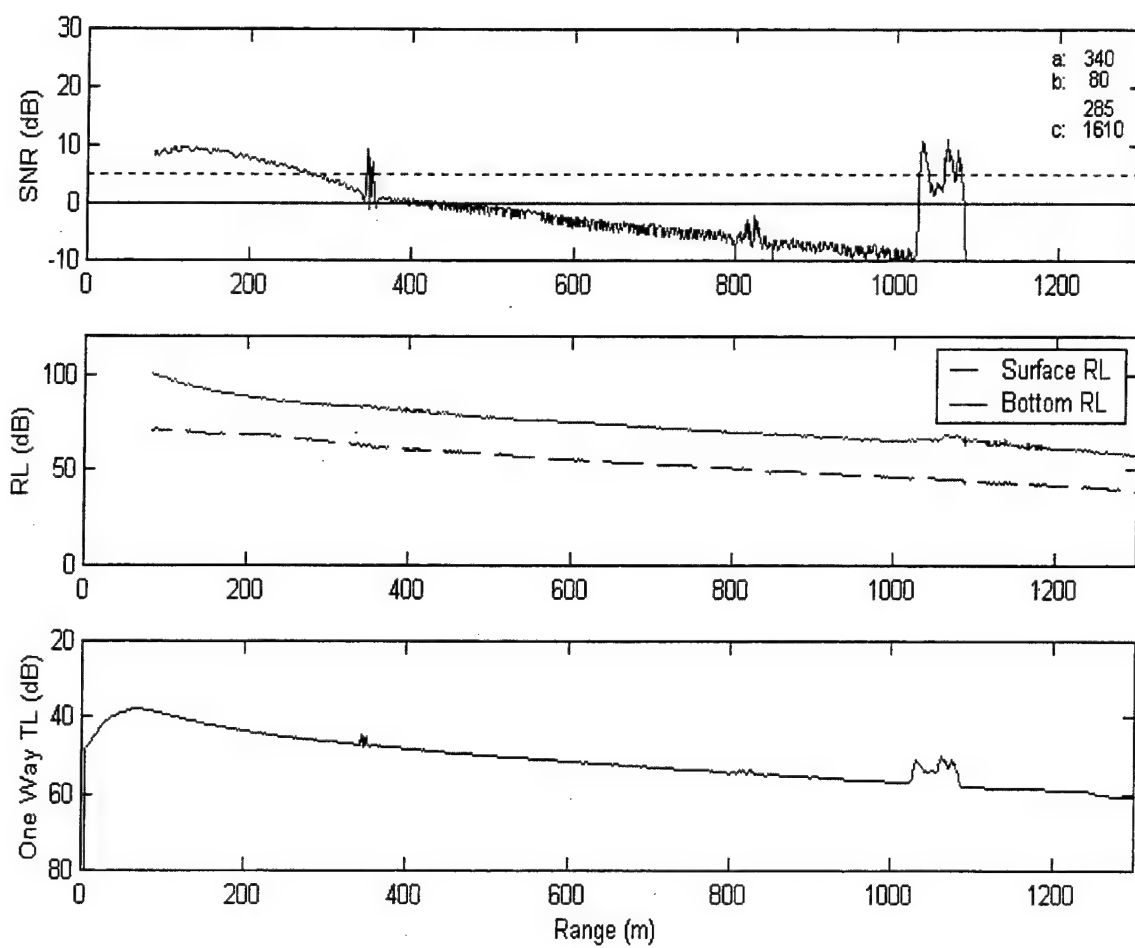


Figure A 5. S\_A40\_05

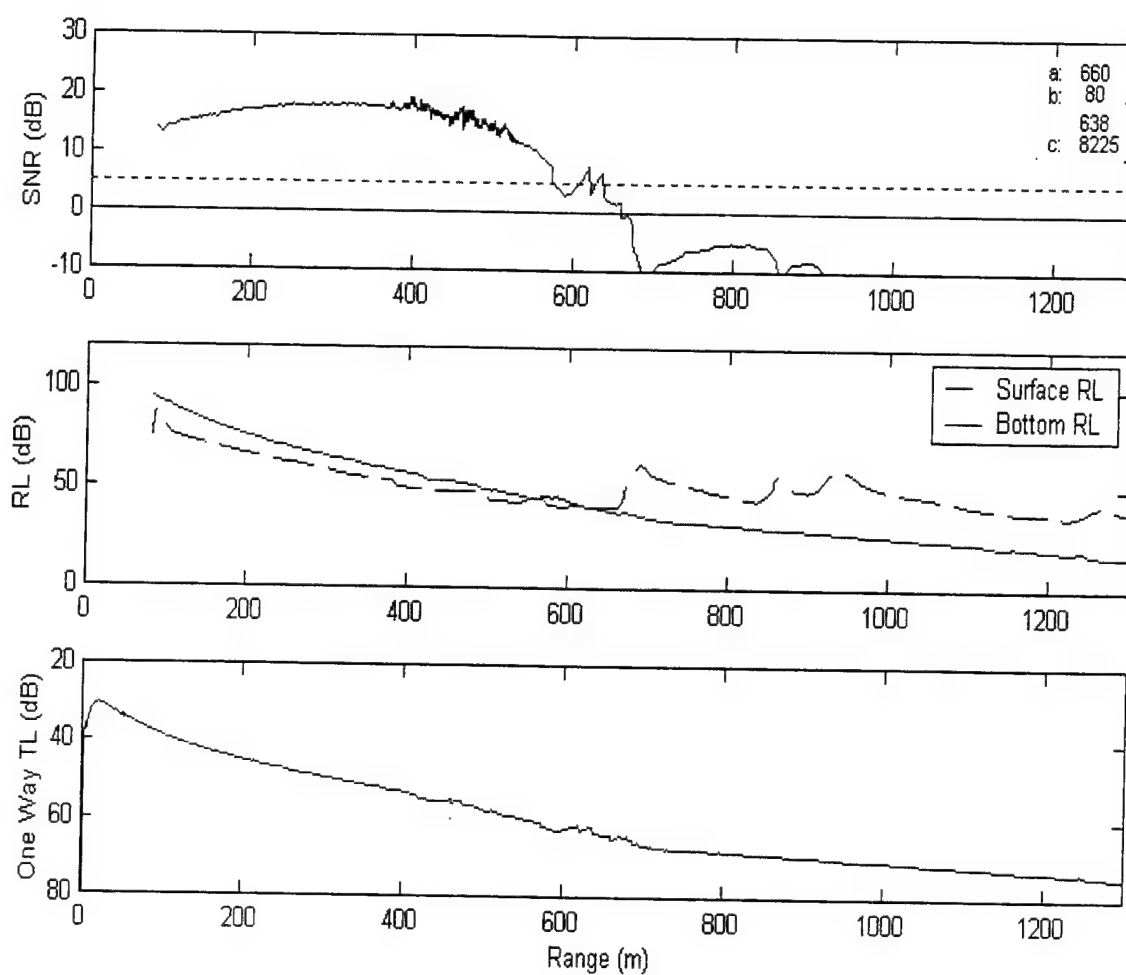


Figure A 6. S\_A40\_06

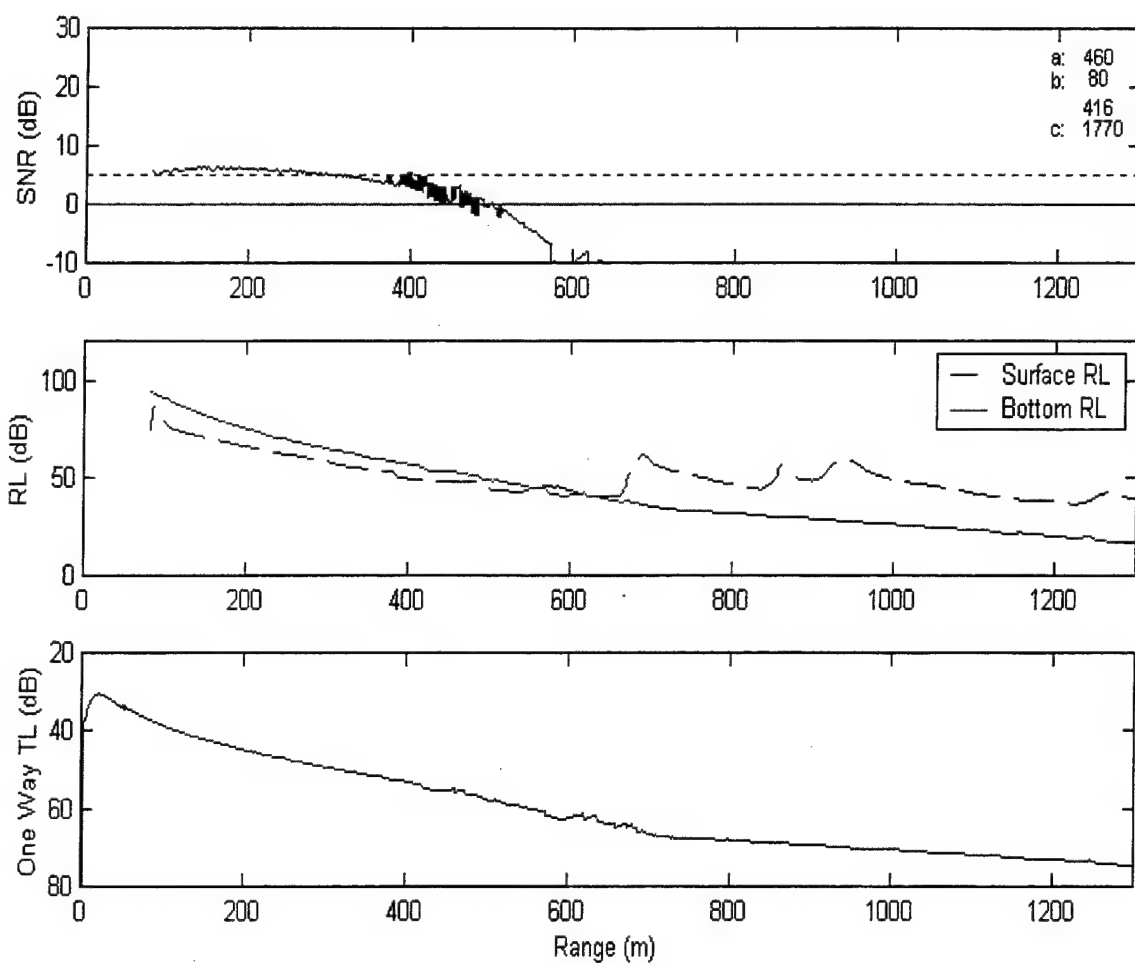


Figure A 7. S\_A40\_07

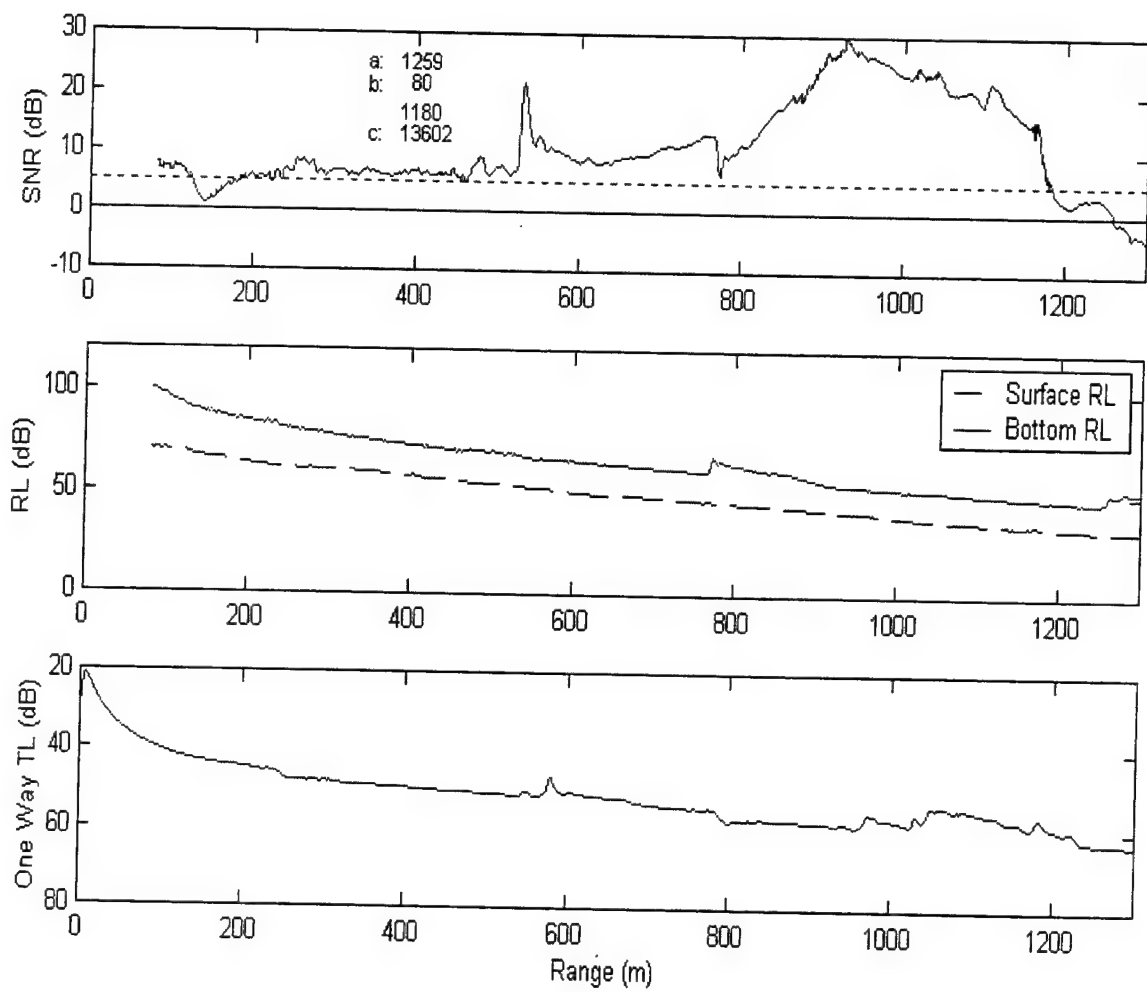


Figure A 8. S\_A40\_08

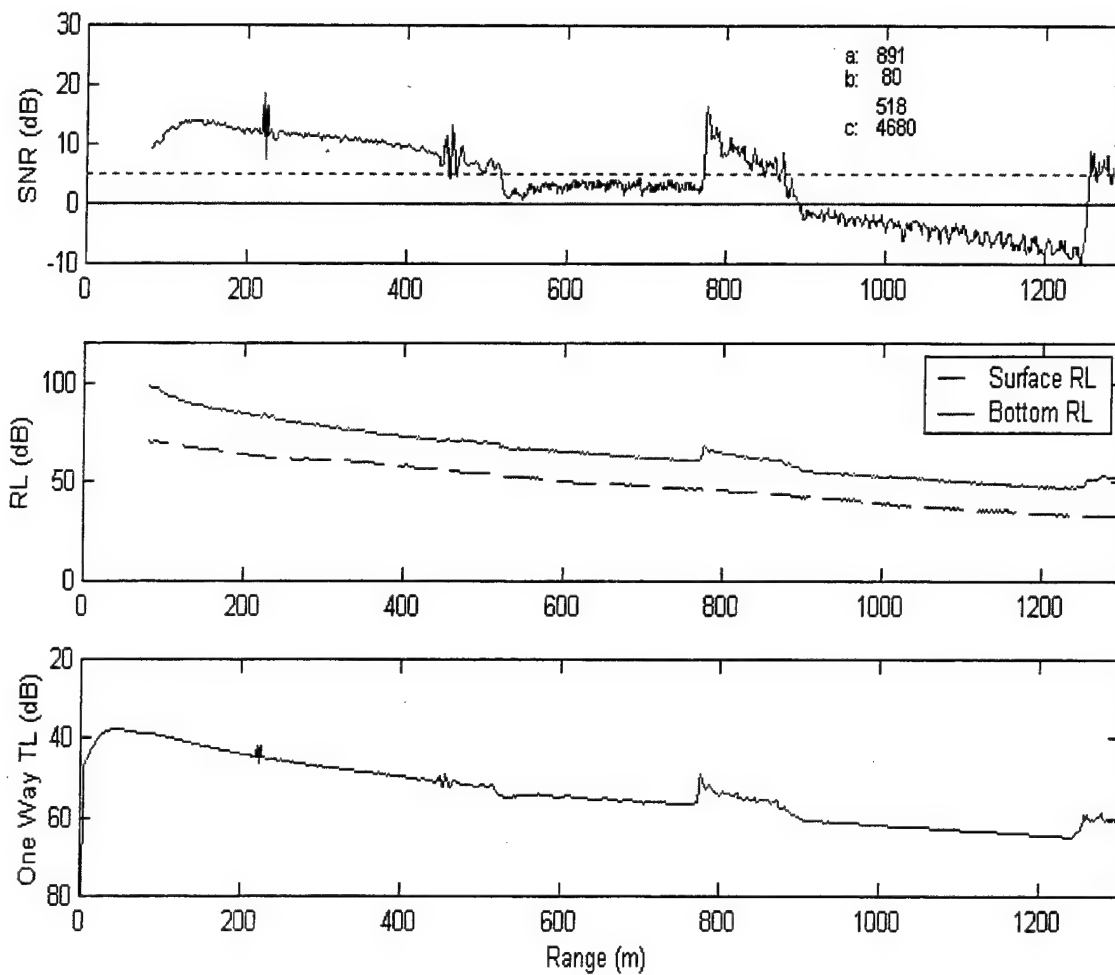


Figure A 9. S\_A40\_09

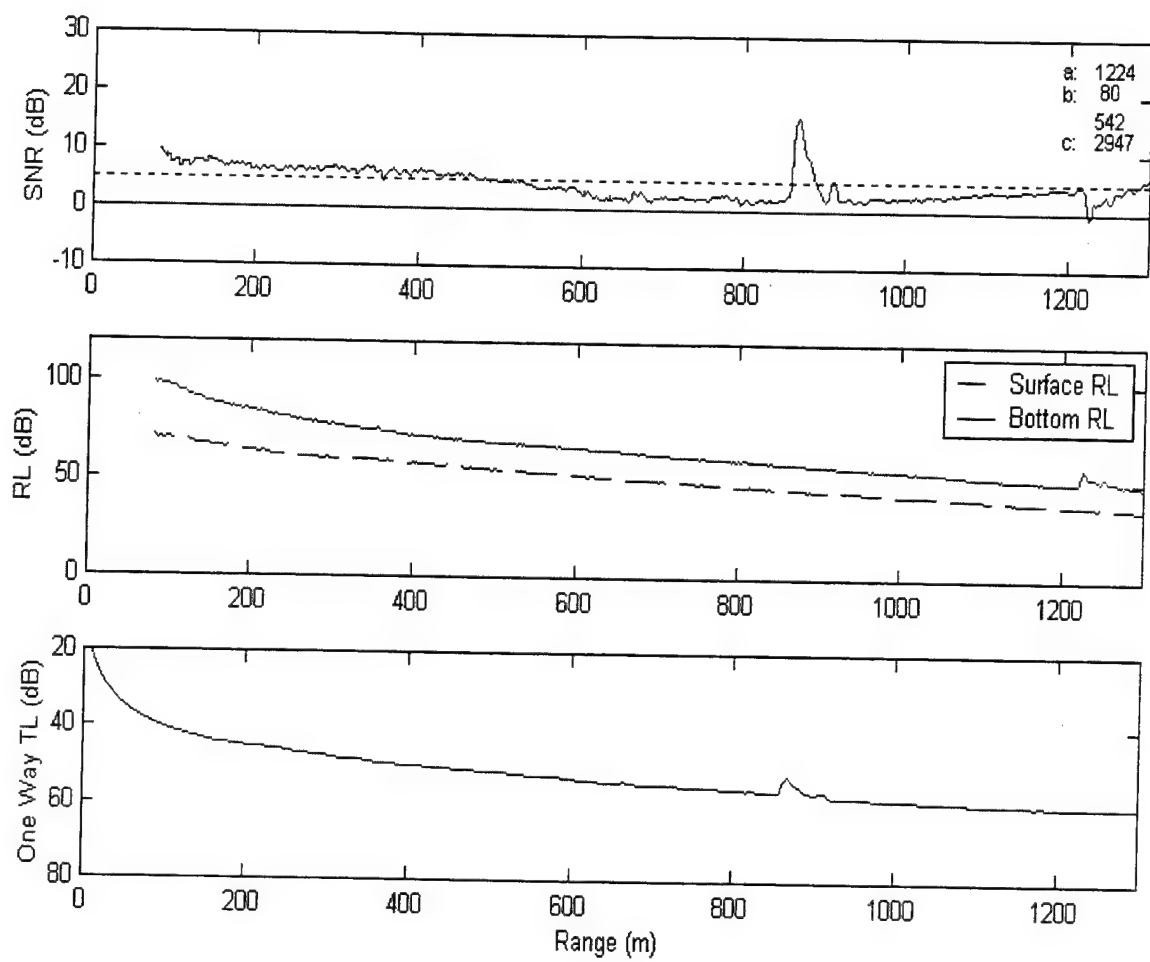


Figure A 10. S\_A40\_10

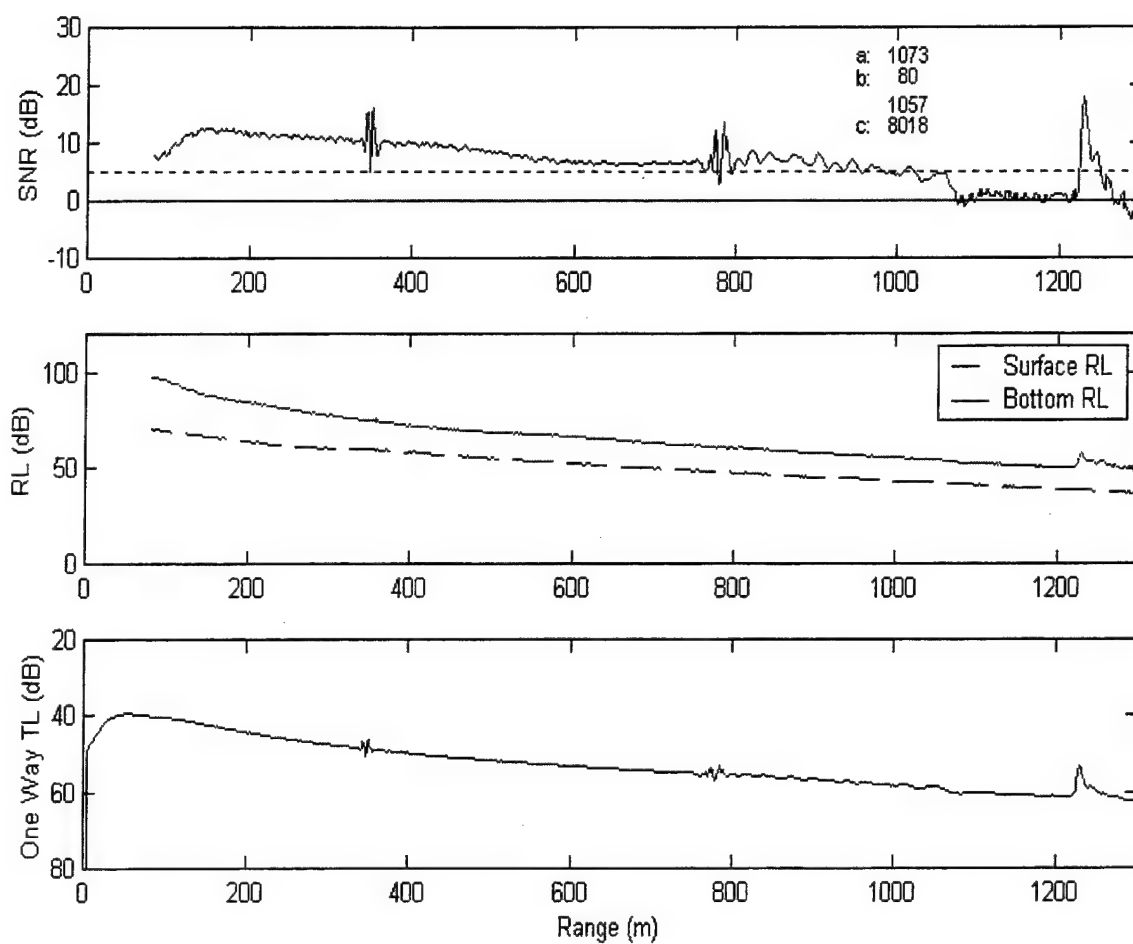


Figure A 11. S\_A40\_11



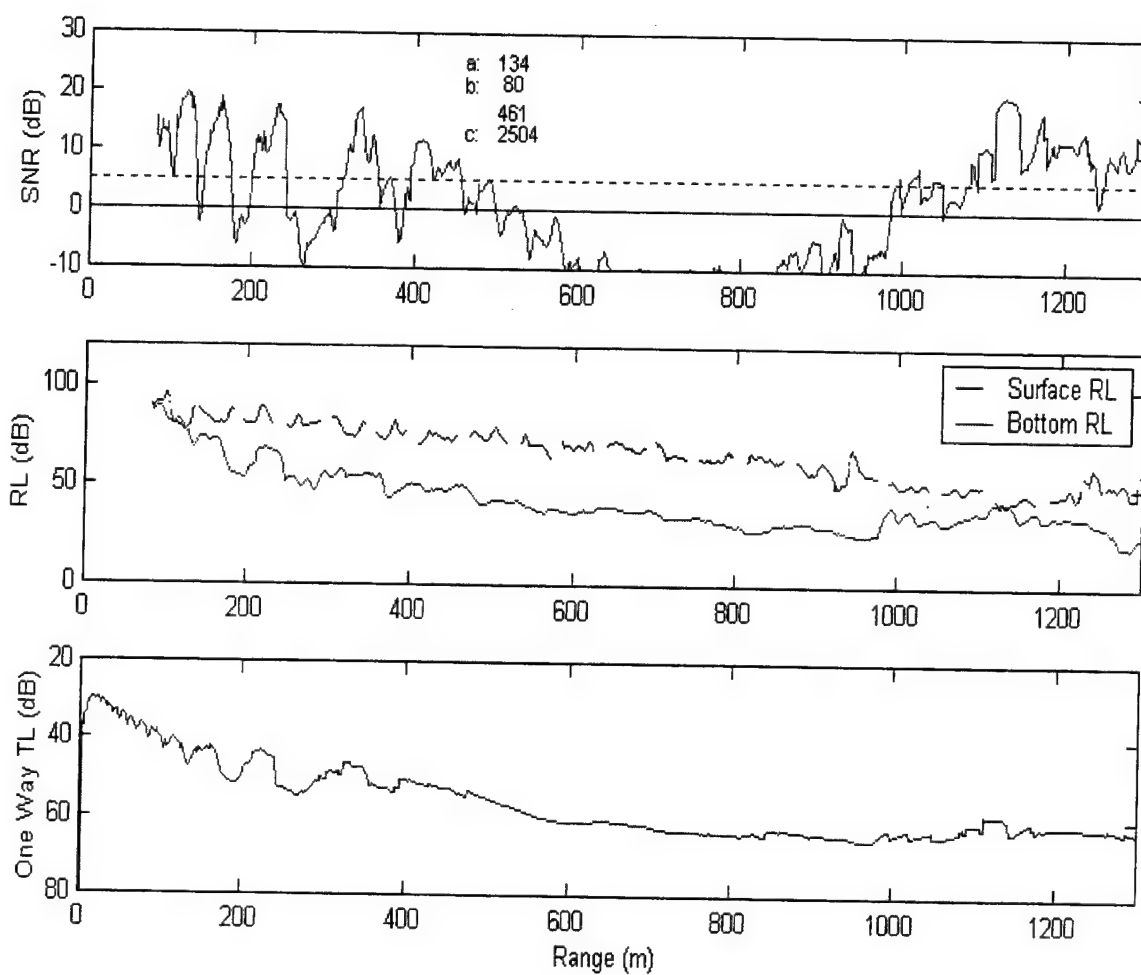


Figure A 12. S\_A40\_12

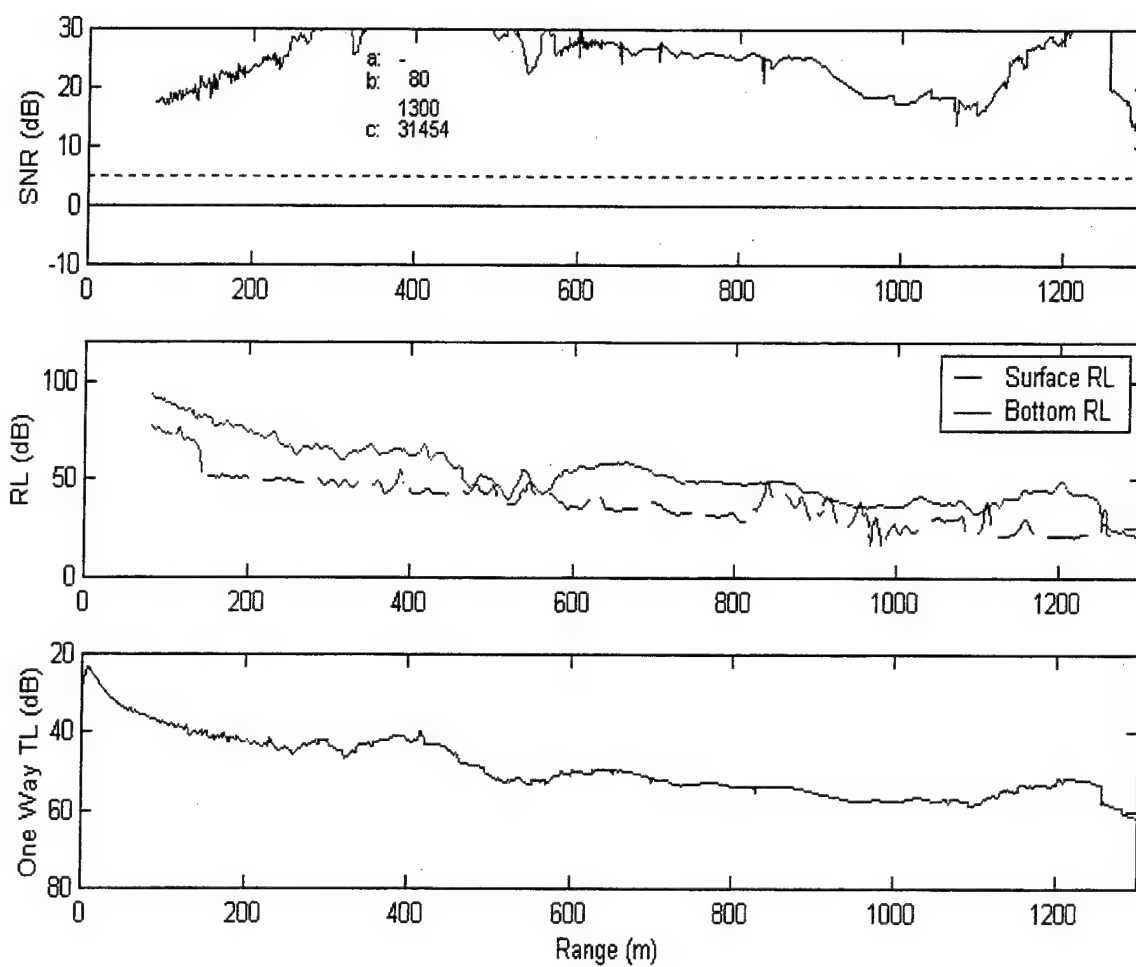


Figure A 13. S\_A40\_13

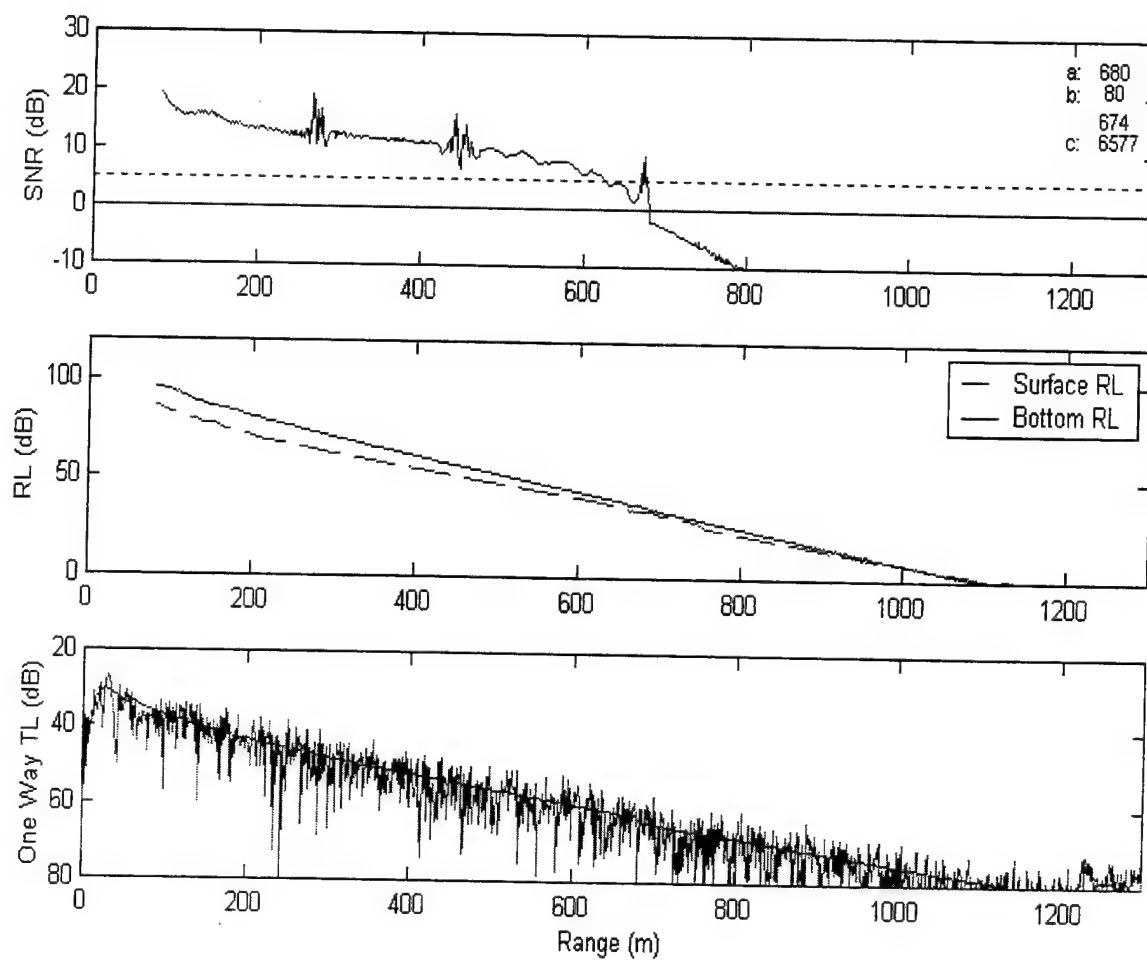


Figure A 14. S\_A90\_01

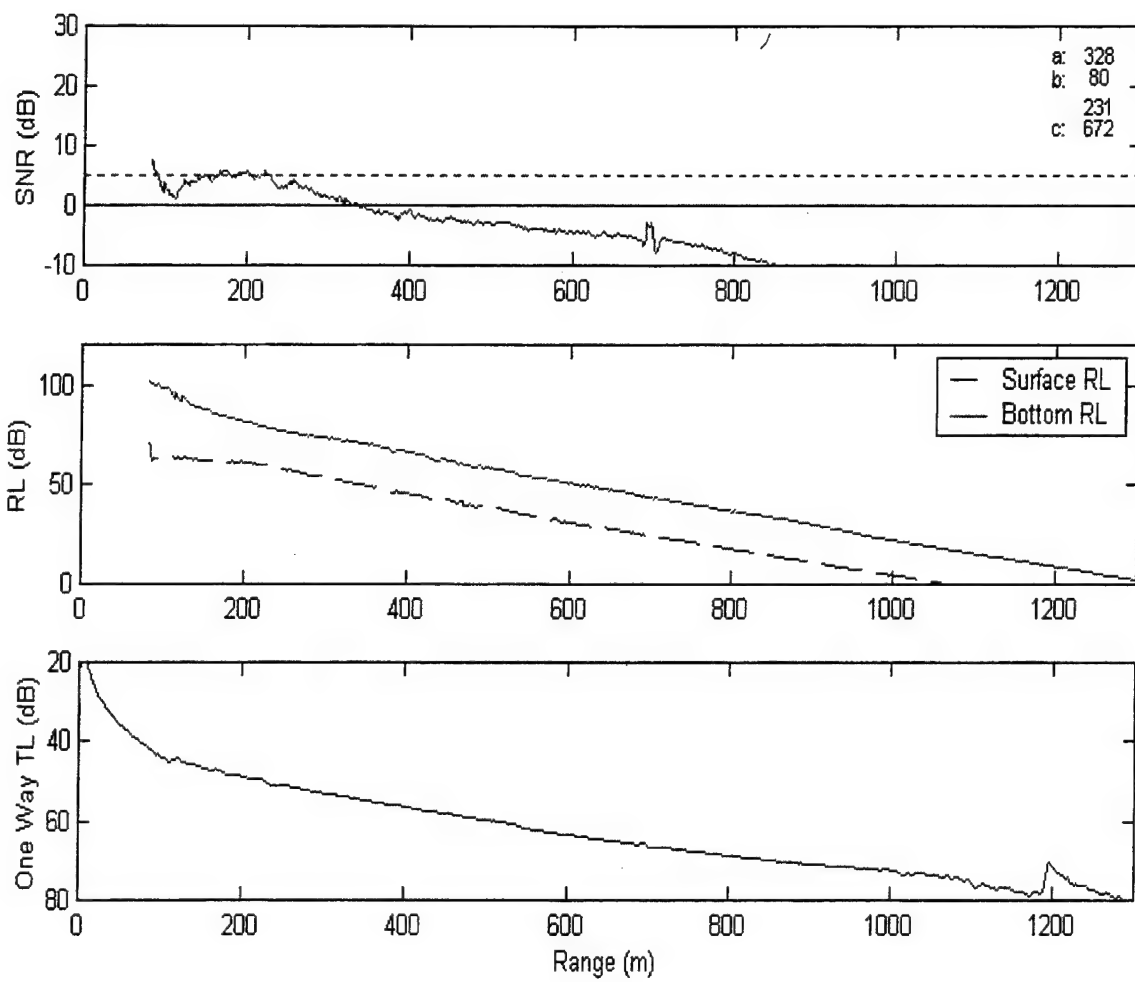


Figure A 15. S\_A90\_02

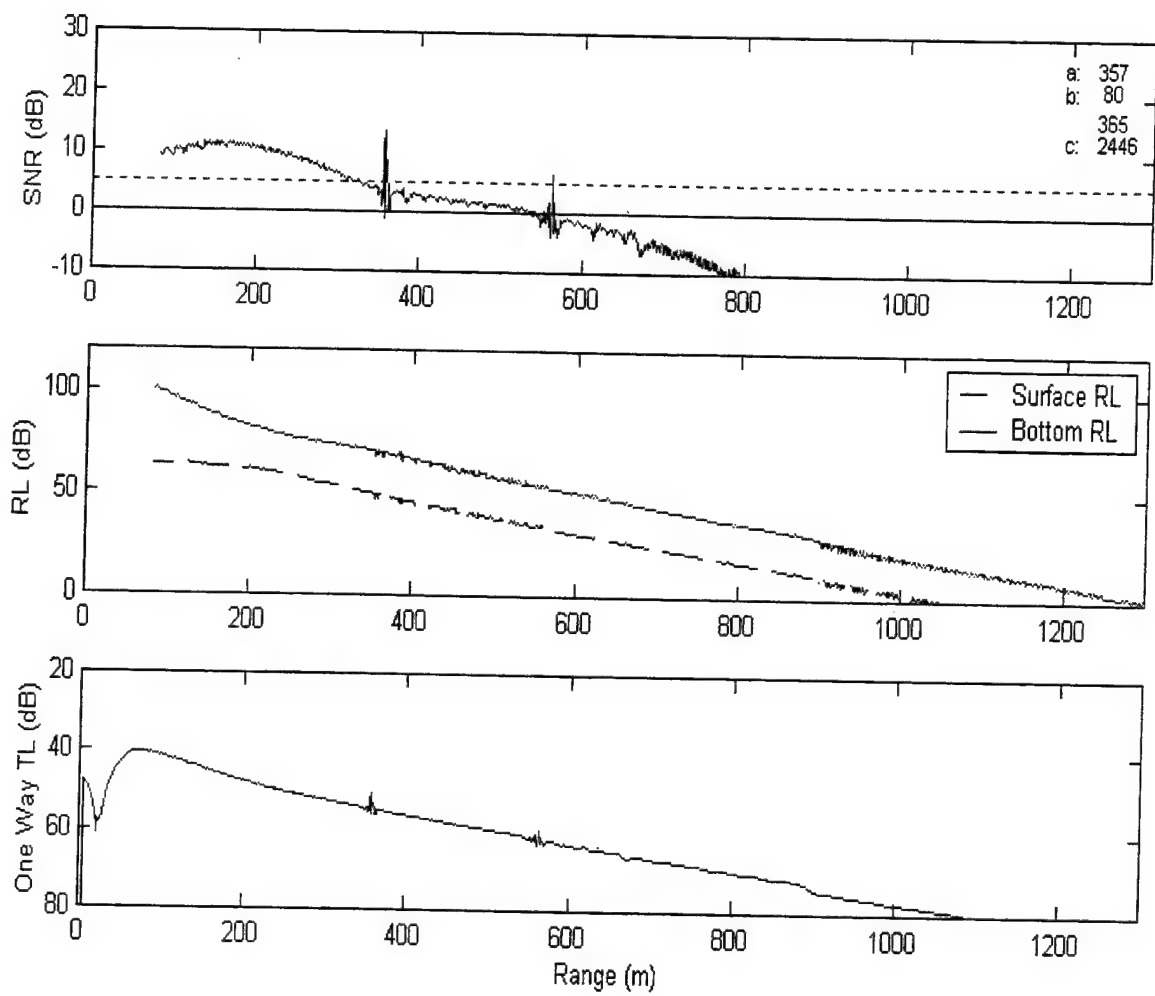


Figure A 16. S\_A90\_03

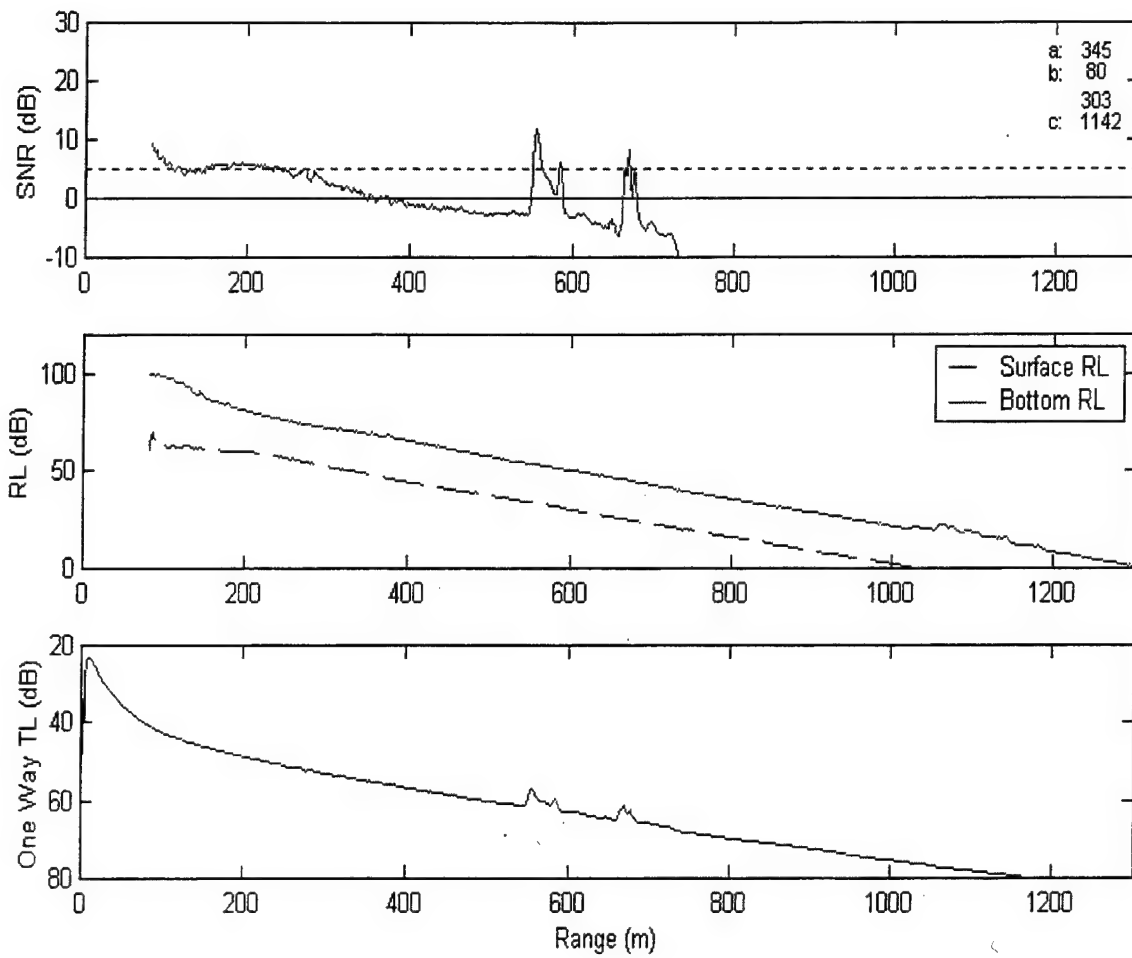


Figure A 17. S\_A90\_04

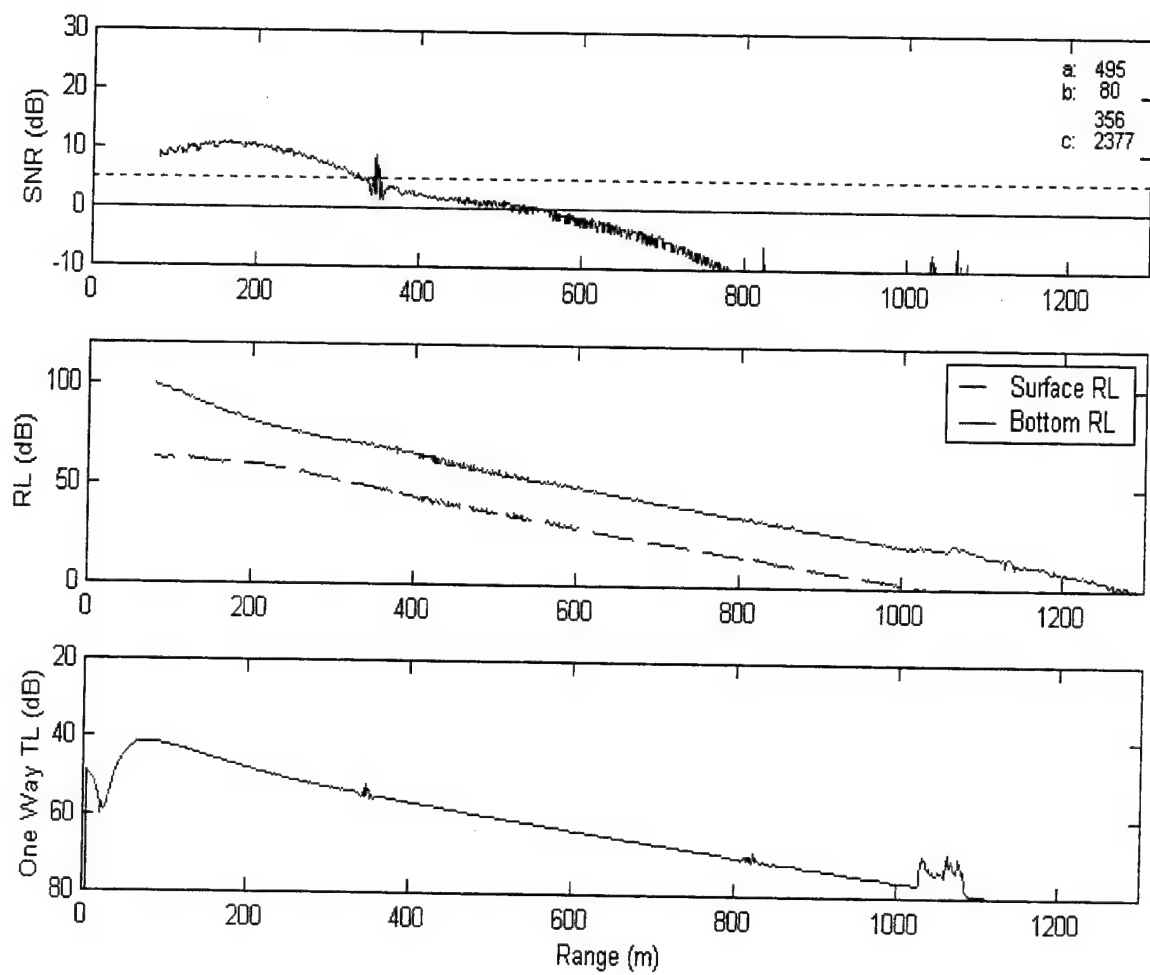


Figure A 18. S\_A90\_05

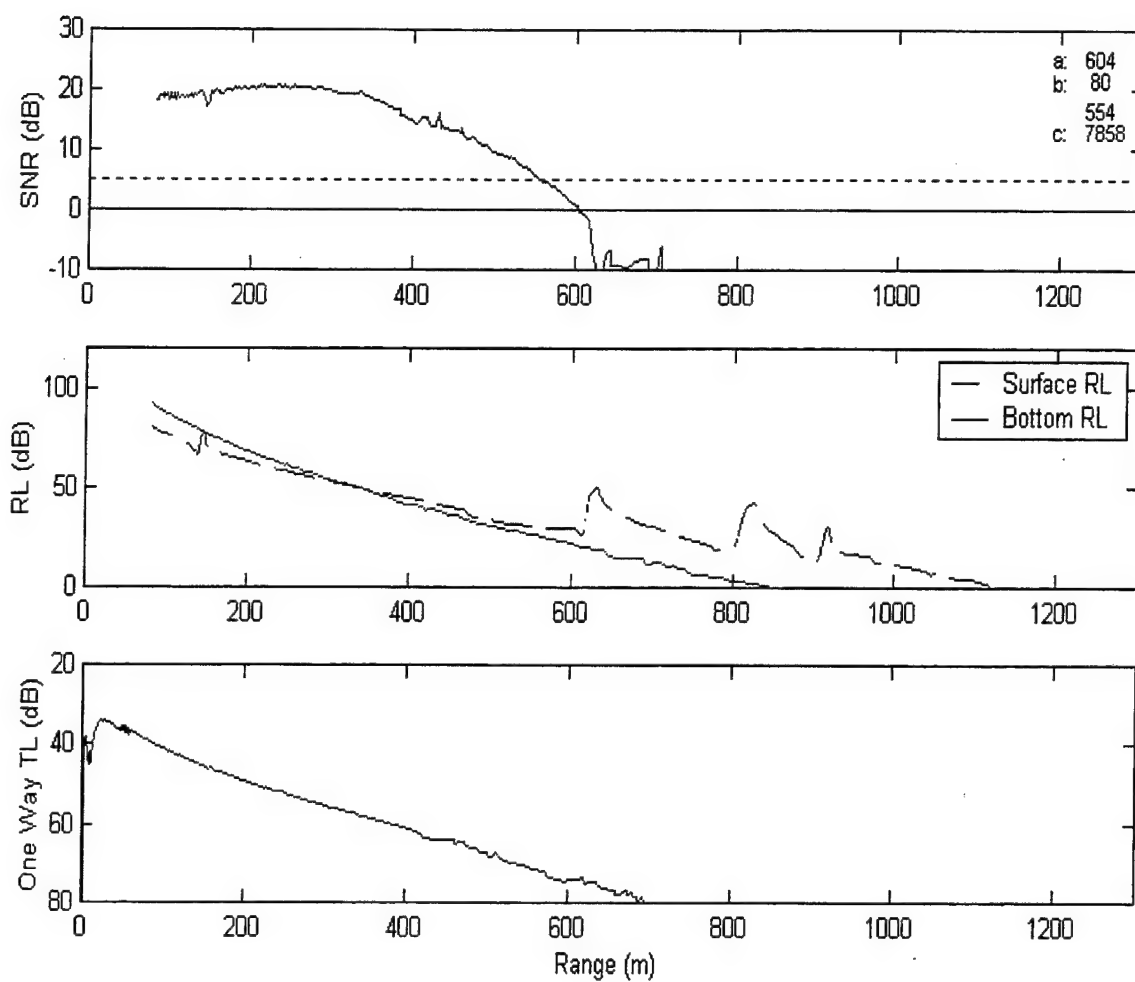


Figure A 19. S\_A90\_06



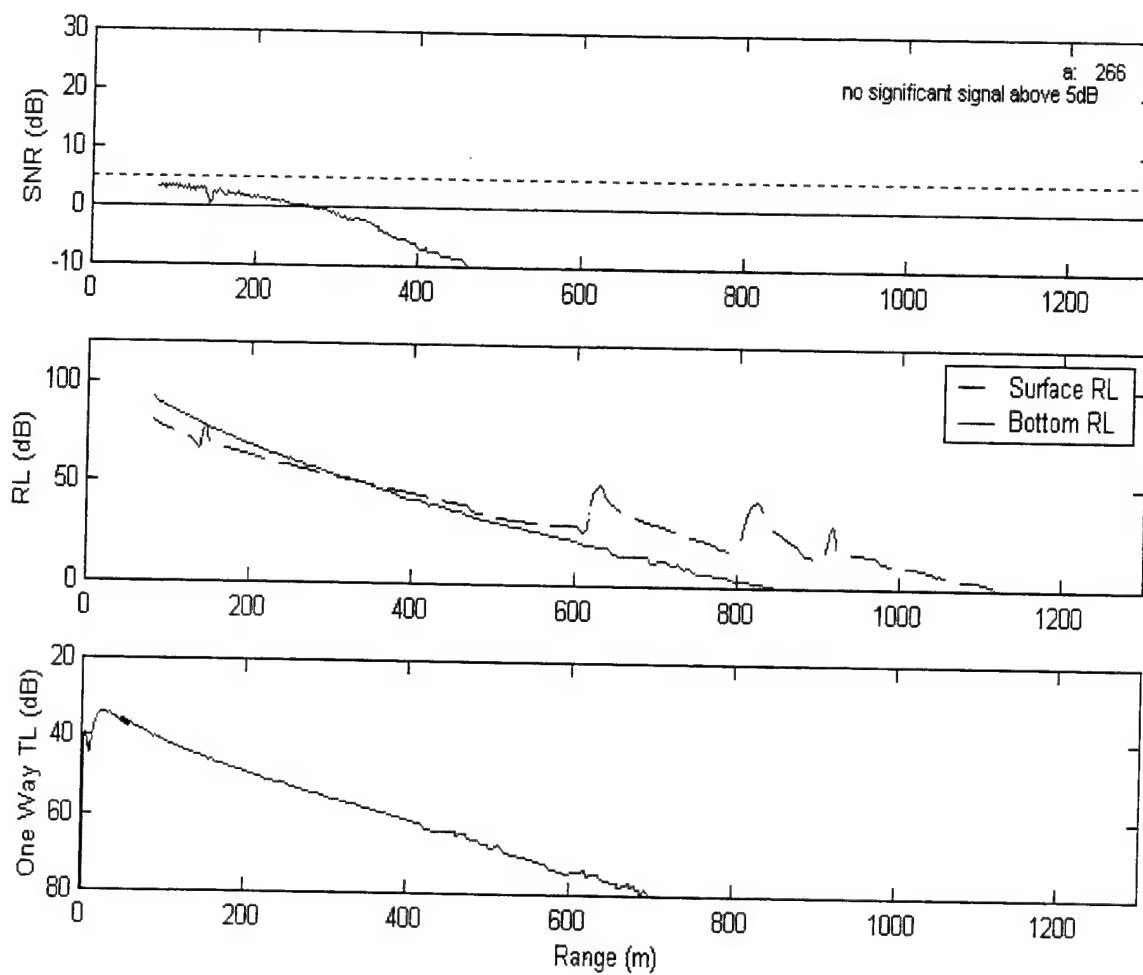


Figure A 20. S\_A90\_07

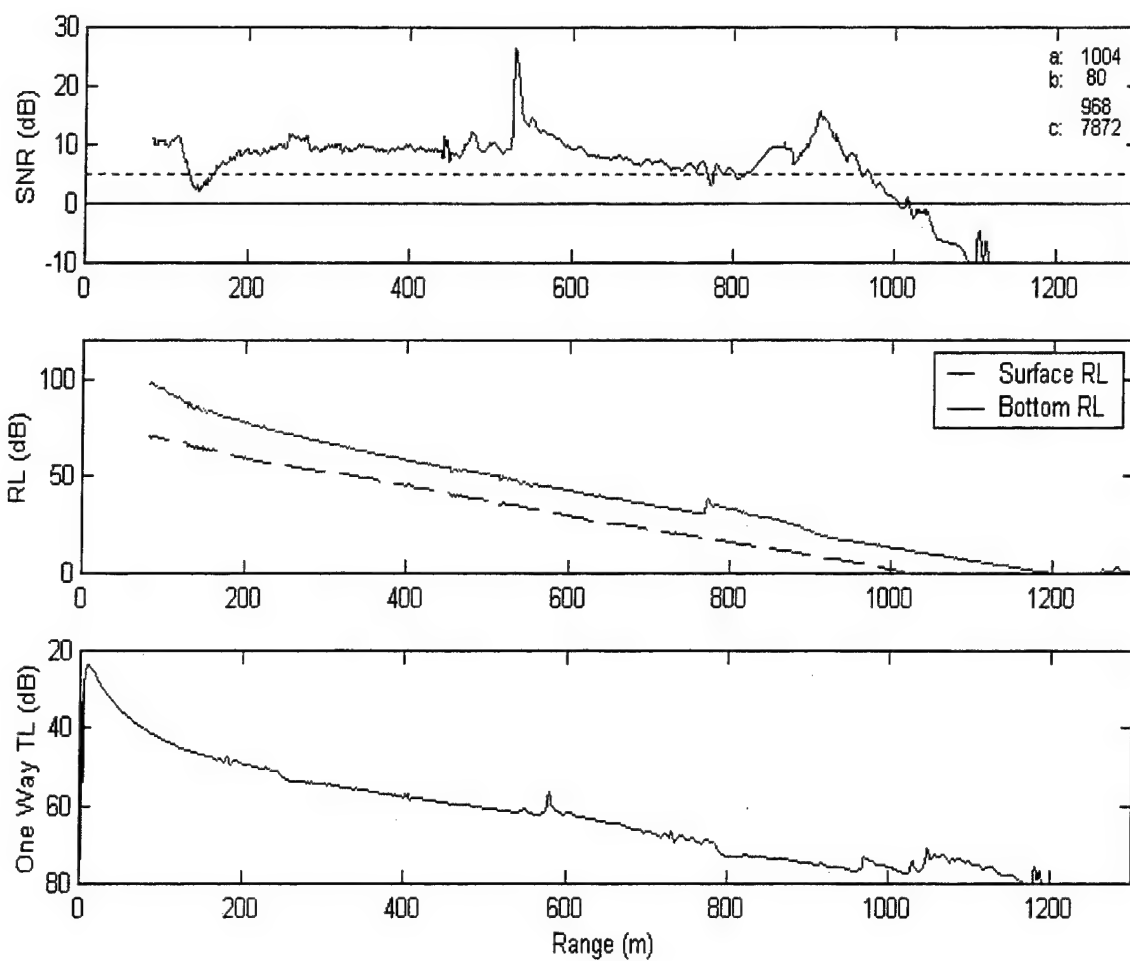


Figure A 21. S\_A90\_08

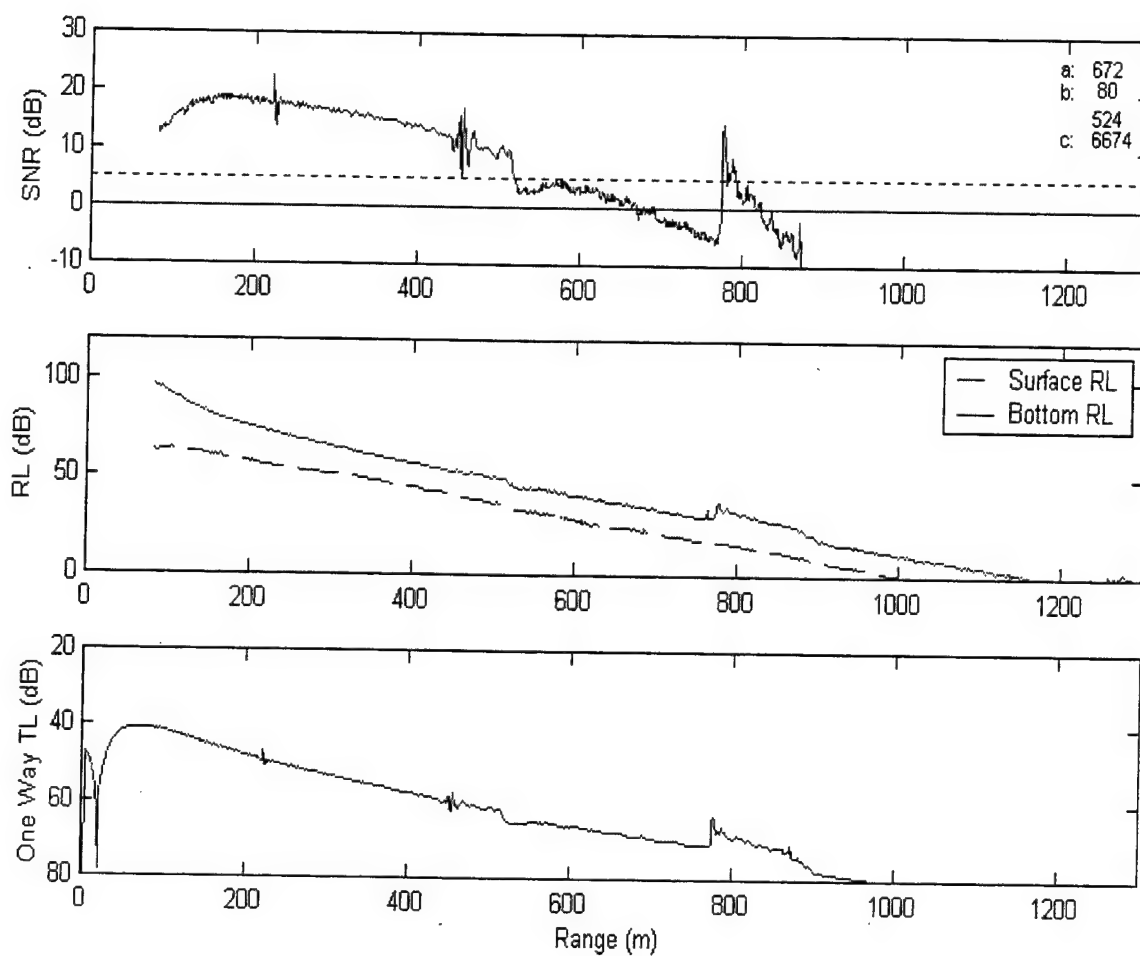


Figure A 22. S\_A90\_09

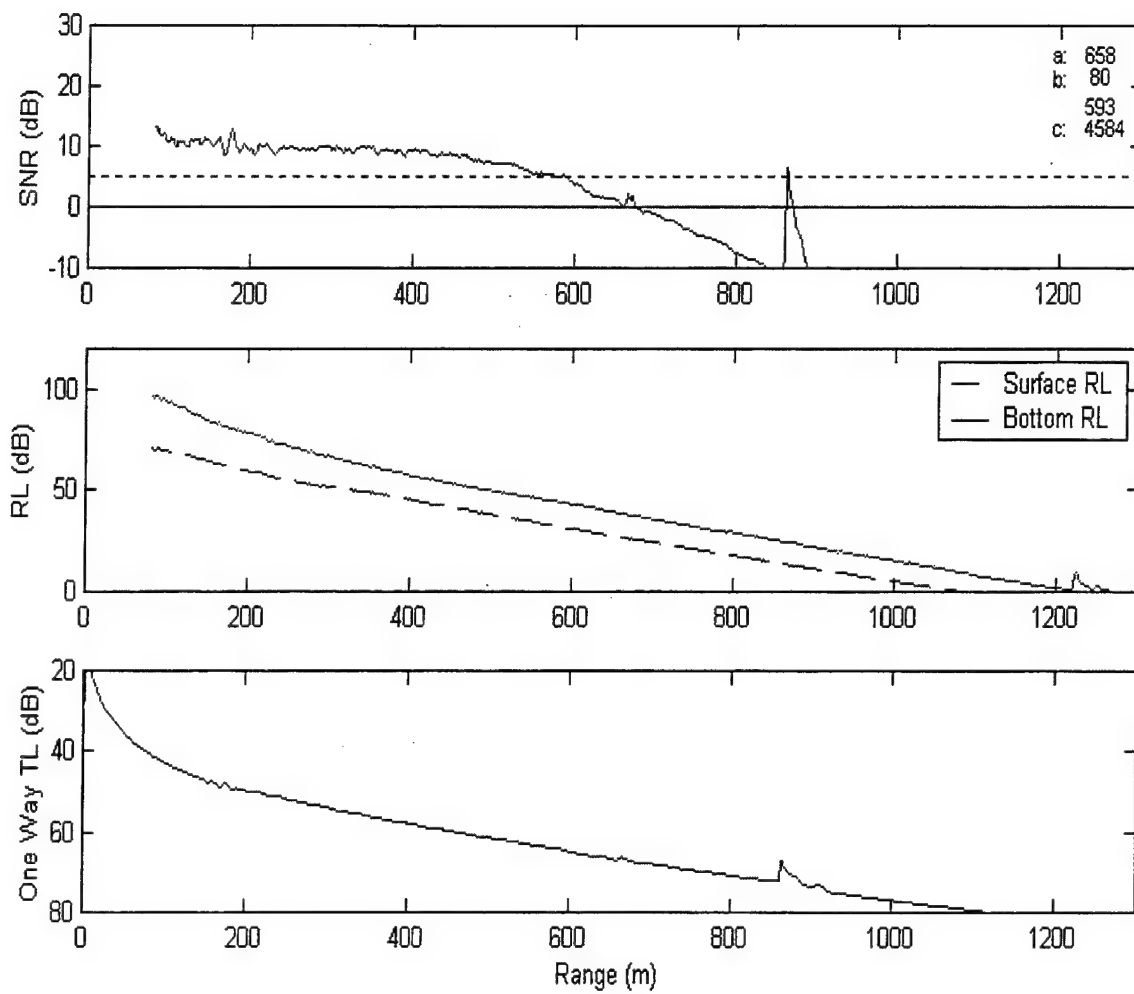


Figure A 23. S\_A90\_10

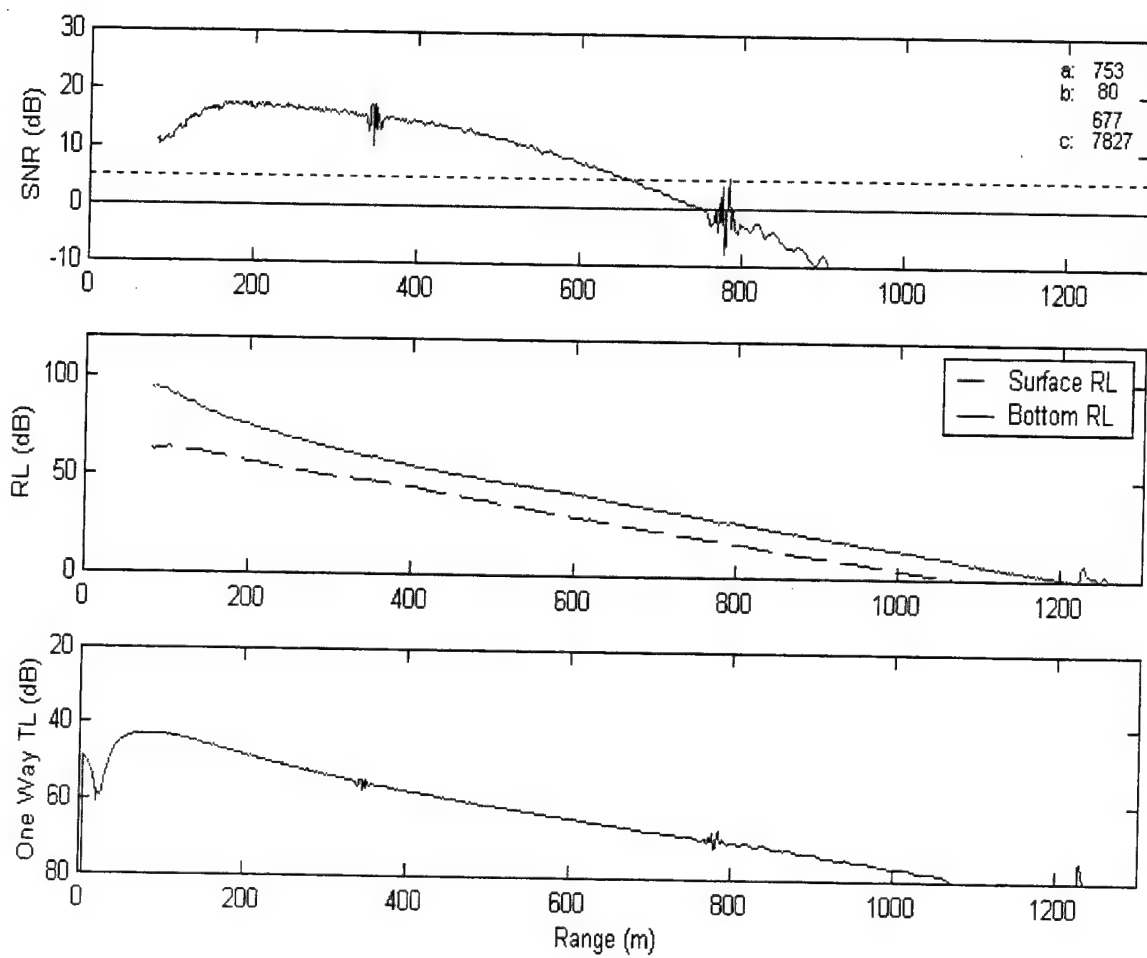


Figure A 24. S\_A90\_11

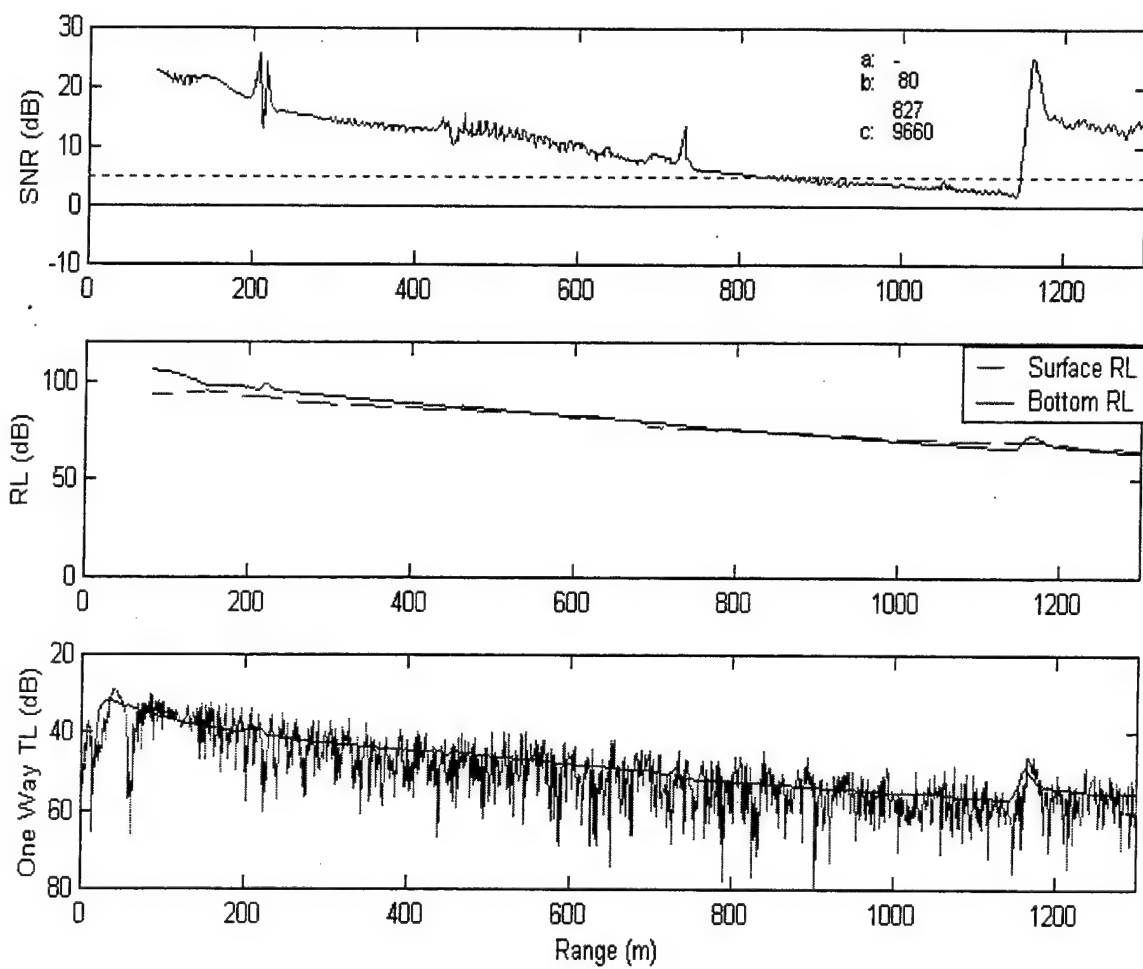


Figure A 25. S\_U35\_01

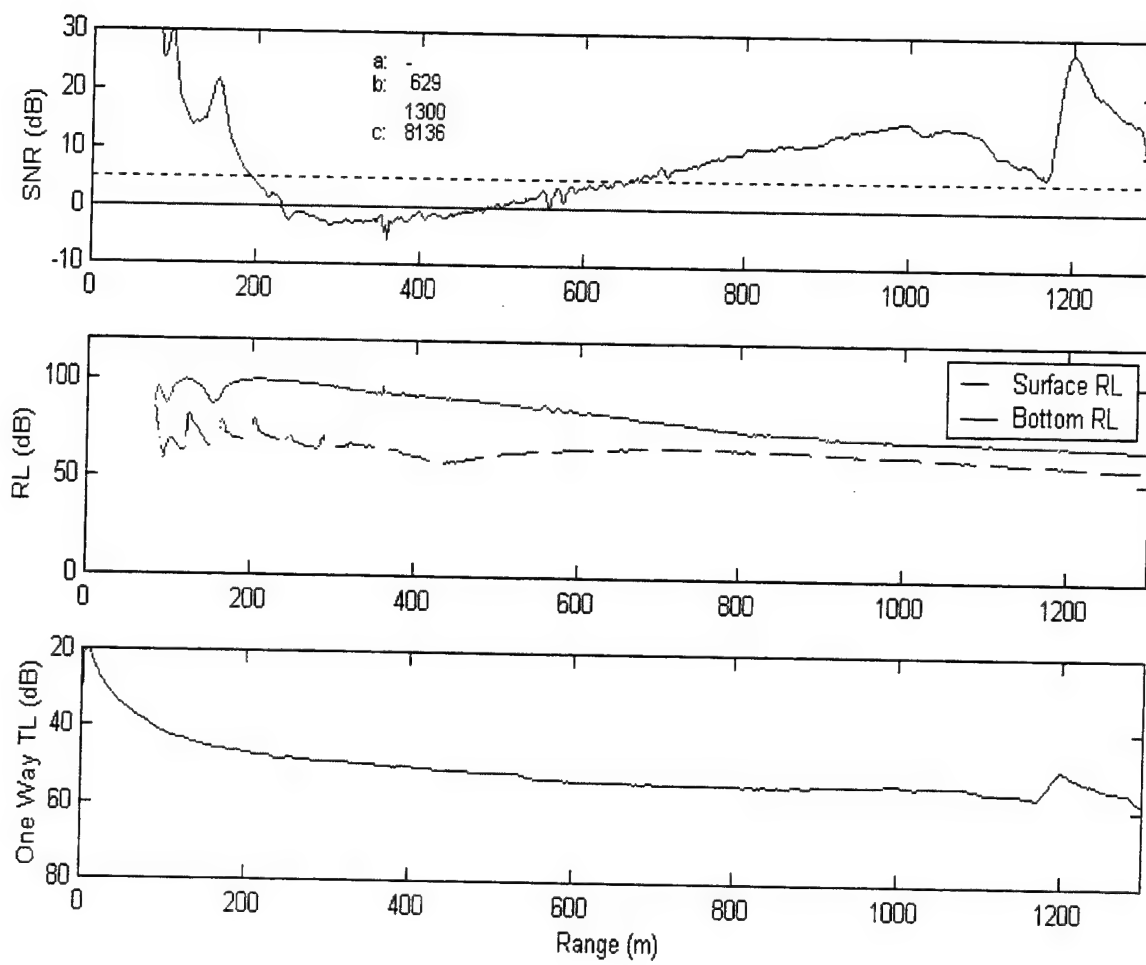


Figure A 26. S\_U35\_02

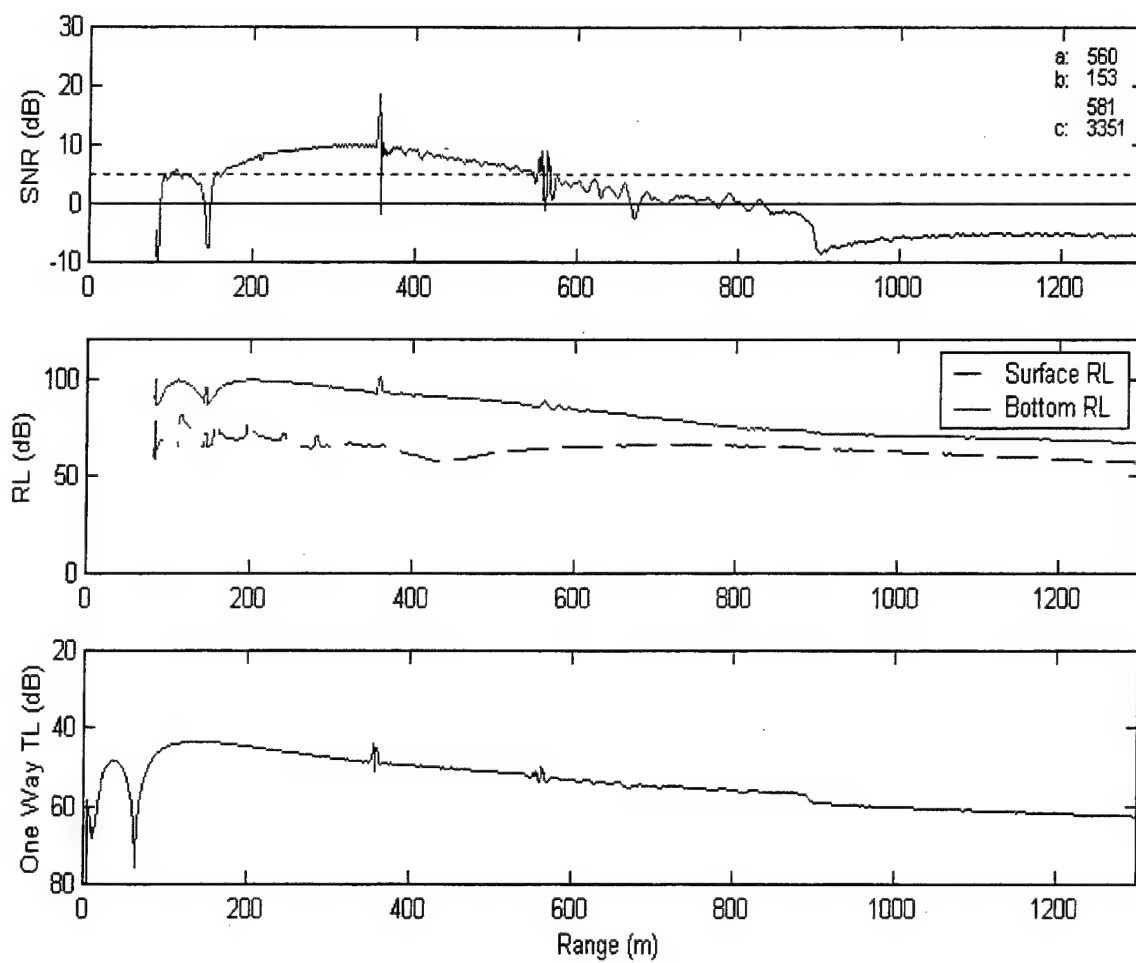


Figure A 27. S\_U35\_03



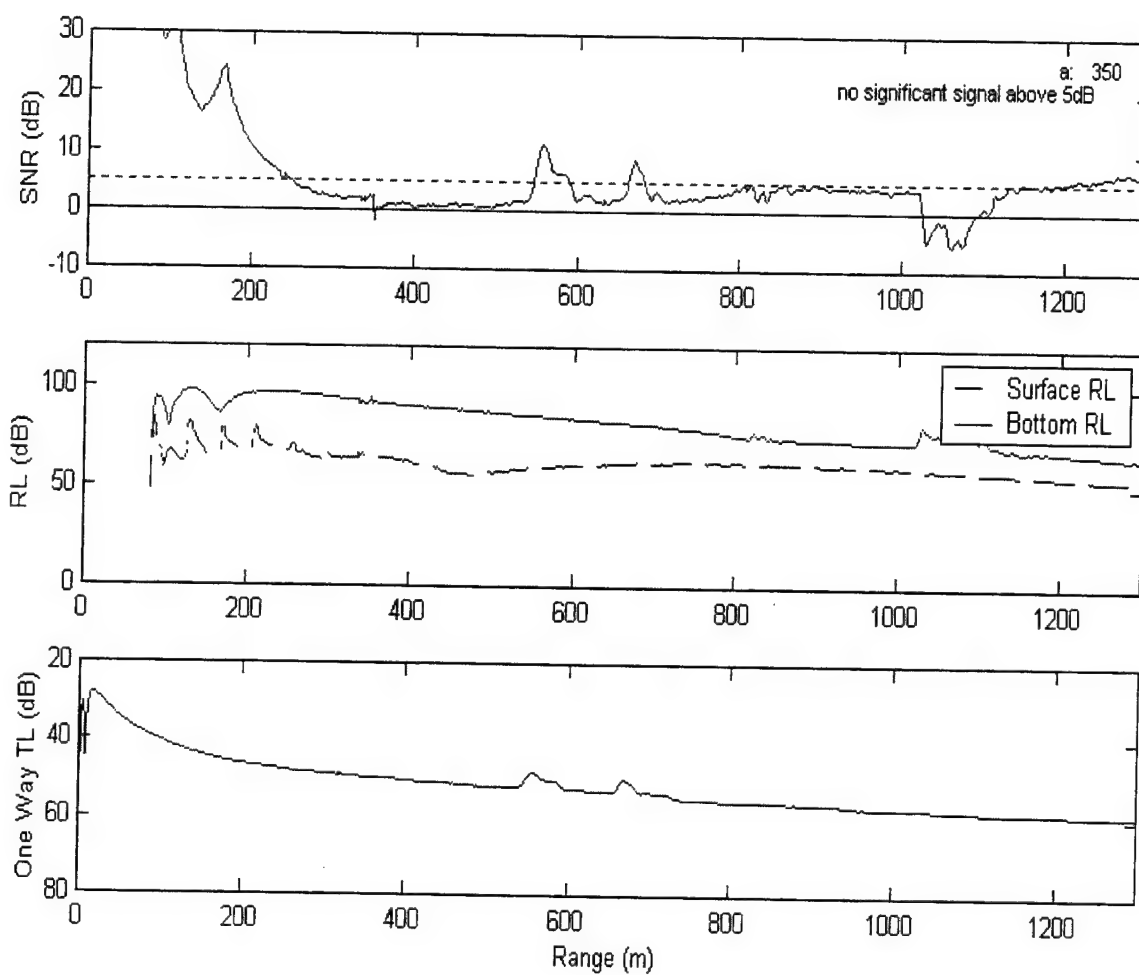


Figure A 28. S\_U35\_04

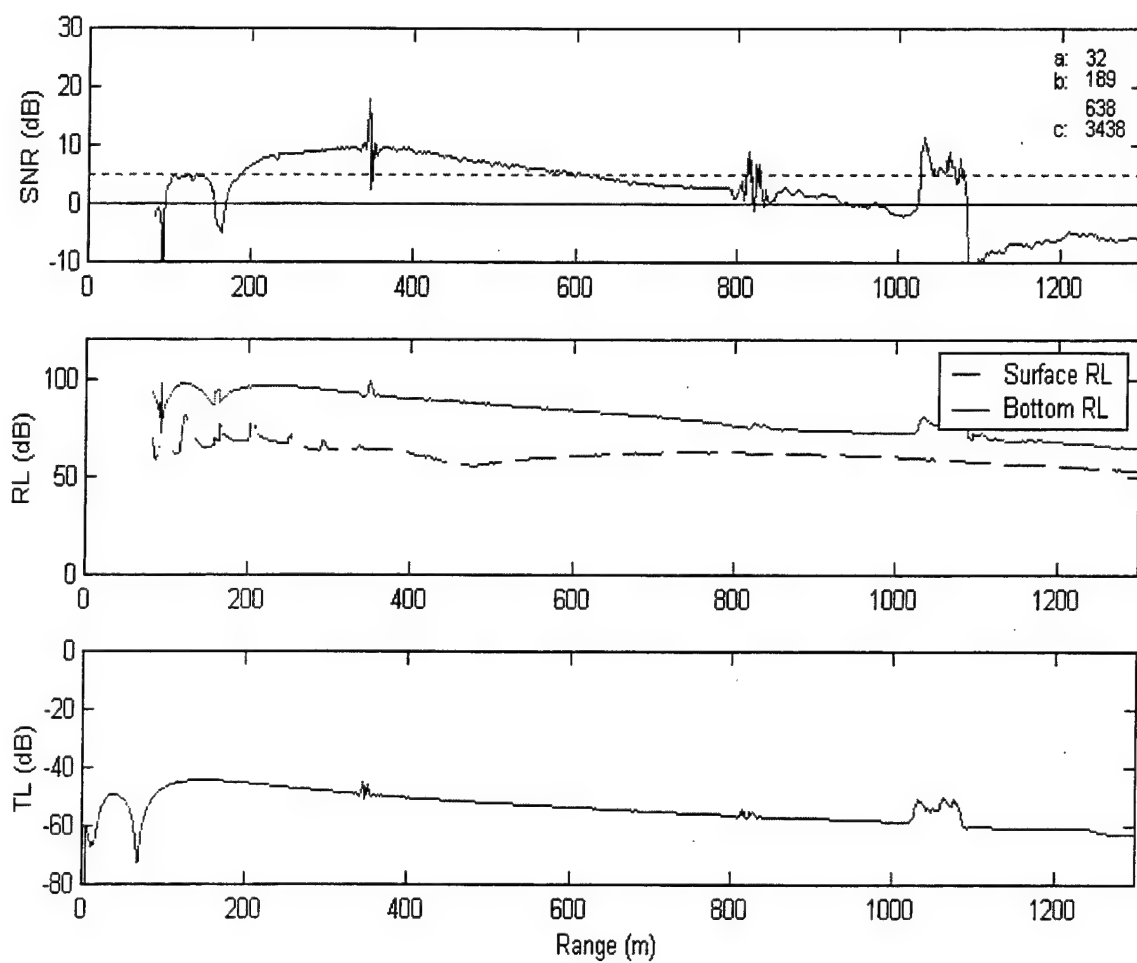


Figure A 29. S\_U35\_05

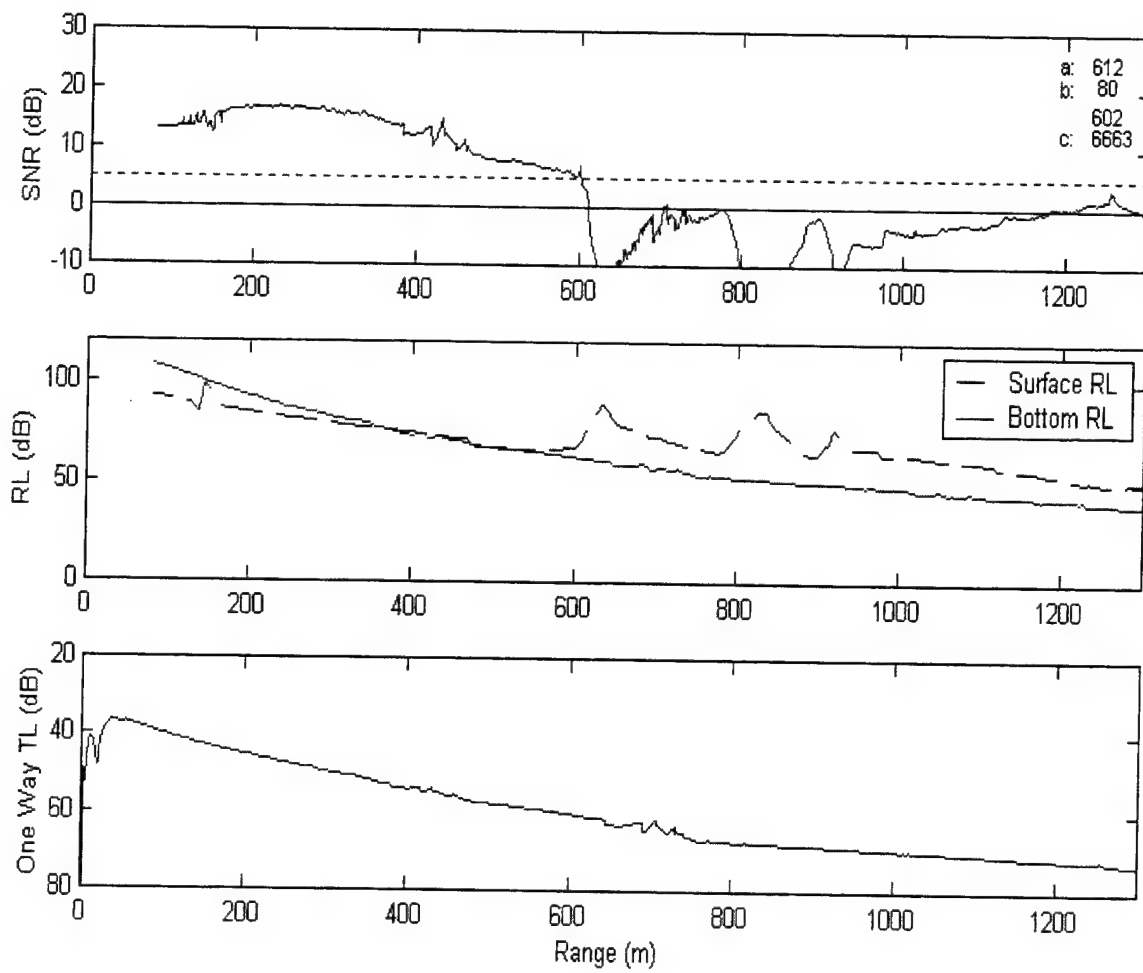


Figure A 30. S\_U35\_06

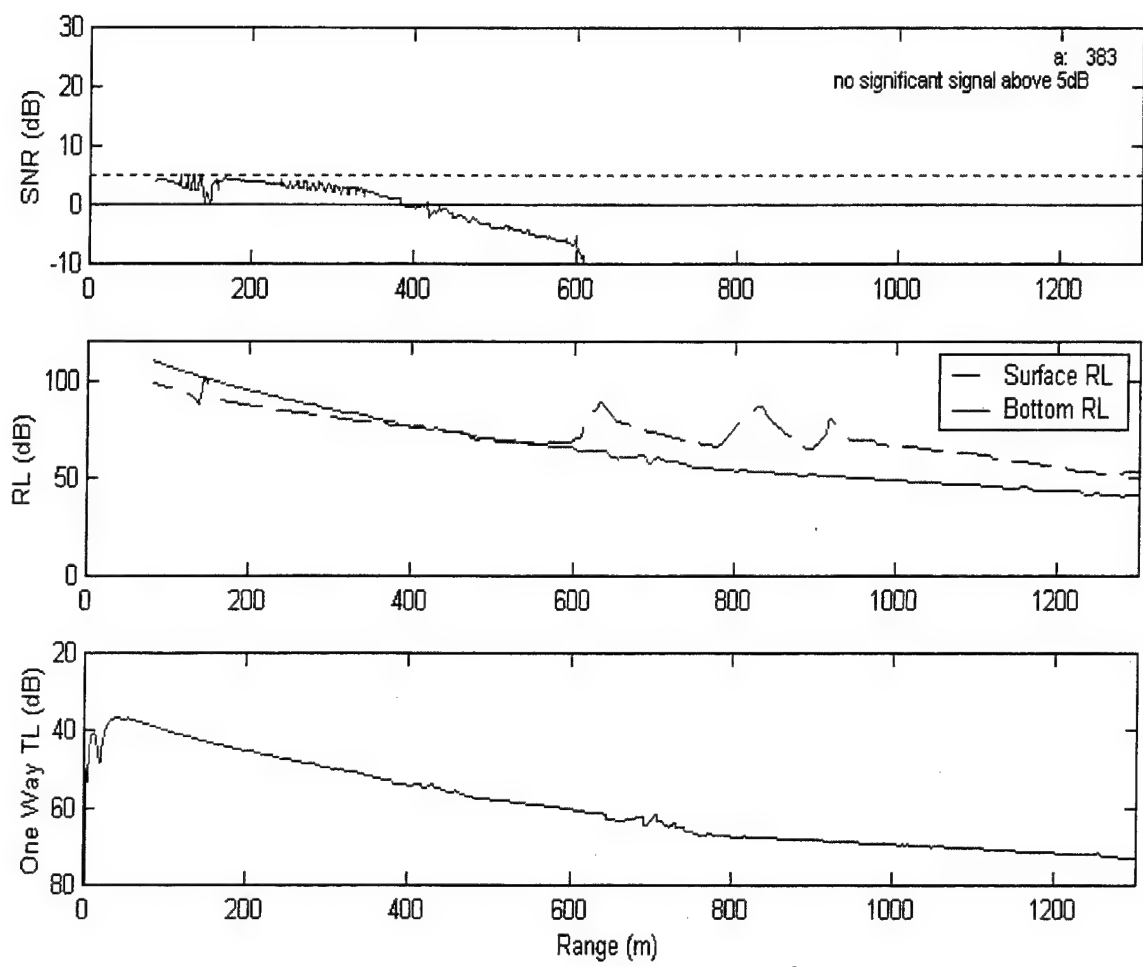


Figure A 31. S\_U35\_07

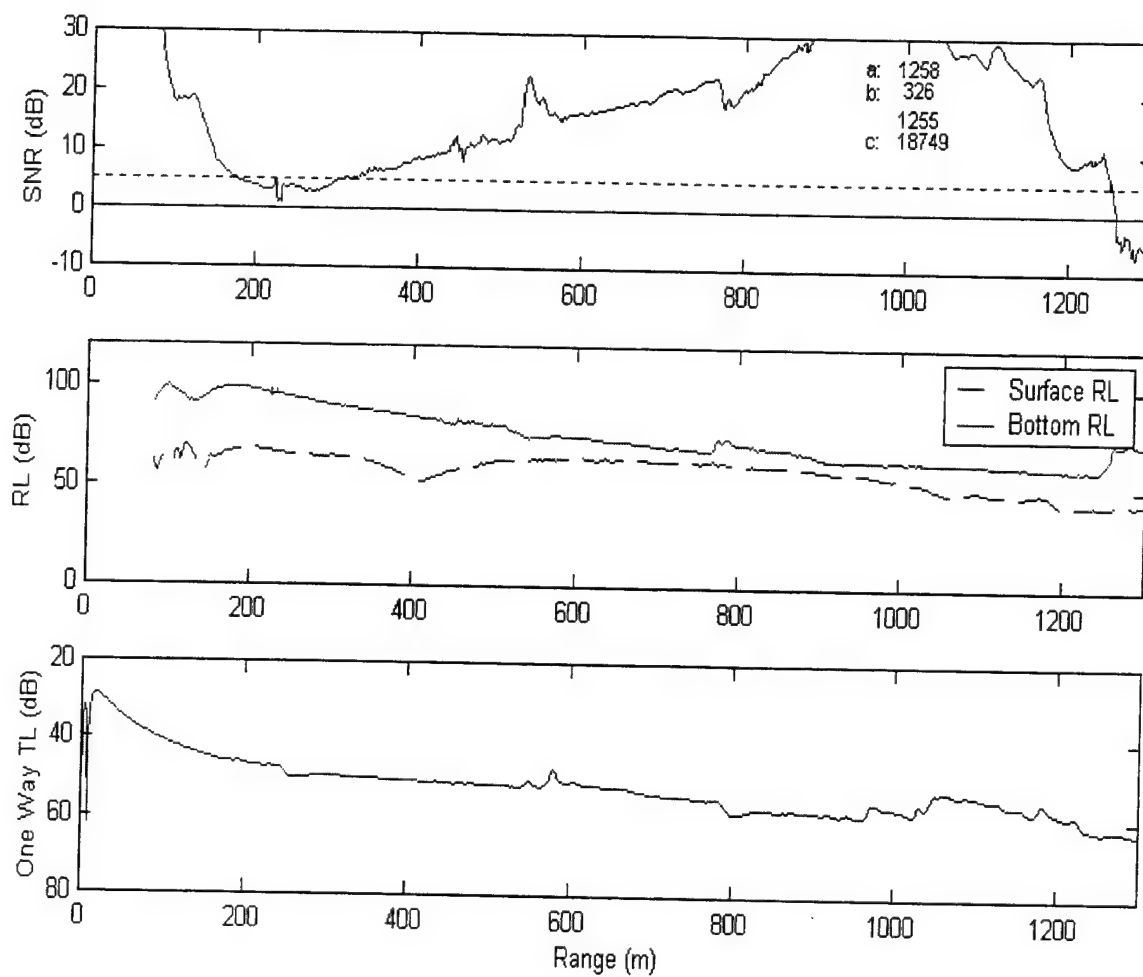


Figure A 32. S\_U35\_08

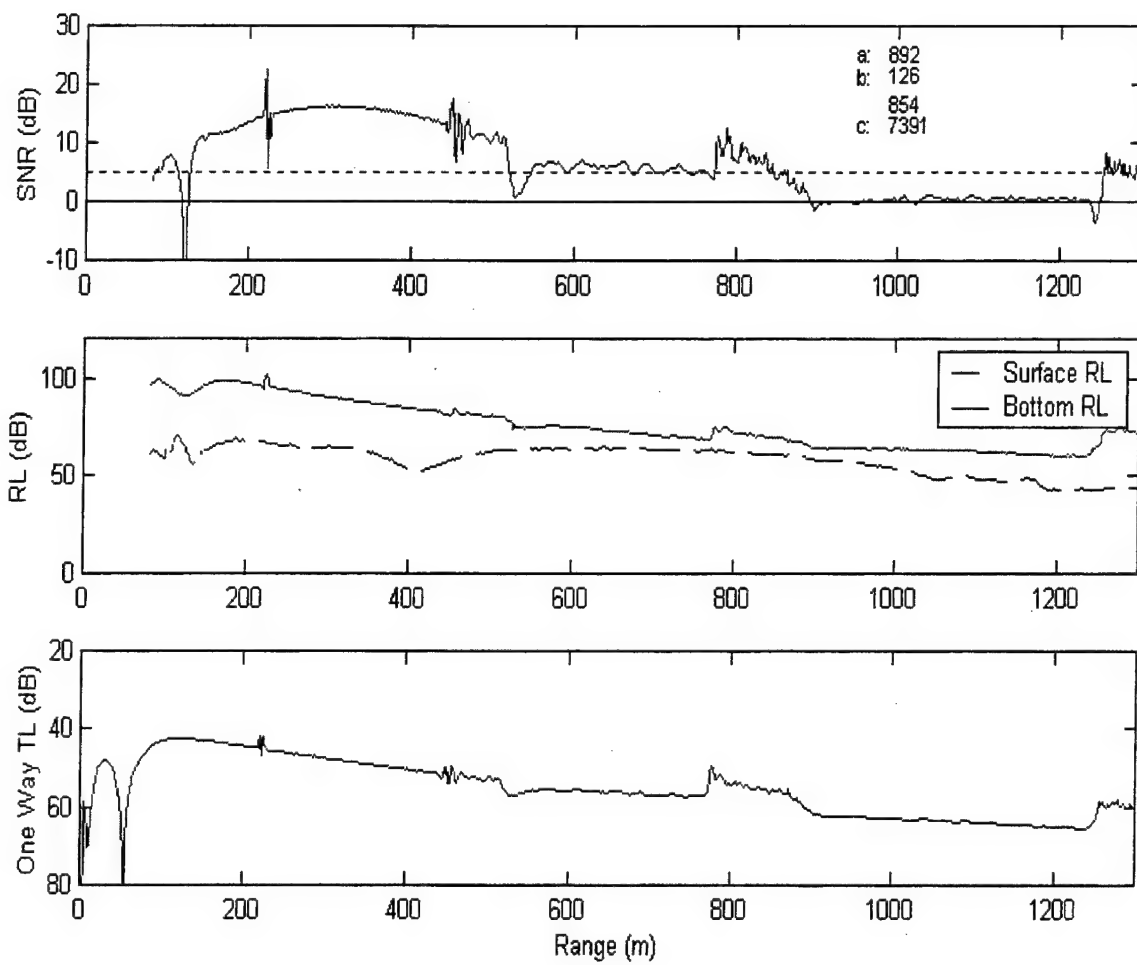


Figure A 33. S\_U35\_09

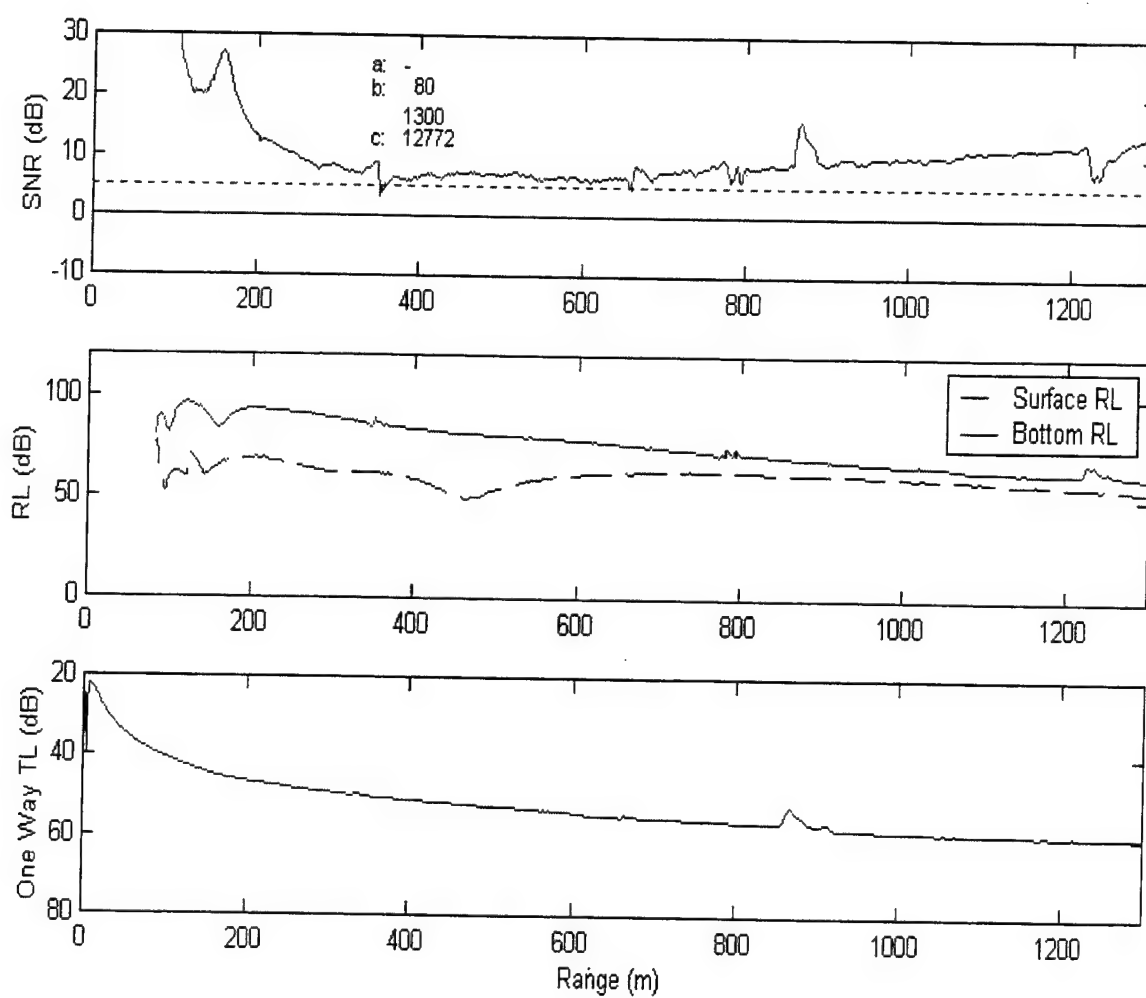


Figure A 34. S\_U35\_10

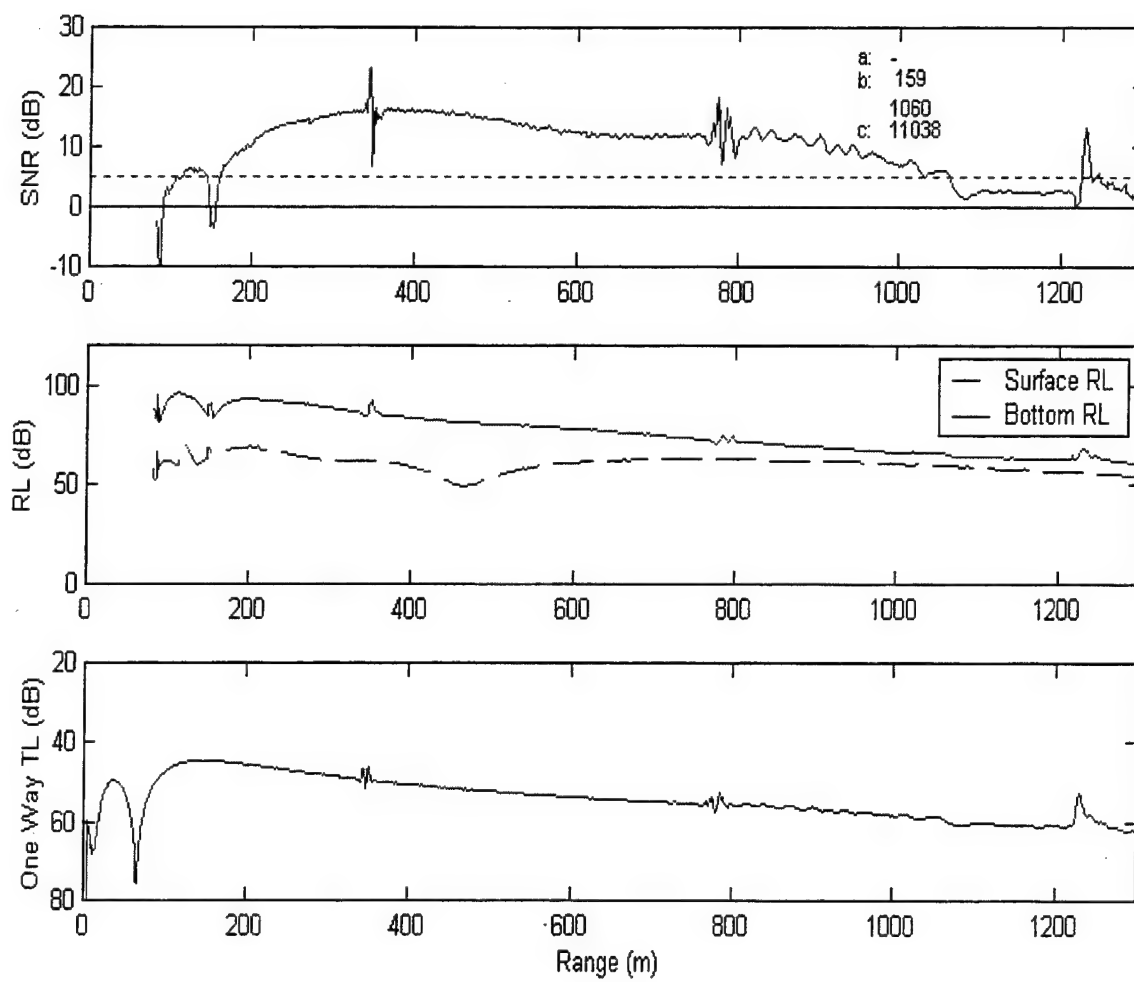


Figure A 35. S\_U35\_11



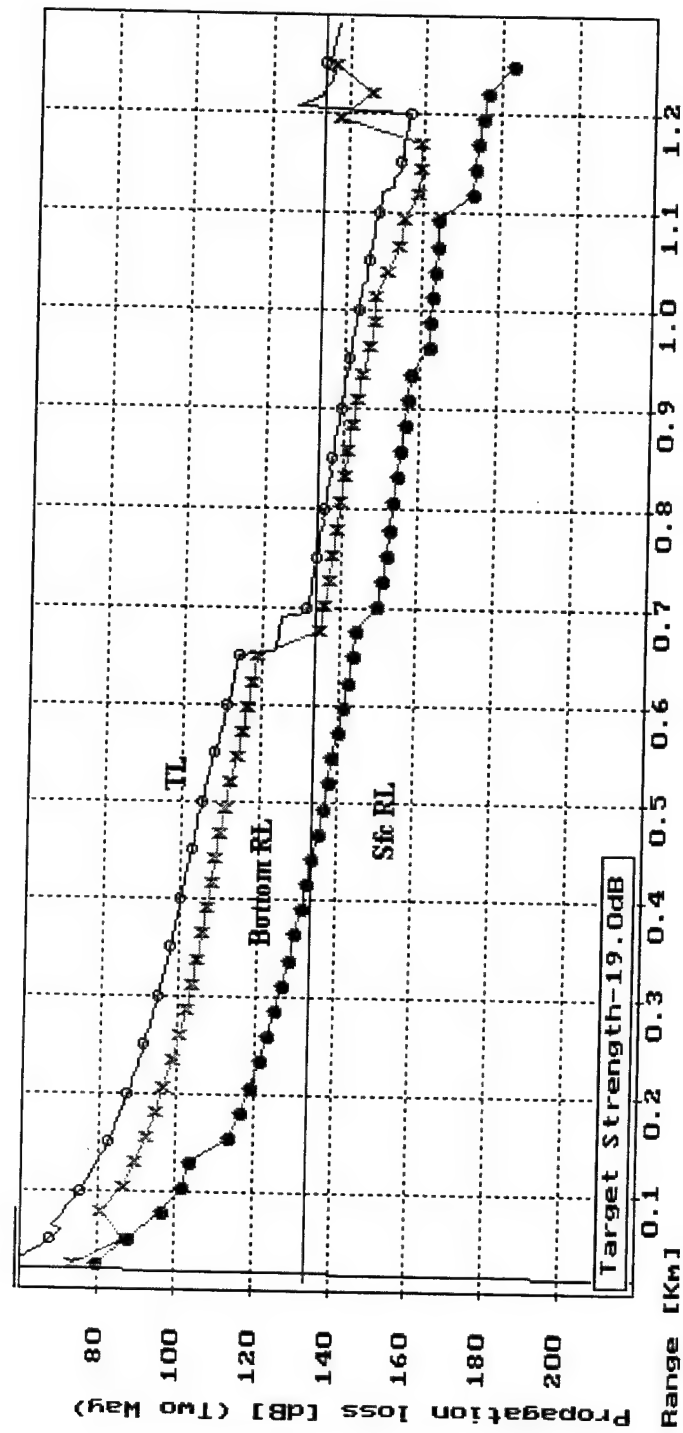


Figure A 36. H\_A40\_01

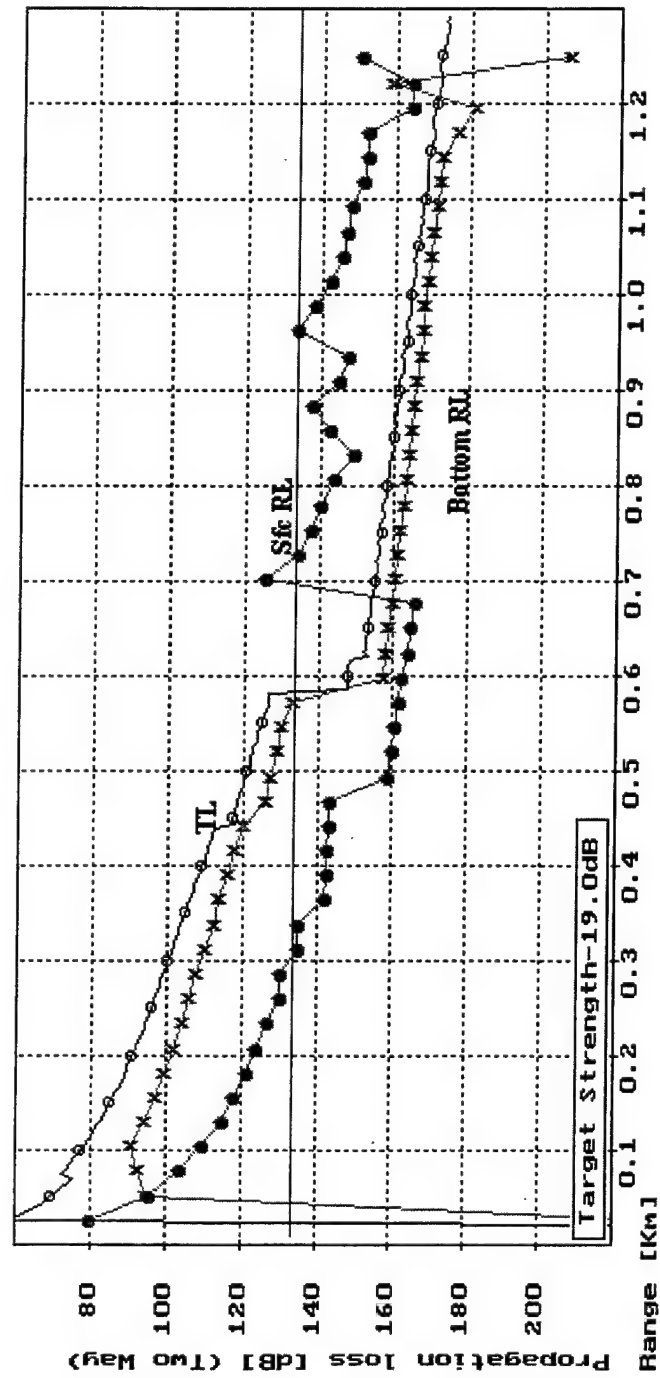


Figure A 37. H\_A40\_06

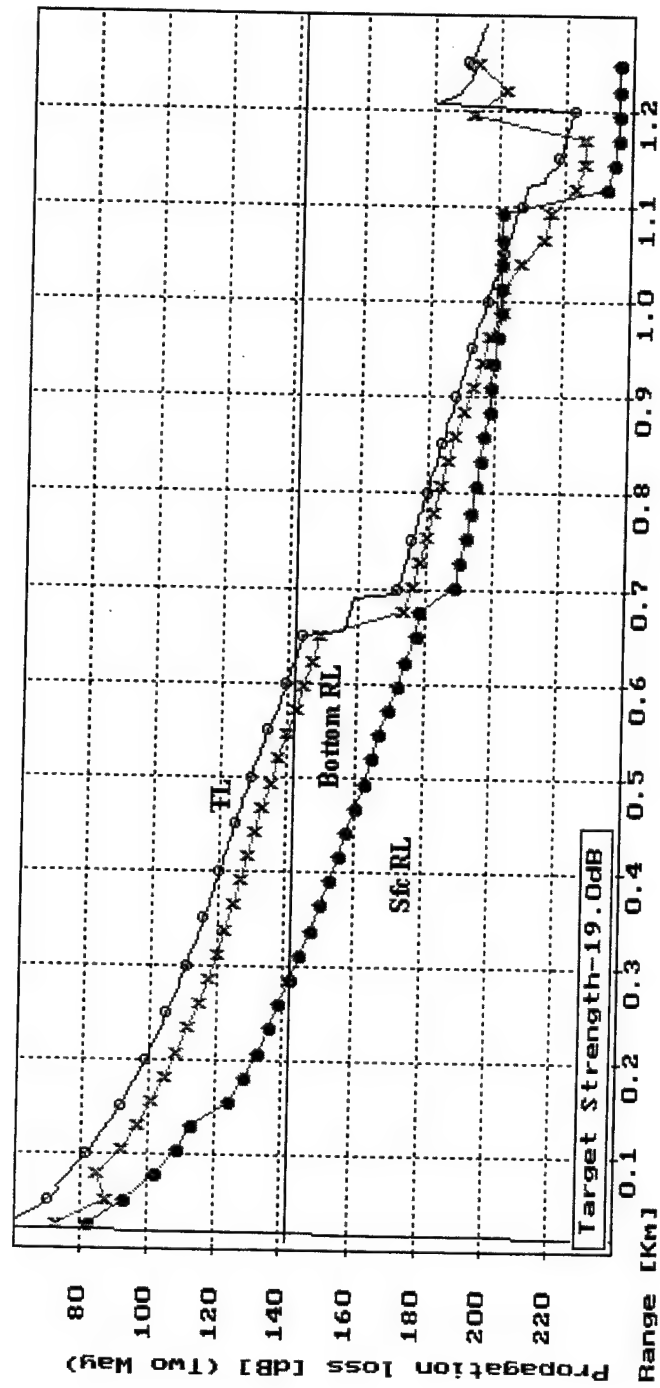


Figure A 38. H\_A90\_01

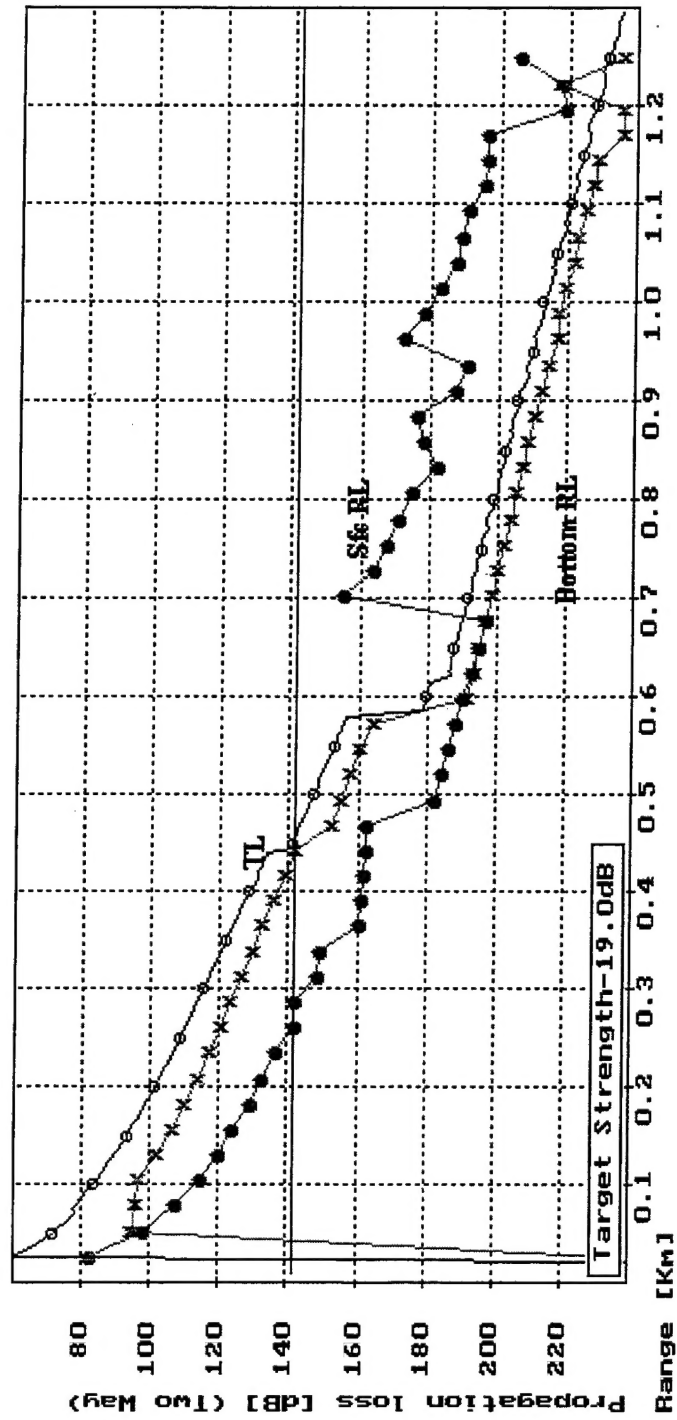


Figure A 39. H\_A90\_06

THIS PAGE INTENTIONALLY LEFT BLANK

## INITIAL DISTRIBUTION LIST

1. Defense Technical Information Center..... 2  
8725 John J. Kingman Road, Suite 0944  
Ft. Belvoir, VA 22060-6218
  
2. Dudley Knox Library..... 2  
Naval Postgraduate School  
411 Dyer Road  
Monterey, CA 93943-5101
  
3. Chairman (Code OC/GD)..... 1  
Department of Oceanography  
Naval Postgraduate School  
Monterey, CA 93943
  
4. Dr. Robert H. Bourke ..... 1  
Department of Oceanography  
Naval Postgraduate School  
Monterey, CA 93943
  
5. Dr. James H. Wilson ..... 2  
Neptune Sciences, Inc.  
4250 Pacific Hwy., Suite 219  
San Diego, CA 92110
  
6. Maritime Commander Australia..... 1  
Maritime Headquarters  
1 Wylde St  
Potts Point NSW 2011
  
7. Director of Oceanography and Meteorology ..... 2  
Maritime Headquarters  
Building 89/90  
Garden Island Dockyard  
NSW, 2011

8. Dr. Stuart Anstee ..... 1  
Maritime Operations Division  
Defence Science and Technology Organisation  
PO Box 44  
Pyrmont, NSW 2011
9. Dr. Gary Sammelmann ..... 1  
Coastal Systems Station  
Dahlgren Division  
Naval Surface Warfare Center  
Panama City, FL 32407
10. LEUT B. K. Dubsky ..... 2  
METOC Services  
Maritime Headquarters  
Building 89/90  
Garden Island Dockyard  
NSW, 2011